UNIVERSITY OF NAPLES FEDERICO II

Dipartimento di Biologia e Patologia Cellulare e Molecolare

"L. Califano"

Doctorate School in Molecular Medicine

Doctorate Program in Genetics and Molecular Medicine

XXIII Cycle 2007-2010

MAPK dysregulation in the brain pathology of Mucopolysaccharidosis IIIB disease

Coordinator

Prof. Lucio Nitsch

Candidate

Dr. Francesca Cecere

Tutor

Prof. Paola Di Natale

TABLE OF CONTENTS

List of pubblications

Villani GRD, Di Domenico C, Musella A, Cecere F, Di Napoli D, Di Natale P. Mucopolysaccharidosis IIIB: oxidative damage and cytotoxic cell involvement in the neuronal pathogenesis. Brain Research 2009;1279:99-108.

Visigalli I, Delai S, Politi LS, Di Domenico C, Cerri F, Mrak E, D'Isa R, Ungaro D, Stok M, Sanvito F, Mariani E, Staszewsky L, Godi C, Russo I, Cecere F, Del Carro U, Rubinacci A, Brambilla R, Quattrini A, Di Natale P, Ponder K, Naldini L, Biffi A. Gene therapy augments the efficacy of hematopoietic cell transplantation and fully corrects Mucopolysaccharidosis type I phenotype in the mouse model. Blood, prepublished online September 16, 2010; DOI 10.1182/blood-2010-04-278234.

Abstract

The accumulation of heparan sulfate (HS) in lysosomes is the primary consequence of the enzyme defect (α-N-acetylglucosaminidase) in Mucopolysaccharidosis type IIIB. This accumulation triggers a cascade of pathological events that progressively leads to CNS pathology. Here we examined the activation of the three major stress kinases in the neuronal tissue of a murine model of the disease. ERK1/2 was significantly higher in the cortex of 1-2-month-old affected animals compared to wild type (Wt) littermates. Similarly, ERK 1/2 was stimulated in neurons cultured from MPS IIIB mice. SAPK/JNK was also found to be activated in the cortex of 1-2-month-old affected animals compared to Wt subjects, and the same was found for cultured neurons. In contrast, the active form of p38MAPK was lower in the cortex of 1-month-old MPS IIIB mice compared to Wt animals, but no significant difference was found between the two p38MAPK analyzed in normal and affected neurons cultured *in vitro*. The differential activation of these kinases in the mouse brain at a very early stage of the disease course suggests a selective stress signature imposed by the lysosomal dysfunction.

Background

1. Lysosomal storage diseases

Pathogenetic events in lysosomal storage diseases

Lysosomal storage diseases (LSD) represent a large group of more than 50 genetic disorders characterized by disruption of normal lysosomal function (Platt and Walkley, 2004). Lysosomes are hydrolase rich organelles, responsible for the degradation of biological macromolecules. Proteins or macromolecular substrates that have to be degraded are delivered to these acidified organelles by various pathways, which among others involve the endocytosis, autophagy and the direct transport across the lysosomal membrane. So lysosomes are component of endosomal/lysosomal (E/L) system which, together with the ubiquitin-proteosomal system and autophagosomal system, represent an important metabolic centre for substrate degradation, influencing several aspects of the cells, from signal transduction to regulation of gene expression.

Early view to explain LSD pathogenesis emanated from the original concept that these disorders are caused by individual lysosomal enzyme deficiencies followed by accumulation of a single major substrate normally degraded by that enzyme. Following the build-up of this non degraded primary substrate, the endosomal/lysosomal system would eventually be overwhelmed, normal cell functions would collapse and cells would simply die as a result of this progressive constipation. This so-called “cytotoxicity hypothesis” is still often cited today to explain the pathogenesis of lysosomal disease, yet modern developments in cell biology and neuroscience offer much richer avenues of explanation (Walkley, 2009). Modern studies, in fact, contribute to overcome the notion of lysosomes as end organelles in the serial degradation of molecules, providing evidence for a greater role of these organelles in cell metabolism. In this respect, recent findings demonstrated the existence of a gene network named CLEAR, regulating the lysosomal biogenesis and function (Sardiello et al., 2009).

As suggested by Tettamanti et al (2003), lysosomal processing include either the degradation or the recycling of break-down products for biosynthetic purpose, known as "metabolic salvage". There is ample evidence that some complex molecules processed by the E/L system do not have to be degraded to their simplest components prior to exit from these organelles. An example are gangliosides, which are synthesized in the Golgi/TGN and delivered to the cell surface by vescicular transport in exocytic vacuoles, followed by insertion in the outer leaflet of the plasmalemma. Following endocytosis, complex gangliosides come into contact with an array of hydrolytic enzymes that facilitate their catabolism to simple gangliosides. However, they may be recycled (or salvaged) after endocytosis prior to their complete degradation. Thus, they may exit the E/L system and be trafficked to the Golgi/TGN, where they would be re-glycosilated and delivered again to the plasmalemma. So, the consequences of this failure to recycle materials (e.g. monosialogangliosides, cholesterol, glycosaminoglycans and others) out of the E/L system is of great importance for LSD. Probably, the first consequence is that lysosomal storage simply overwhelms the cell's capacity for volume expansion and causes death. Another possibility is that sequestered substrates like GM_1 ganglioside could interact with IP-3 receptor influencing the activity of this channel, with the resulting efflux of Ca^{2+} from ER to mitochondria and, finally, the activation of apoptotic pathway (d'Azzo et al, 2009).

Most LSD show wide-spread tissue and organ involvement. Brain disease however, is particularly prevalent, involving two-thirds of all lysosomal diseases. For LSD affecting brain, the pathogenic events appears to be more complex for several reasons. Among these, the wide variety of enzyme and non-enzyme proteins implicated in causing lysosomal disease; the complexity of brain itself in terms of heterogeneity of the neuronal and glial cell types that typically exhibit distinct metabolic identities and interrelationship; the potential role of the E/L system in signal transduction and in cellular homeostatic control (Walkley, 2009). In neurons, endocytic events govern a variety of signaling

mechanisms, such as those associated with neurotransmitter actions. For example, endocytic mechanisms are known to control the avaibility of neurotransmitter receptors at excitatory synapses. In addition to a possible compromise of neurotransmitter receptor recycling, another prominent aspect of signaling that may be altered in lysosomal disease involves growth factors. Growth factors receptors are known to be internalized by endocytosis, with this occurring both in the somatodendritic as well as axonal domains. Growth factors are also endocytosed at synaptic terminals and transported along with their receptors back to the neuronal cell body to recruit appropriate second-messenger cascades for signal transduction purposes. In LSD, disruption of E/L function in neurons has the capacity to compromise many normal cell operation and to generate a host of downstream consequences. For example, the possible compromise in cycling of receptors critical for synaptic plasticity, secondary to lysosomal system compromise, could account for ectopic dendritogenesis that characterized many LSD. Analogously, the formation of spheroids (collection of mitochondria, autophagosomal-like and multivescicular-like bodies) may be contributing to compromise signaling events blocking endosomes carrying a growth factor-receptors complex essential for cell survival (Walkley, 2009).

Failure to recycle materials out of the E/L system in lysosomal diseases may also lead to deficiency of precursor pools of metabolites and thereby alter cellular homeostatic functions leading to changes in synthetic pathways. The first consequence, in fact, might be the up-regulation of precursor synthesis, an event that if occurred would not solve the deficit but would simply add further problems to the storage process. Another possibility, that has come under increased focus in lysosomal disease, is the block, or in some cases the increase, of autophagy that is closely allied to protein degradative mechanisms associated with chaperone-mediated autophagy and the ubiquitin-proteosomal system (Settembre et al, 2008).

Taking into consideration what previously described, it is possible to

conclude that the complexity of the pathogenetic events in LSD derive, at least in part, from disruption of interrelated components of the greater lysosomal system such as macroautophagy, UPS, endocytosis (Walkley, 2009). Furthermore, all these evidences support the new concept of lysosomes as the central element in the lysosomal system that function as link between the endocytic streams from axonal domains and the "salvage pathway" (Fig 1).

New therapeutic options for lysosomal storage diseases

Although at present the sequence of pathological events in LSD is not completely understood, there is no doubt that accumulation of storage materials is the first pathogenetic factor which by triggering secondary structural and biochemical alterations leads to disease initiation and progression. Removal of this material should be the first therapeutic goal. Essentially, this target can be achieved by different therapeutic approaches such as enzyme replacement therapy, application of small molecules that could inhibit enzyme responsible for substrate synthesis (substrate deprivation) or act as chaperone to increase the residual activity of the lysosomal enzyme (enzyme enhancing therapy), and finally, gene therapy.

The early in vitro studies demonstrated that the metabolic defect of cultured fibroblasts from mucopolysaccharidosis patients can be compensated by the addition of corrective factors which are secreted by cells not having the same defect and that the corrective factors are enzymes that are taken up from outside the cell into the lysosomal compartment by receptor-mediated endocytosis via the mannose 6-phosphate receptor (Fratantoni et al., 1968). On the basis of these early studies it was considered that LSD should be generally treatable by administration of the intact lysosomal enzyme, the so called

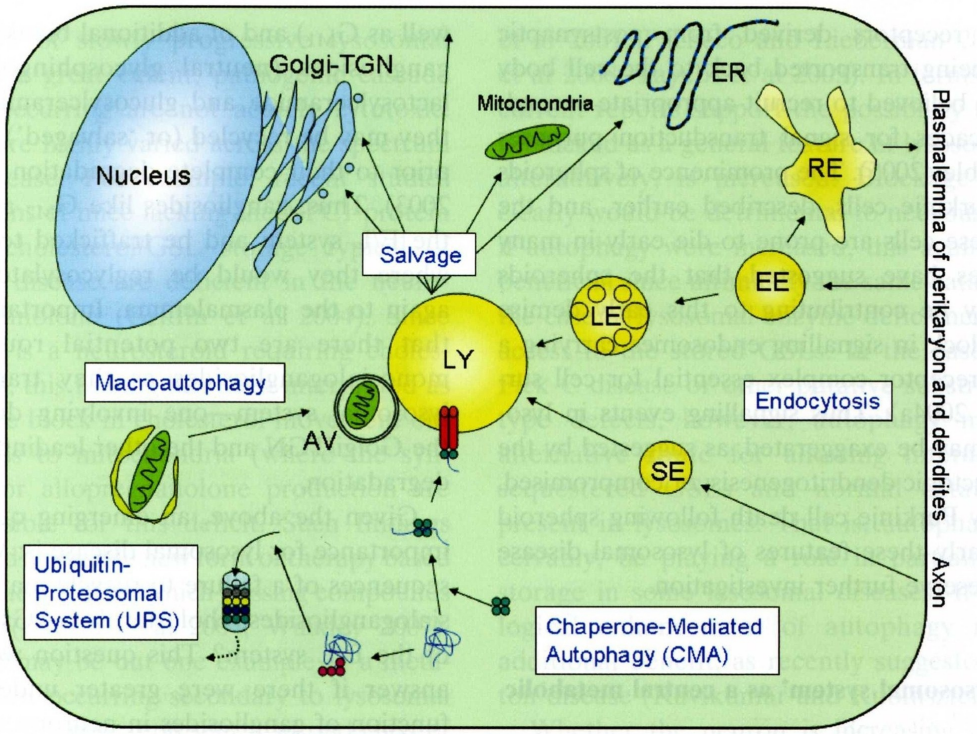

Fig. 1 Schematic summarizing the concept of the lysosome as a central element in the greater lysosomal system of neurons with links to the endocytic streams from somadendritic and axonal domains, and to the macroautophagy stream and its close allies, the ubiquitin-proteosomal system (UPS) and chaperone-mediated autophagy (CMA) components. What flows into this system must also leave in some form, depicted here as the salvage pathway with delivery to the Golgi/TGN, mitochondria, and other sites in the cell. The complexity of the disease cascades in lysosomal disorders is conjectured to emanate in part from disruption of these interrelated components of the greater lysosomal system, as described in the text. (EE, early endosome; RE, recycling endosome; LE, late endosome; LY, lysosome; SE, signaling endosome; AV, autophagic vacuole; ER, endoplasmic reticulum). (From: Walkley, 2009)

enzyme replacement therapy (ERT). The first thing that must be taken into consideration for development of an effective ERT therapy is that various cell types use specific receptors for uptake of lysosomal enzymes. For example, the hepatocyte membrane contains galactose receptors, macrophages require mannose residues for uptake, whereas most cells bind exogenous enzymes via the mannose-6-phosphate receptor. In addition, the diversity in the density of the M6P receptor in different tissue could account for a different response of tissues to exogenously administered enzyme. So successfully ERT will require targeting to multiple cell types and the ideal drug may be that one that includes enzymes with various sugar residues, designed to use the many cellular receptors involved in endocytosis (Beck, 2007).

Since ERT has been successfully introduced for patients with Gaucher disease, this principle of treatment has been taken into consideration for other LSD as well. Clinical trial for Mucopolysaccharidoses, Fabry disease, Pompe disease were set up with results that confirm the efficacy of the administration of enzyme preparation. However, it has been taken into consideration that currently available replacement therapies are not able to treat all symptoms of a disorder in the same degree. For example in mucopolysaccharidoses the enzyme preparation do not have a beneficial effect on the skeletal system, heart valve or brain. Another important limitation for ERT is the risk of developing antibodies that may lead to allergic reactions and/or inactivate enzyme activity following the regular intravenous administration of a protein. Humoral immune response to recombinant protein was investigated in MPS I patients showing increased IgG antibodies titers that did not inhibit enzyme activity. In most of the patients, after continue administration, antibody levels declined until dropped into the normal range suggesting that the patients developed immune tolerance to the recombinant human enzyme. Similar observation were made in clinical trials of ERT in patients with MPS VI and MPS II. In Gaucher disease, inhibitory antibodies were found, although most of them were transient. In general, the presence of inhibitory antibodies was not associated with a

reduction in efficacy of the enzyme preparation. Generally it can be stated that enzyme replacement therapy is well tolerated, and the patients who exhibit seroconversion show a decrease in their antibody titers with time and mostly continue to tolerate the enzyme preparation (Beck, 2007).

Whereas enzyme replacement therapy is aimed at removal of storage material accumulating within the lysosome, the principle of substrate reduction therapy is to partially inhibit the biosynthetic cycle to reduce substrate influx into the catabolically compromised lysosome. Imino-sugar for example were known to reduce the activity of the enzyme ⋄-glucosidase and were administered in clinical trials in patients with Gaucher disease unable to receive or to continue ERT or in combination with ERT (Cox et al, 2000). As glucosylceramide represents the precursor of several glycosphingolipids, imino-sugar were also considered as a treatment option for patients with G_1-G_2 gangliosidoses with positive results in mice treated with this drug. Similar results were obtained in mouse model of Niemann-Pick disease type C in which treatment delayed the onset of neurological dysfunction, increase life span and reduct ganglioside accumulation in the brains of animals. However, in Tay-Sachs disease the enzyme inhibitor could not arrest the progressive clinical deterioration.

Imino-sugar do not only act as enzyme inhibitors but also have an effect as the so called chaperones. Chaperones, together with the ubiquitin system and the proteasome system, have the task to control the quality of newly synthesized proteins eliminating misfolded or unstable mutant proteins. In genetic disorders, certain missense mutations and some small in-frame deletions may cause polypeptide misfolding, but may not impair the functionally essential domains of the mutant protein (the active site, receptor-binding site). Small molecule chemical chaperones (like imino-sugar) increase the stability of the mutant protein, restoring the native conformation of misfolded protein (Fig. 2). So, small molecule chemical chaperones may be

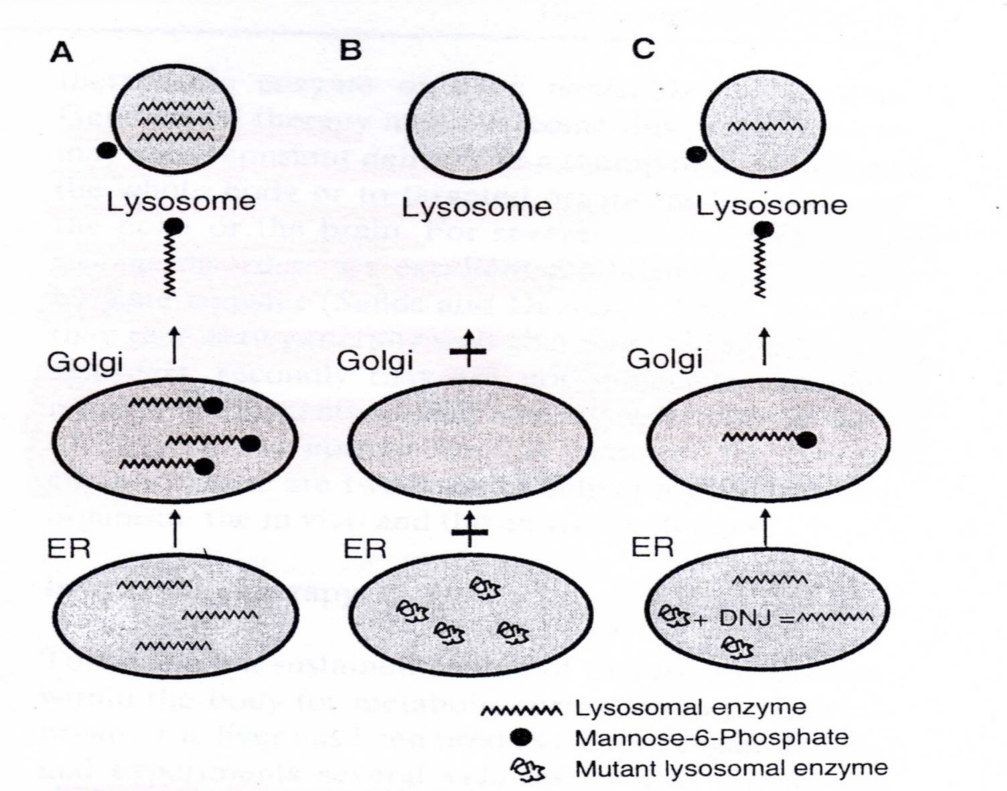

Fig. 2 A Normally, the lysosomal enzymes are synthesized in the endoplasmic reticulum (ER) and trasported to the Golgi apparatus, where they receive the mannose-6-phosphate marker that is essential for receptor-mediated sorting into the lysosomes. **B** The mutant enzyme is misfolded and retained in the ER, enzyme activity is lacking in the lysosome. **C** *N*-butyldeoxynojirimycin increases the stability of the mutant enzyme that now is able to enter the Golgi apparatus and-after binding the mannose-6-phosphate receptor-becomesactive within lysosome (From: Beck, 2007).

therapeutically useful for various lysosomal storage disorders caused by mutant but yet catalytically active enzymes (Beck, 2007).

Although enzyme replacement therapy has become a therapeutic option for some lysosomal storage disorders, it has been shown to be of limited efficacy, especially regarding the effect on bone and brain manifestation. Protein delivery poses serious challenges when sustained administration is required and when the central nervous system (CNS) and peripheral nervous system (PNS) are the major disease targets. In fact, the blood-brain and the blood-nerve barriers may severely limit access of systemically administered therapeutic molecules to these tissues. Gene-based delivery may allow the establishment of a sustained source of therapeutic proteins within the body for peripheral organs correction, or within the nervous system, overcoming the anatomical barriers that limit enzyme diffusion from the circulation.

Gene therapy by retroviral vectors

LSD are excellent candidates for therapy by gene transfer. They represent generally well-characterized single gene disorders, are not subject to complex regulation mechanisms and enzyme activity of only 15-20% of the normal level is sufficient for clinical efficacy (Beck, 2007). At present, various vector delivery systems exist that can be used for direct in vivo gene transfer into the CNS and delivery of therapeutic molecules to brain regions vulnerable to neurodegenerative diseases. Direct injection of gene transfer vectors into CNS has achieved long-term protein expression and therapeutic benefit in several disease model of LSD (for review see Biffi and Naldini, 2005). The occurrence of enzyme or vector crossing the blood-brain barrier seems unlikely and is not supported by clear experimental findings. However the reduction of storage materials in CNS could reflect progressive CNS engraftment of circulating, cross-corrected monocytes, giving rise to enzymatically active microglia, which could provide a partial benefit.

The main cellular target of lentiviral vectors (LV) in the CNS is neurons whereas glial cells are transduced in vivo to a lower efficiency. Cross-correction from transduced neurons may have the advantage of achieving a widespread enzyme distribution within the CNS, thanks to the long-range reach of neural processes. Direct CNS gene delivery by viral vectors is an effective strategy to restore the biologic functions of LSD brains. Moreover, this strategy not only halt disease progression but also reverse the disease phenotype once it has been established. The mechanisms by which such correction could be achieved remain to be elucidated. An intriguing hypothesis is that endogenous neural stem cells are targeted by the vector, and that their progeny may be capable of replacing, at least in part, the damaged tissue. It is thus possible that the correction of nervous system pathology observed in some studies may be due to neuroregeneration from gene-corrected progenitors (Biffi and Naldini, 2005). The cellular mechanisms responsible for the widespread distribution of therapeutic enzyme within the injected brain could be diffusion into the extracellular space or, more likely, axonal transport within secretory vescicle that may be released at nerve endings, taken up, and retrogradely transported along neural processes. The latter mechanism would allow long-distance active transport and crossing of the midline.

Regarding the evaluation of the immune responses against the therapeutic protein and the vector used for in vivo gene transfer, several studies reported the occurrence of cellular and/or humoral immune responses after administration of pure enzyme and liver directed in vivo gene-therapy, responsible for the clearance of the transduced cells and/or the disappearance of enzyme activity from the circulation. However some studies indicate that under specific experimental conditions, in vivo gene delivery in adult mice may escape immune responses, such as by using hepatocyte-specific promoters that restrict transgene expression within antigen-presenting cells (Biffi and Naldini, 2005).

Direct injection of gene transfer vectors, or ex vivo engineered cells into

the CNS achieved long-term protein expression and therapeutic benefit in several disease models. However, the probable requirement for multiple injections and the invasiveness of the procedure may limit its application to humans. Furthermore, intravenous delivery of viral vectors has been demonstrated to be of limited efficacy in enzyme delivery to tissues protected by physiological barriers such as the brain or poorly vascularized like skeleton (Biffi et al., 2004). Thus, an alternative strategy is represented by allogeneic hematopoietic stem cells transplantation (HSCT). This strategy has been performed with positive results in several LSD. Several works have demonstrated that following bone marrow transplantation, donor derived cells have been detected within the CNS supporting the notion that donor bone marrow-derived (BM-derived) cells replaced a fraction of the CNS macrophage/microglia population in a probable process of physiological turnover and that this phenomenon was enhanced upon tissue damage.

Although allogeneic HSCT has been used with increased frequency to treat LSD patients, the therapeutic impact of bone marrow transplantation depends on the specific enzymatic deficiency and the stage of the disease; for example, visceral symptoms can usually be improved, whereas the established skeletal lesions remain relatively unaffected and the effect on neurologic symptoms varies. Clinical evidence in patients with metachromatic leukodystrophy and ⋄-mannosidosis indicate that HSCT has led to promising results provided that the transplantation is performed in early presymptomatic stage, especially before that extensive CNS injury becomes evident (Malm et al., 1996; Krivit et al., 1999). However, the lack of adequate donors and the high morbidity and mortality related to allogeneic transplant greatly reduce the overall number of candidate patients for HSCT. Furthermore, based on the positive clinical experience with bone marrow transplantation in some LSD, hematopoietic stem cell-mediated gene therapy was considered as an attractive alternative for the treatment of LSD. The autologous procedure is associated with reduced transplant-related morbidity and mortality and avoids the risks of graft-versus-

host disease. Moreover, autologous cells may be genetically modified to constitutively express higher levels of the therapeutic enzyme and become a quantitatively more effective source of enzyme than wild-type cells, possibly also at the level of the nervous system.

HSCs are elective targets for gene therapy because of the ease with which they can be manipulated ex vivo and returned to the host. Moreover, the largely quiescent nature of HSCs, combined with the need for vector integration to ensure gene delivery to the HSC progeny, makes them prime candidates for LV transduction. Therapeutic efficacy of HSC-based ex vivo gene therapy approaches in controlling disease manifestations has been shown in preclinical experiments on LSD models. Metachromatic leukodystrophy (MLD) represent one of the first LSD on which RV-based and, later, LV-based ex vivo gene therapy was tested. By transplanting HSCs transduced with a third generation LV carrying the therapeutic arylsulfatase A (ARSA) cDNA, enzyme activity was reconstituted in the hematopoietic system of MLD mice at supranormal levels and the development of major CNS and PNS disease manifestations at the functional, histopathological and behavioral levels was almost completely prevented. Remarkably, ex vivo gene therapy had a significantly better therapeutic impact than did wild-type HSC transplantation, indicating a critical role for enzyme overexpression in HSC progeny (Biffi et al., 2004).

More recently, this therapeutic approach has been also tested in MPS I mouse model (Visigalli et al., 2010) in which previous transduction of several viral vectors was not able to adequately correct the CNS and skeletal disease. Indeed, the results shown by Visigalli and coworkers demonstrated that gene-corrected cells are capable of effective delivery of the functional IDUA enzyme to diseased tissues, including the CNS, where supra-normal enzymatic activity was measured. The efficient delivery of IDUA was associated with metabolic correction of the affected tissues, as shown by the clearance of accumulated glycosaminoglycan (GAGs) within hematopoietic and non-hematopoietic cells, suggesting an active secretion of the functional enzyme by the gene corrected

progeny of the transplanted cells and its re-uptake by resident populations.

These promising results achieved by LV-mediated HSC gene therapy both in MLD (for which this therapeutic approach has now entered clinical testing) and in MPS I, indicate that this approach represents an efficacious strategy for the treatment of storage diseases with systemic and CNS involvement, capable of addressing the disease manifestations refractory to correction by ERT and HCT.

2. Mucopolysaccharidosis IIIB

Mucopolysaccharidosis IIIB (MPS IIIB) is a lysosomal storage disease due to a deficiency of a lysosomal hydrolase (⋄-N-acetylglucosaminidase, NAGLU, E.C. 3.2.1.50) necessary for the stepwise degradation of the saccharide chains of the heparan sulfate (HS) glycosaminoglycan (GAG). As for the majority of LSD, in the MPS IIIB the deficiency of a single lysosomal enzyme causes the accumulation, in patients' cells, of its undegraded substrate. The build-up of HS is believed to be primarily responsible of the disease pathogenesis.

The disease is chronic and progressive and its manifestations are most pronounced in the CNS, with severe mental retardation and behavioral problems (Neufeld and Muenzer, 2001). A mouse model of MPS IIIB, that recapitulated the pathology observed in human patients, has been created in 1999 by Li and coworkers for the purpose of studying the pathophysiology of the disease and for developing treatment (Li et al., 1999). At date, however, there is no effective therapy for MPS IIIB although gene therapy based on adeno-associated vector (Cressant et al., 2004) and lentiviral vector (Di Natale et al., 2005; Di Domenico et al., 2009) has been tested in mice with some success and management of this difficult disease is all that can be offered. Probably, the lack of an effective therapy relies on the fact that pathogenic mechanism due to abnormal HS oligosaccharide catabolism and the consequent neurodegeneration are not yet well understood. Pathological studies of affected

mouse brain revealed progressive onset and aggravation of chronic brain inflammation and widespread CNS pathology (Ohmi et al., 2003; Ausseil et al., 2008). At this regard, microglia activation followed by secretion of toxic cytokines (Li et al., 2002; Ohmi et al., 2003; Villani et al., 2007) and involvement of T-cell-mediated cytotoxicity (DiRosario et al., 2009; Villani et al., 2009) have been shown to contribute to neuropathology. In addition alteration in neuroplasticity (Li et al., 2002), neurotrophins (Villani et al., 2007) and increased degradation of synaptophysin (a protein associated to synaptic vesicles) by the proteasome (Vitry et al., 2009) have been found to account for neurodegeneration. A characteristic feature of brain disease in MPS IIIB is that in contrast to somatic cells which accumulate primarily heparan sulfate, neurons accumulate a number of apparently unrelated metabolites that do not need the participation of NAGLU for their metabolism such as subunit c of mitochondrial ATP synthase (Ryazantsev et al., 2007), GM3 ganglioside (Ohmi et al., 2003), cholesterol (McGlynn et al., 2004) and more recently hyperphosphorylated tau protein (Ohmi et al., 2009). Interestingly, the accumulation of these secondary products and of the primary product is not dispersed throughout the brain, but is limited to neurons in certain areas, especially enthorinal and somatosensory cortex.

However, despite all the efforts to clarify the MPS IIIB disease pathogenesis, the sequence of events from the enzyme deficiency to the cellular dysfunction and CNS pathology is not known.

Aims of the PhD thesis

We have found oxidative stress as one of the main factors implicated in the pathogenesis of the MPS IIIB murine model (Villani et al., 2007; 2009). Our previous works demonstrated the involvement of the reactive oxygen species (ROS) in the disease pathogenesis, showing the upregulation of the component of NADPH oxidase, the major source of ROS during inflammation expressed mainly by microglia, as well as the overproduction of superoxide ions throughout the CNS. In addition, by evaluating the effect of the stress on the cellular macromolecules we have found that oxidative stress results primarily in protein oxidation and that it is present in MPS IIIB -/- animals, in the cerebrum and cerebellum tissues early in the disease course, i.e. at one month from birth (Villani et al., 2009). One of the consequences of increased ROS levels in brain of affected mice would be the activation of the mitogen-activated protein kinases (MAPK).

The mammalian family of MAPK includes extracellular signal regulated kinase (ERK), c-Jun NH2 terminal kinase (JNK; also known as stress-activated protein kinase SAPK) and p38 (Kim et al., 2010). Once activated, these Serine-Threonine kinases mediates a variety of cellular responses: extracellular regulated kinase 1/2 (ERK 1/2) typically regulates growth, proliferation and differentiation (McCubrey et al., 2006; Dhillon et al., 2007), whereas stress activated protein kinase/Jun kinase (JNK) and p38 MAPK are activated in response to osmotic shock, UV irradiation, inflammatory cytokines, oxidative stress (Haddad, 2004).

To test the hypothesis of MAPK activation in the brain pathology of Mucopolysaccharidosis IIIB disease, in the present thesis we analyzed the expression of these three major stress kinases in the neuronal tissue of the murine model of the disease. In particular, we studied the activation of phospho ERK1/2, SAPK/JNK and p38 MAPK in the cortex and in embryonic neurons cultured from MPS IIIB mice.

This thesis refers to the experimental work performed in the last two years of the PhD course (2008-2010).

Materials and Methods

Chemicals

Hanks' Balanced Salt Solution and MEM were purchased from Gibco. Fetal Bovine Serum, L-glutamine, penicillin G and streptomycin were obtained from Cambrex. Cell Signaling Technology supplied the first antibodies raised against phospho ERK1/2, phospho SAPK/JNK and phospho p38MAPK and the goat anti-rabbit IgG horseradish peroxidase (HRP) conjugated secondary antibody. Poly D-lysine, cytosine arabinoside and trypsin were purchased from Sigma, as were the mouse anti--tubulin monoclonal primary antibody and the goat anti-mouse IgG HRP conjugated secondary antibody.

Animals

The mice were genotyped by PCR performed on DNA samples extracted from tail biopsy at 1 month after birth, as previously described (Di Natale et al., 2005). For the study on adult mouse cortices, homozygous mutant mice and wildtype (Wt) control mice of 1, 2, 3, and 6 months of age were used. At the time of killing, the mice were sacrificed by cervical dislocation after profound anesthesia. The cerebrum was rapidly removed and the cortex isolated by using a stereomicroscope (Zeiss) on ice-cold tissue culture plate. The cortices were then transferred to microcentrifuge tubes and immediately stored at -80 ^{0}C until used. For the preparation of primary neuronal cultures, timed-pregnancies of MPS IIIB and Wt mice were set up and embryos were obtained by cesarean section of pregnant mice 16 days after coitum. All experimental protocols were approved by the Italian Ministry of Public Health.

Western blotting

Brain cortices were homogenized on ice in lysis buffer (20 mM Tris-HCl, pH 7.5, 150 mM NaCl, 1 mM Na_2EDTA, 1 mM EGTA, 1% Triton, 2.5 mM

sodium pyrophosphate, 1 mM beta-glycerophosphate, 1 mM Na_3VO_4) supplemented with protease inhibitors (1µg/ml leupeptin, 1µg/ml aprotinin, 1 mM PMSF) and incubated for 30 minutes on ice. After centrifugation at 14000 rpm at 4°C for 30 minutes, the supernatants were used for protein determination by the Bradford method (Bradford, 1976) using BSA as a standard. The same protocol was used for the preparation of total protein extract from neuronal cells. Western blotting analysis was carried out on equal amounts of protein extracts. Briefly, 30 µg of total protein extract were boiled for 5 minutes in SDS/reducing loading buffer, run on a 10% SDS-PAGE and then transferred onto nitrocellulose membranes (Millipore). The membranes were blocked for 1 hour at room temperature with 5% BSA (or 5% skim-milk powder for anti-tubulin) in T-TBS (30 mM Tris-HCl, 125 mM NaCl, 0.1% Tween 20). The blots were then incubated overnight at 4°C with the specific primary antibody, appropriately diluted in T-TBS containing 5% BSA for the phospho-MAPK antibodies or 2% milk for the tubulin antibody. The primary antibodies used were rabbit anti-phospho ERK1/2 (1:1000), rabbit anti-phospho SAPK/JNK (1:500), rabbit anti-phospho p38MAPK (1:500) and mouse anti-tubulin (1:10000). After washing in T-TBS (30 mM Tris-HCl, 125 mM NaCl, 0.05% Tween 20), the membranes were incubated for 1 hour at room temperature with goat anti-rabbit or anti-mouse HRP conjugated secondary antibody diluted in T-TBS containing 2% milk (1:3000). The proteins were visualized by an enhanced chemiluminescence reaction using E.C.L. detection reagent (Amersham) followed by exposure to film (Fuji). The same blots were stripped and re-probed with -tubulin monoclonal antibody to confirm equal loading of proteins in all lanes. Films were scanned using an HP scanner and subjected to densitometric analysis with ImageJ software.

Primary cortical neuronal cultures

Neuronal cultures were prepared from embryonic day-16 (E16) mouse cortices as described by Scorziello and colleagues (2001) with some

modifications. Brains of mouse embryos, obtained from time-pregnant MPS IIIB and Wt mice, were collected and placed in ice-cold Hanks' balanced salt solution supplemented with 5 mg/ml glucose, 7 mg/ml saccharose and 0.3 mg/ml sodium bicarbonate. Cortices were then isolated under a stereomicroscope by removing the attached meninges and incubated with 0.25% trypsin for 20 minutes at 37 °C. After centrifugation at 600g for 5 minutes, the cells were dissociated by careful titration through a constricted Pasteur pipette. Dissociated neurons were resuspended in minimal essential medium (MEM) containing glucose, 5% heat-inactivated fetal bovine serum, 5% heat-inactivated horse serum, 2 mM L-glutamine, 100 U/ml and 100 µg/ml of a mixture of penicilin-streptomycin and seeded at a density of 2 X 10^6 cells on 35 mm Petri dishes precoated overnight with 0.1 mg/ml poly-D-lysine. After 24 h the medium was replaced with freshly prepared medium of similar composition as before and neuronal cells were maintained in humidified 5% CO_2/95% air atmosphere at 37°C until used. Cytosine  -D-arabino-furanoside (10 µM) was added at 5 days *in vitro* (DIV) to prevent glial proliferation and experiments were performed on cultures that were 8 DIV. The data of each experiment were obtained from at least three individual culture preparations (i.e., one embryo was used for one culture preparation) and each experiment was repeated at least three times.

Confocal immunofluorescence analysis

The purity of the cultures was verified using the neuron-specific marker microtubule-associated protein-2 (MAP2) and the astrocyte marker glial fibrillary acidic protein (GFAP). Primary cortical neurons cultured on glass coverslips were rinsed in cold 0.01M saline phosphate buffer at pH 7.4 (PBS) and fixed in 4% (w/v) paraformaldehyde (Sigma, Milan, Italy) for 20 min at RT at 8-10DIV. Following three washes in PBS, cells were blocked with 3% (w/v) bovine serum albumin and 0.05% Tryton-X (Biorad, Milan, Italy) for 1 h at room temperature (RT). The coverslips were then incubated with the primary

antibody anti-Map2 (mouse monoclonal, 1:2000 dilution, Sigma, Milan, Italy), or anti-GFAP (rabbit polyclonal, 1: 1000 dilution, Sigma, Milan, Italy), at 4 ◦C overnight. Following three washes in PBS, the coverslips were incubated in the dark with the corresponding secondary antibodies: Alexa fluor 594 anti-mouse IgG and Alexa-fluor 488 anti-rabbit IgG (Molecular Probes, Eugene, OR; dilution 1:200) for 1 h at RT. After the final wash, the coverslips were mounted with Vectashield mounting medium (Vector Labs, Burlingame, CA,). Images were observed using a Zeiss LSM510 META/laser scanning confocal microscope. Single images were taken with an optical thickness of 0.7 μm and a resolution of 1024X1024.

Measure of HS levels in cultured neurons

The level of HS in embryonic neurons cultured from MPS IIIB and Wt animals was measured according to Bjornsson (1993) with some modifications. Briefly, the total extract from neuron pellets (300μg) was resuspended in 0.9% NaCl/0.2% Triton X-100, rotated at 4˚C overnight and centrifuged to remove debris. GAGs were precipitated with Alcian Blue and absorbance was measured at 600 nm. Heparan sulfate from porcine intestinal mucosa was used as a standard.

Statistical analysis

All results are presented as histograms and data are expressed as means SD of five independent experiments. Student's *t* test was used to assess whether there were significant differences between MPS IIIB and control mice.

Results

Our work was aimed at the dissection of the intracellular pathways that might be switched on/off in the cortex and in cultured neurons of the MPS IIIB mice. Three major protein kinase pathways have been shown to be responsive to insults such as stress, the ERK 1/2, JNK and p38MAPK (Seger and Krebs, 1995). MAPKs are activated by phosphorylation on specific Thr and Tyr sites by upstream kinases. Therefore, we examined by Western blot the level of the three MAPKs by using antibodies specific for each phosphorylated form of these enzymes.

Selective activation of ERK and JNK in the cortex of MPS IIIB mice

We evaluated the activation status of ERK1/2 in the cortex of MPS IIIB and Wt mice by Western blot on the homogenates of cortex derived from mice at different ages. We used a primary monoclonal antibody raised against phospho-(Thr202/Tyr204)-ERK, selective for the two isoforms of the enzyme, corresponding to phospho-ERK1 and phospho-ERK2 with an apparent molecular weight of 44 kDa and 42 kDa, respectively. We found that both p44 and p42 were significantly activated in 1-2-month-old MPS IIIB mice, as shown in Fig. 3. The quantitative analysis performed comparing the density of the corresponding bands to that of tubulin is shown in Figs. 3B and 3C, respectively. The levels of both p44 and p42 in MPS IIIB mice (black bars) were two-fold higher than in Wt littermates (white bars) and the increase was statistically significant. Selective upregulation of ERK1/2 was lost with older mice (3 and 6 months).

The activation status of SAPK/JNK was evaluated by Western blot using a polyclonal antibody raised against phospho-(Thr183/Tyr185)-SAPK-JNK, showing only two major bands at an apparent molecular weight of 54 kDa and 46 kDa. Fig. 4A indicates that SAPK-JNK is activated in the first two months from birth of MPS IIIB mice compared to Wt controls. The quantitative analyses performed comparing the density of the corresponding bands to that

of tubulin are illustrated in Figs. 4B and 4C, respectively. A significant increase was evident only at 1-2 months of age. As for pERK1/2, the selective upregulation of JNK decreased with age.

Selective downregulation of p38MAPK in the cortex of MPS IIIB mice

In order to evaluate the activation status of p38MAPK, a Western blot was performed using an anti-phospho p38MAPK antibody raised against phospho-(Thr180/Tyr182)- p38MAPK, showing one single major band at an apparent molecular weight of 38 kDa. Fig. 5A shows a representative Western blot showing that activation of p38 is present in the cortex of MPS IIIB mice but is lesser than that found in the cortex of Wt mice. A quantitative analysis of the data found in Wt (white bars) and MPS IIIB (black bars), performed by comparison to the tubulin band, is shown in Fig. 5B. The data show that p38MAPK is less phosphorylated in the cortex of MPS IIIB mice at each time considered from birth, although the difference is statistically significant only at 1 month of age.

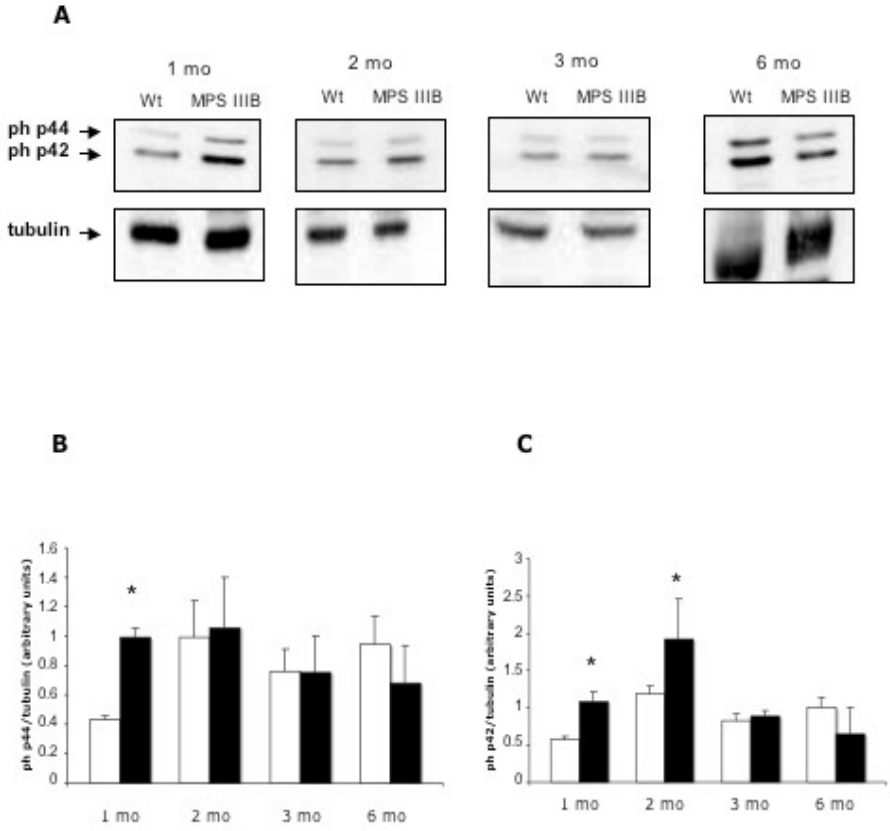

Fig. 3. ERK is activated in the cortex of 1-month-old MPS IIIB mice. Activation of ERK was visualized using specific antibody for its phosphorylated form. (A) Representative Western blot analysis of phospho ERK 1/2 (p44/p42) on homogenates of the cortex of Wt and MPS IIIB mice; Western blot analysis of tubulin, performed on the same gel, is shown for comparison. ERK phosphorylation was quantitated after scanning as ratio between p-ERK1 and tubulin (B) and between p-ERK2 and tubulin (C). Each band density was calculated separately. The levels of phospho p44 and phospho p42 in 1-2-month-old MPS IIIB mice were significantly higher than in Wt (* 1-month-old $P< 0.005$; * 2-month-old $P<0.1$, Student's *t*-test). White bars: Wt mice, n=5; Black bars: affected mice, n=5.

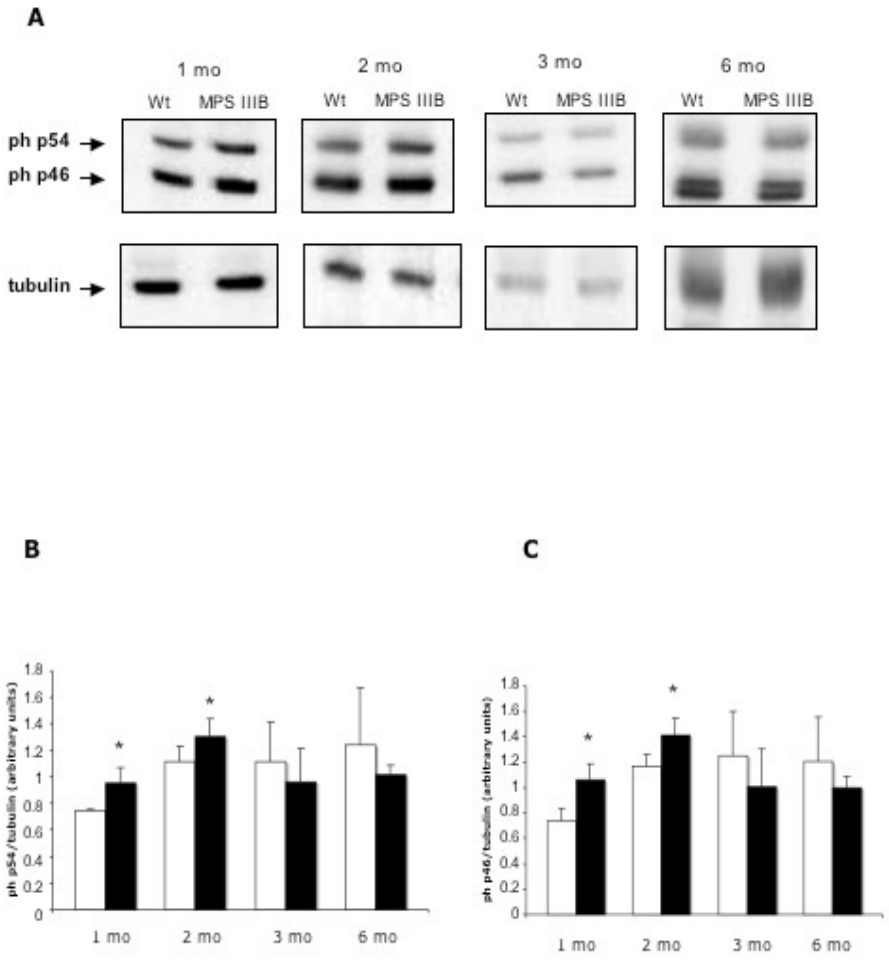

Fig. 4. Activation of SAPK/JNK in the cortex of 2-month-old MPS IIIB mice. Activation of SAPK/JNK was visualized using specific antibody for its phosphorylated form. (A) Representative Western blot analysis of phospho SAPK/JNK (p54/p46) on homogenates of the cortex of Wt and MPS IIIB mice; Western blot analysis of tubulin, performed on the same gel, is shown for comparison. (B, C) Quantitative analysis of activated SAPK/JNK performed comparing the immunopositive band of phospho p54 (B) or phospho p46 (C) with that of tubulin run on the same gel. Each band density was calculated separately. The levels of phospho p46 in 1-2-month-old MPS IIIB mice were significantly higher than in Wt (* 1-month-old $P< 0.1$; * 2-month-old $P<0.05$, Student's *t*-test); White bars: Wt mice, n=5; Black bars: affected mice, n=5.

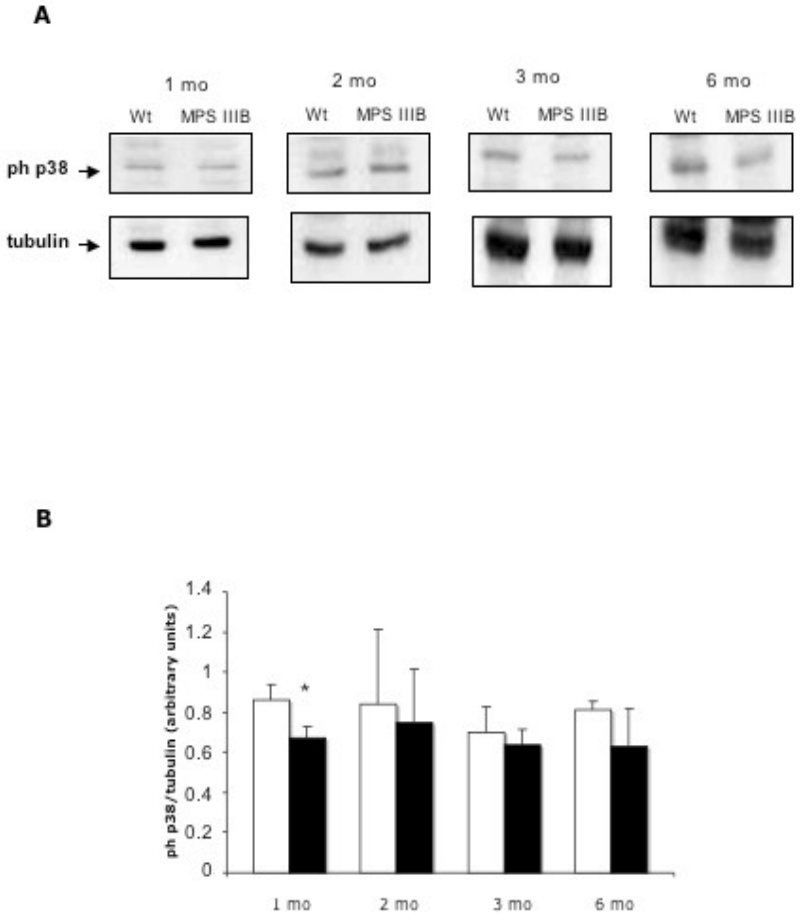

Fig. 5. p38MAPK is less activated in the cortex of 1-month-old MPS IIIB mice. Activation of p38MAPK was visualized using specific antibody for its phosphorylated form. (A) Representative Western blot analysis of phospho p38MAPK on homogenates of the cortex of Wt and MPS IIIB mice; Western blot analysis of tubulin, performed on the same gel, is shown for comparison. (B) Quantitative analysis of activated p38MAPK performed comparing the immunopositive band of phospho p38MAPK with that of tubulin run on the same gel. The levels of phospho p38MAPK in 1-month-old MPS IIIB mice were significantly lower than in Wt (* $P< 0.05$, Student's t-test). White bars: Wt mice, n=5; Black bars: affected mice, n=5.

Primary cortical neurons: isolation and measure of GAGs levels

Neurons were isolated from the cortex of Wt and MPS IIIB mice at embryonic day E16. The purity of the cultures was verified to be 98% using the neuron-specific marker microtubule-associated protein-2 (MAP2) and the astrocyte marker glial fibrillary acidic protein (GFAP) (Fig. 6).

The levels of GAGs measured on cultured cells were significantly higher (P <0.005, Student's t test) in neurons from affected mice with respect to those found in Wt controls (Table 1).

Activation of MAPKs in cultured neurons from MPS IIIB mice

In order to evaluate whether the alterations in the MAPK pathway identified in the cortex of MPS IIIB mice are present already at an early stage of cortex development, we analyzed the phosphorylation status of MAPKs in neurons cultured from MPS IIIB and Wt mice. The activation of MAPKs in cultured neurons was analyzed by Western blotting on protein extract obtained from MPS IIIB and Wt cortical neurons at 8 days *in vitro* (8 D.I.V.). Both ERK and SAPK/JNK showed an increase in the phosphorylated bands in MPS IIIB neurons (Figs. 7A, C). A quantitative analysis performed comparing the immunopositive bands of each kinases with that of tubulin reveals that the differences between MPS IIIB (black bars) and Wt (white bars) are statistically significant (Figs. 7B, D). Increased phosphorylation of the p38MAPK band is also present in MPS IIIB cultured neurons (Fig. 7E), although not statistically significant as shown by quantitative analysis (Fig. 7F).

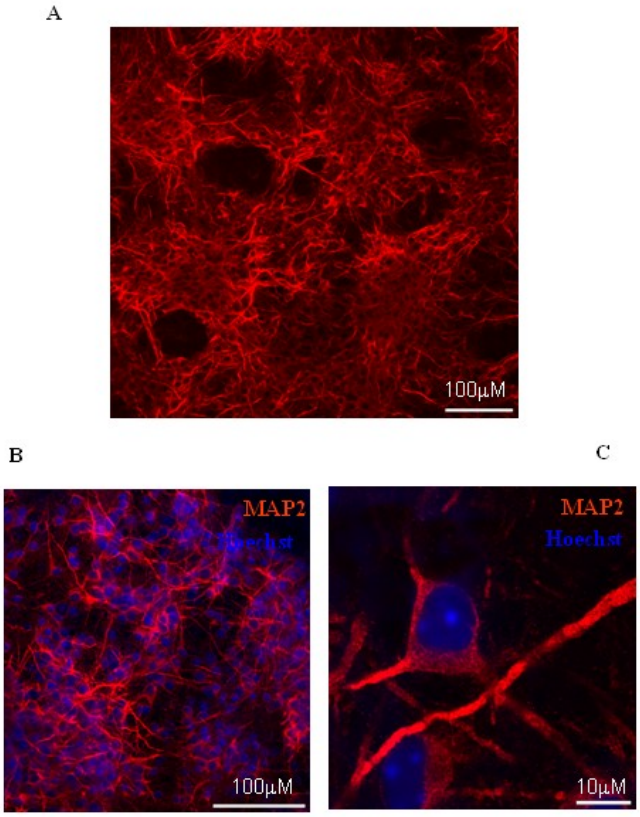

Fig. 6. Confocal immunofluorescence analysis of MAP-2 expression in primary culture of neurons from wild-type mice. MAP2 immunolabelling in perikarya and dendritic processes of neurons is shown at lower (panels A and B) and at higher magnification (panel C). Nuclei were stained with Hoechst-33258. Scale bars: A and B: 100µM; C: 10µM

TABLE 1. Measure of GAGs levels in cortical neurons cultured from E16 embryos

Animals examined	µgGAGs/mg protein
Wt mice	2.8±0.65
MPS IIIB mice	8.3±1.1

GAG concentration was determined by the Alcian Blue, as described under Materials and Methods. Values are means ± SD from three experiments, in which three neuronal cultures were established from different mice.
A significant difference was obtained in MPS IIIB mice ($P<0.05$, Student's t test) with respect to wild type mice.

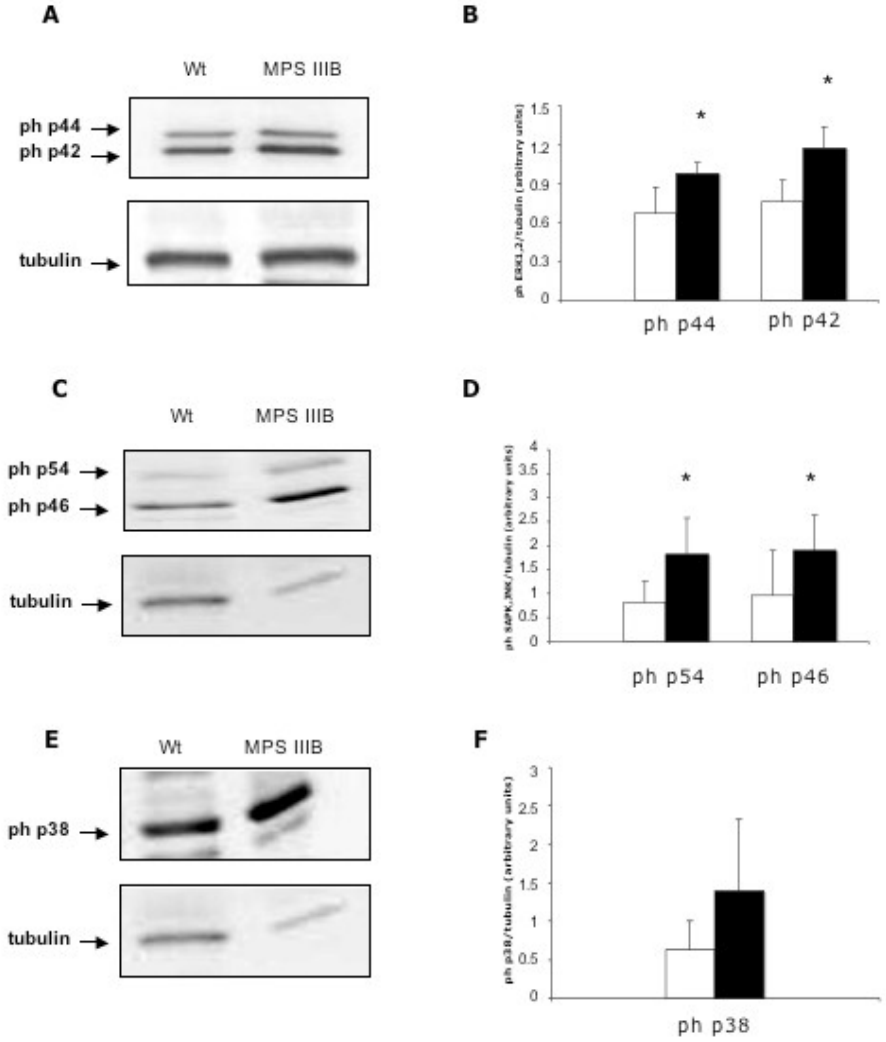

Fig. 7. Activation of MAPKs in cultured neurons from MPS IIIB mice. Phosphorylation status of MAPKs ERK 1/2, SAPK/JNK and p38MAPK were visualized using specific antibody for their phosphorylated form on cellular extracts obtained from cortical neurons of MPS IIIB and Wt mice at 8 days *in vitro* (A, C, E). Representative Western blot analysis of phospho-ERK1/2 (A), SAPK/JNK (C) and p38MAPK (E); Western blot analysis of tubulin performed on the same gel is shown for comparison. (B, D, F) Quantitative analysis of activated kinases performed comparing the immunopositive band of phospho ERK1/2 (B), SAPK/JNK (D) and p38MAPK (F) with that of tubulin run on the same gel. Each band density was calculated separately. The levels of phospho p44 and phospho p42 in cultured neurons from MPS IIIB mice were significantly higher than in Wt (p44 *$P < 0.1$ and p42 *$P < 0.05$, Student's *t*-test); the levels of phospho p54 and phospho p46 (* $P < 0.1$, Student's *t*-test) were also higher. No significant differences were observed for p38 kinase. White bars: Wt mice, n=5; Black bars: affected mice, n=5.

Discussion

In the present work, we studied the activation of the three main stress kinases (MAPK) in an MPS IIIB mouse model and showed that a selective activation of MAPK is involved in the disease pathogenesis.

The mammalian family of MAPK includes extracellular signal-regulated kinase (ERK), c-Jun NH2 terminal kinase (JNK; also known as stress-activated protein kinase SAPK) and p38 (Kim et al., 2010). Extracellular regulated kinase 1/2 (ERK 1/2) typically regulates growth, cell proliferation and differentiation, whereas stress activated protein kinase/Jun kinase (JNK) and p38MAPK are activated in response to osmotic shock, UV irradiation, inflammatory cytokines and oxidative stress (Haddad, 2004). Moreover, JNK has been associated with the neurofibrillary pathology (Willaime-Morawek et al., 2003), and its upregulation has been shown to overlap with phosphorylated tau (Zhu et al., 2001). Once activated, these serine-threonine kinases mediate a variety of cellular responses including cell proliferation, differentiation, survival, death and transformation (McCubrey et al., 2006; Dhillon et al., 2007). However, although it is well established that ERK activation has beneficial effects on the cells, recent findings on neural cells show that ERK may exert an opposite effect, in that its activation can either promote neuron survival or cause cell death. For example, in a number of neural cell systems it has been shown that chronic activation of ERK is able to impair the physiological response to neurotrophic factors and/or to drive cells to death (Colucci-D'Amato et al., 2003). Moreover, ERK activation was suggested to play a role in a caspase-independent mechanism of cell death involving an alteration of the plasma membrane (Subramaniam et al., 2004).

Our data show an increased activation of ERK and SAPK/JNK in the first two months after birth in the cortex of MPS IIIB animals, and this is consistent with the clinical onset of the disease, in which the neurological manifestations are evocative of a frontal pathology. However, although the increased MAPK expression was detected in the cortex, at present we cannot exclude that it

could also be present outside the cortical area. Our results are in agreement with the findings of early activation of ERK in some neurodegenerative diseases: phosphorylated ERK immunoreactivity has been found in neurons in Pick's disease, progressive supranuclear palsy and corticobasal degeneration (Ferrer et al., 2001), in hippocampal neurons with neurofibrillar degeneration in Alzheimer's disease (AD) (Perry et al., 1999) and in astrocytes from AD patients (Webster et al., 2006).

The alterations in the CNS in MPS IIIB shared some features with other neurodegenerative diseases, especially AD, like the accumulation of abnormal products, activation of microglia and alteration of the lysosomal and autophagic degradation pathway. To this regard, it is interesting to note that Ohmi and coworkers recently described for the first time the presence of a hyperphosphorylated form of microtubule-associated protein tau in the brain of MPS IIIB mice (Ohmi et al., 2009), a characteristic of many storage diseases associated with dementia. An accumulation of HS is the primary consequence of the enzyme defect in MPS IIIB and triggers a cascade of pathological events that progressively leads to CNS pathology. Ausseil and coworkers detected GAG accumulation in the brain of MPS IIIB mice already at the age of 10 days (Ausseil et al., 2008), but we observed a storage of HS starting during embryonic life, as seen by the HS accumulation in neuron cultures from the brain of E16 MPS IIIB mice. It has been demonstrated that heparin is able to promote tau aggregation *in vitro* and so it is likely that this function is carried out by heparan sulfate *in vivo* (Pandel et al., 1999). This observation suggests that HS accumulation in the early stage of the MPS IIIB disease could promote tau aggregation and consequent hyperphosphorylation through the activation of MAPK, as demonstrated in other models of neurodegeneration (Perez et al., 2008). Alternatively, early activation of ERK and SAPK/JNK may represent a first response to the onset of MPS IIIB pathology and thus may be linked to neuroprotective pathways. In fact, as discussed above, different kinetics of ERK activation can account for its dual

effects, i.e. survival or death of neuronal cells (Colucci-D'Amato et al., 2003). Interestingly, the rise in pERK and pSAPK/JNK immunoreactivity were transient and more characteristic of the early stage of disease and, therefore, may be a reaction to ongoing neuronal damage. Thus, the increase in ERK and SAPK/JNK phosphorylation may be a reaction to microglia activation caused by HS, a feature that Ausseil and coworkers (2008) identified in the early stage of MPS IIIB brain pathology.

Our results obtained in the cortex of MPS IIIB mice were confirmed by the study of embryonic cultured cortical neurons, in which the patterns of ERK and SAPK/JNK phosphorylation reflect those observed in the brain of post-natal mice and permit us to speculate that this activation is present already during fetal life. Moreover, our data obtained in pure neuronal cultures, devoid of astrocytes and microglia, allow us to reasonably assume that this phenomenon is not secondary to the activation of microglia, and this is in agreement with the assumption of Ausseil and coworkers (2008) that in the early stage of MPS IIIB disease, the pathology of the central nervous system is cell autonomous rather than environmental.

We found that p38MAPK was downregulated in the cortex of MPS IIIB mice compared to Wt littermates. Increased activation of p38MAPK has been found in brain homogenates in all the tauopathies (Ferrer et al., 2005), and often phosphorylated p38MAPK immunoreactivity has been found in co-localization with activated SAPK/JNK (Ferrer et al., 2001; Giovannini et al., 2008). It is widely accepted that the activation of p38MAPK is related to the production of pro-inflammatory cytokines but also to an aggravation of the inflammatory processes, a feature shared by most chronic neurodegenerative diseases. However, the lesser phosphorylation of p38 that we found in the brain cortex of 1-month-old MPS IIIB mice can be explained if we consider that the inflammatory pathology is prominent only in the late disease course (Ausseil et al., 2008). Alternatively, the inhibition of p38MAPK phosphorylation could support the hypothesis that early activation of ERK and

SAPK/JNK represent a first response to the onset of the pathology.

The experiments conducted in this study show that a selective activation of MAPK is present in the murine model of MPS IIIB. In particular, the early stages of the disease are characterized by simultaneous activation of ERK and SAPK/JNK pathways and inhibition of p38MAPK phosphorylation. These results together with our findings in pure neuronal cultures allow us to suggest not only that the alteration of the MAPK pathways is involved in the pathophysiological changes that occur early on in the brain of MPS IIIB mice, but also that these events are cell autonomous and not dependent on environmental alterations, at least in the early stages of brain disease.

We propose a model for the pathological mechanisms involved in MPS IIIB disease (Fig.8), where the selective activation of stress kinases could be included in the pathogenetic cascade following enzymatic deficit. It could well be, in fact, that an increased ROS production (Villani et al., 2007; 2009) might lead to the activation of MAPK (this thesis). However, whether or not this leads to cell death, as suggested for other lysosomal diseases (for review see Walkley, 2009), remains to be demonstrated for MPS IIIB. To this regard, previous data on apoptotic or non-apoptotic mechanisms in brain disease of MPS IIIB are controversial (Li et al., 2002; Villani et al., 2007; 2009). Finally, although further studies are required to define the exact sequence of pathological events in MPS IIIB brain disease, our experiments have demonstrated for the first time that cell signaling transduction alterations are involved in the MPS IIIB neuronal pathology.

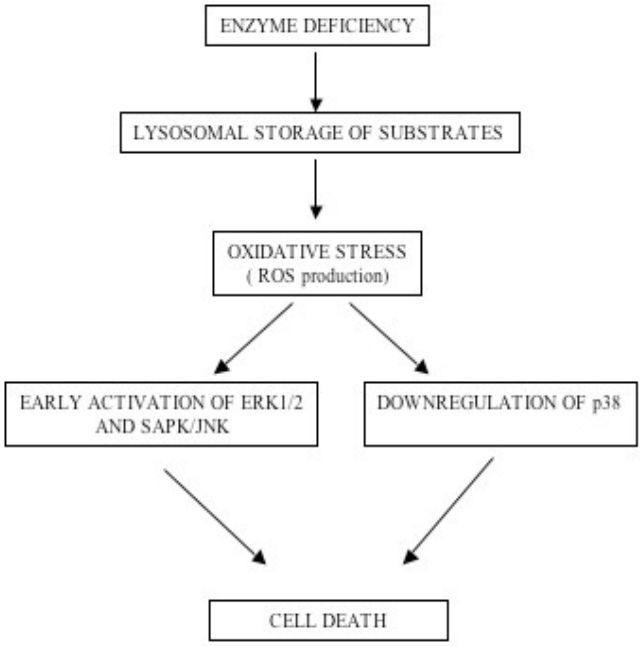

Fig. 8. A proposed model for pathogenesis of MPS IIIB. A defect in α-N-acetylglucosaminidase results in the accumulation of the primary substrate, the glycosaminoglycan heparan sulfate. This leads to oxidative stress (Villani et al., 2007; 2008) and kinase activation (this paper). The final step is cell death.

Conclusions

In the present thesis we have studied the activation of the main mitogen-activated protein kinase (MAPK) in MPS IIIB mouse model, showing that a dysregulation of MAPK is involved in the brain disease of young mice. In particular, we found a simultaneous activation of ERK 1/2 and SAPK/JNK pathways and inhibition of p38MAPK phosphorylation. These results, confirmed in pure neuronal cultures, allow us to suggest that the alteration of the stress kinases is cell-autonomous and not dependent on environmental alterations (i.e. microglia activation), at least in the early stages of brain disease.

Our results add a new insight in the pathological cascade of MPS IIIB disease. We suggest that an increased ROS production, previously demonstrated in our laboratory (Villani et al., 2007; 2009) would lead to the activation of MAPK, and finally to cell death.

Our work, to our knowledge, is the first study reporting that cell signaling transduction alterations are involved in the MPS IIIB neuronal pathology.

References

Beck M. New therapeutic options for lysosomal storage disorders: enzyme replacement, small molecules and gene therapy. Hum. Genet. 2007;121(1):1-22.

Biffi A, De Palma M, Quattrini A, Del Carro U, Amadio S, Visigalli I, Sessa M, Fasano S, Brambilla R, Marchesini S, Bordignon C, Naldini L. Correction of metachromatic leukodystrophy in the mouse model by transplantation of genetically modified hematopoietic stem cells. J. Clin. Invest. 2004;113(8):1118-29.

Biffi A, Naldini L. Gene therapy of storage disorders by retroviral and lentiviral vectors. Hum. Gene Ther. 2005;16(10):1133-42.

Bjornsson S. Simultaneus preparation and quantitation of proteoglycans by precipitation with alcian blu. Anal. Biochem. 1993;210:282-91.

Bradford MM. A rapid and sensitive method for the quantitation of microgram quantities of protein utilizing the principle of protein dye binding. Anal. Biochem. 1986; 72:248-54.

Colucci-D'Amato L, Perrone-Capano C, di Porzio U. Chronic activation of ERK and neurodegenerative diseases. BioEssays 2003;25:1085-95.

Cox T, Lachmann R, Hollak C, Aerts J, van Weely S, Hrebicek M, Platt F, Butters T, Dwek R, Moyses C, Gow I, Elstein D, Zimran A. Novel oral treatment of Gaucher's disease with N-butyldeoxynojirimycin (OGT 918) to decrease substrate byosinthesis. Lancet 2000;355:1481-85.

Cressant A, Desmaris N, Verot L, Brejot T, Froissart R, Vanier MT, Maire I, Heard JM. Improved behaviour and neuropathology in the mouse model of Sanfilippo type IIIB disease after adeno-associated virus-mediated gene transfer in the striatum. J. Neurosci. 2004;10 24(45): 10229-39.

Dhillon AS, Hagan S, Rath O, Kolch W. MAP kinase signalling pathways in cancer. Oncogene 2007;26: 3279-90.

Di Domenico C, Villani GR, Di Napoli D, Nusco E, Calì G, Nitsch L, Di Natale P. Intracranial gene delivery of LV-NAGLU vector corrects neuropathology in murine MPS IIIB. Am. J. Med. Genet. A. 2009; 149 A (6):1209-18.

Di Natale P, Di Domenico C, Gargiulo N, Castaldo S, Gonzales Y Reyero E, Mithbaokar P, De Felice M, Follenzi A, Naldini N, Villani GR. Treatment of the mouse model of mucopolysaccharidosis type IIIB with lentiviral-NAGLU vector. Biochem. J. 2005;388(Pt.2):639-46.

DiRosario J, Divers E, Wang C, Etter J, Charrier A., Jukkola P, Auer H, Best V, Newsom DL, McCarty D, Fu H. Innate and adaptive immune activation in the brain of MPS IIIB mouse model. J. Neurosci. Res. 2008;87(4):978-90.

Ferrer I, Blanco R, Carmona M, Ribera R, Goutan E, Puig B, Rey MJ, Cardozo A, Vinals F, Ribalta T. Phosphorylated map kinase (ERK1, ERK2) expression is associated with early tau deposition in neurones and glial cells, but not with increased nuclear DNA vulnerability and cell death, in Alzheimer disease, Pick's disease, progressive supranuclear palsy and corticobasal degeneration. Brain Pathol 2001;11(2):144-58.

Ferrer I, Gomez-Isla T, Puig B, Freixes M, Ribé E, Dalfó E, Avila J. Current advances on different kinases involved in tau phosphorylation, and implications in Alzheimer's disease and tauopathies. Curr. Alzheimer Res. 2005;2(1):3-18.

Fratantoni JC, Hall CW, Neufeld EF. Hurler and Hunter syndromes: mutual correction of the defect in cultured fibroblasts. Science 1968;162:570-72.

Fu H, Samulski RJ, McCown TJ, Picornell YJ, Fletcher D, Muenzer J. Neurological correction of lysosomal storage in a mucopolysaccharidosis IIIB mouse model by adeno-associated virus-mediated gene delivery. Mol. Ther. 2002;5:42–49.

Giovannini MG, Cerbai F, Bellucci A, Melani C, Grossi C, Bartolozzi C, Nosi D, Casamenti F. Differential activation of mitogen-activated protein kinase signalling pathways in the hyppocampus of CRND8 transgenic mouse, a model of Alzheimer's disease. Neuroscience 2008;153:618-33.

Haddad F, Adams GR. Inhibition of MAP/ERK kinase prevents IGF-I-induced hypertrophy in rat muscles. J Appl Physiol. 2004;96(1):203-10.

Kim EK, Choi E. Pathological roles of MAPK signaling pathways in human diseases. Biochimica et Biophysica Acta 2010;1802:396-405.

Krivit W, Peters C, Shapiro EG. Bone marrow transplantation as effective treatment of central nervous system disease in globoid cell leukodystrophy, metachromatic leukodysptrophy, adrenoleukodystrophy, mannosidosis, fucosidosis, aspartylglucosaminuria, Hurler, Maroteaux-Lamy, and Sly syndromes, and Gaucher disease type III. Curr. Opin. Neurol. 1999;12:167-176.

Li HH, Yu WH, Rozengurt N, Zhao HZ, Lyons KM, Anagnostaras S, Fanselow MS, Suzuki K, Vanier MT, Neufeld EF. Mouse model of Sanfilippo syndrome type B produced by targeted disruption of the gene encoding alpha-N-acetylglucosaminidase. Proc.Natl.Acad.Sci 1999; 96(25):14505-10.

Li HH, Zao HS, Neufeld EF, Cai Y, Gomez-Pinilla F. Attenuated plasticity in neurons and astrocytes in the mouse model of Sanfilippo syndrome type B. J.Neurosci.Res. 2002;69(1):30-38.

Malm G, Ringden O, Winiarski J, Grondahl E, Uyebrant P, Eriksson U, Hakansson H, Skjeldal O, Mansson JE. Clinical outcome in four children with metachromatic leukodystrophy treated by bone marrow transplantation. Bone Marrow Transplant 1996;17:1003-1008.

McCubrey JA, Lahair MM, Franklin RA. Reactive oxygen species-induced activation of the MAP kinase signalling pathways. Antioxid. Redox Signal 2006;8:1775-89.

McGlynn R, Dobrenis K, Walkley SU. Differential subcellular localization of cholesterol, gangliosides and glycosaminoglycans in murine models of mucopolysaccharide storage disorders. The J. Comp. Neurol. 2004;480:415-26.

Myerowitz R, Lawson D, Mizukami H, Mi Y, Tifft CJ, Proia RL. Molecular pathophysiology in Tay-Sachs and Sandhoff diseases as revealed by gene expression profiling. Hum. Mol. Genet. 2002;11(11):1343-50.

Neufeld EF and Muenzer J. The mucopolisaccaridoses. In: Scriver CR, Beaudet AL, Sly WS, Valle D Editors. The metabolic and moleclular bases of inherited disease. 8th Ed New York: McGraw-Hill; 2001. pp 3421-3452.

Ohmi K, Greenberg DS, Rajavel KS, Ryazantsev S, Li HH, neufeld EF. Activated microglia in cortex of mouse models of mucopolysaccaridosis I and III B. Proc. Nat. Acad. Sci. USA 2003;100:1902-07.

Ohmi K, Kudo LC, Ryazantsev S, Zhao HZ, Karsyen SL, Neufeld EF. Sanfilippo syndrome type B, a lysosomal storag disease, is also a tauopathy. PNAS 2009;106(20):8332-37.

Pacheco CD, Lieberman AP. Lipid trafficking defects increase Beclin-1 and activate autophagy in Niemann-Pick type C disease. Autophagy 2007; 3(5):487-9.

Perry G, Roder H, Nunomura A, Takeda A, Friedlich AL, Zhu X, Raina AK, Holbrook N, Siedlak SL, Harris PL, Smith MA. Activation of neuronal extracellular receptor kinase (ERK) in Alzheimer disease links oxidative stress to abnormal phosphorylation. Neuroreport, 1999;10(11):2411-15.

Platt FM, Walkley SU. Chapter 2, Lysosomal Defects and Storage. In: Platt FM, Walkley SU, editors. Lysosomal Disorders of the Brain. Oxford University Press; 2004. pp. 32-49.

Rothwell NJ, Luheshi GN. Interleukin 1 in the brain: biology, pathology and therapeutic target. Trends Neurosci. 2000;23(12):618-25.

Ryazantsev S, Yua WH, Zao HS, Neufeld EF, Ohmi K. Lysosomal accumulation of SMACS (Subunit c of Mitochondrial ATP Synthase) in neurons of the mouse model of mucopolysaccaridosis IIIB. Mol. Genet. Met 2007; 90(4):393-401.

Sardiello M, Palmieri M, di Ronza A, Medina DL, Valenza M, Gennarino VA, Di Malta C, Donaudy F, Embrione V, Polishchuk RS, Banfi S, Parenti G, Cattaneo E, Ballabio A. A gene network regulating lysosomal biogenesis and function. Science, 2009; 325(5939):473-7.

Sano R, Annunziata I, Patterson A, Moshiach S, Gomero E, Opferman J, Forte M, d'Azzo A. GM-1ganglioside accumulation at the mitochondria-associated ER membranes links ER stress to Ca(2+)-dependent mitochondrial apoptosis. Mol. Cell. 2008;36(3):500-11.

Scorziello A, Pellegrini C, Forte L, Tortiglione A, Gioielli A, Iossa S, Amoroso S, Tufano R, Di Renzo G, Annunziato L. Differential vulnerability of cortical and cerebellar neurons in primary culture to oxygen glucose deprivation followed by reoxygenation. J. Neurosci. Res., 2001;63(1):20-6.

Seger R, Krebs EG. The MAPK signaling cascade. FASEB J. 1995; 9(9):726-35.

Settembre C, Fraldi A, Jahreiss L, Spampanato C, Venturi C, Medina D, de Pablo R, Tacchetti C, Rubinsztein DC, Ballabio A. A block of autophagy in lysosomal storage disorders. Hum Mol Genet. 2008;17(1):119-29.

Subramaniam S, Zirrgiebel U, von Bohlen und Halbach O, Strelau J, Lalibertè C, Kaplan DR, Unsicker K. ERK activation promotes neuronal degeneration predominantly through plasma membrane damage and indipendently of caspase-3. Journal of Cell Biology 2004;165 (3):357-369.

Tettamanti G, Bassi R, Viani P, Riboni L. Salvage pathways in glycosphingolipid metabolism. Biochimie. 2003;85:432-37.

Villani GRD, Gargiulo N, Faraonio R, Castaldo S, Gonzales y Reyero E, Di Natale P. Cytochines, neurotrophins, and oxidative stress in brain disease from mucopolysaccaridosis IIIB. J.Neurosci. Res. 2007;85:612-622.

Villani GRD, Di Domenico C, Musella A, Cecere F, Di Napoli D, Di Natale P. Mucopolysaccharidosis IIIB: oxidative damage and cytotoxic cell involvement in the neuronal pathogenesis. Brain Research 2009;1279:99-108.

Visigalli I, Delai S, Politi LS, Di Domenico C, Cerri F, Mrak E, D'Isa R, Ungaro D, Stok M, Sanvito F, Mariani E, Staszewsky L, Godi C, Russo I, Cecere F, Del Carro U, Rubinacci A, Brambilla R, Quattrini A, Di Natale P, Ponder K, Naldini L, Biffi A. Gene therapy augments the efficacy of hematopoietic cell transplantation and fully corrects Mucopolysaccharidosis type I phenotype in the mouse model. Blood 2010

Vitry S, Ausseil J, Hocquemiller M, Bigou S, Dos Santos Coura R, Heard JM. Enhanced degradation of synaptophysin by the proteasome in mucopolysaccharidosis type IIIB Mol. Cell Neurosci. 2009;41(1):8-18.

Walkley SU. Pathogenetic cascades in lysosomal disease- Why so complex? J. Inherit. Metab. Dis. 2009;32:181-189.

Webster B, Hansen L, Adame A, Crews L, Torrance M, Thal L, Masliah E. Astroglial activation of extracellular–regulated kinase in early stages of Alzheimer disease. J. Neuropathol. Exp. Neurol. 2006;65(2):142-151.

Willaime-Morawek S, Brami-Cherrier K, Mariani J, Caboche J, Brugg B. C-Jun N-terminal kinase/c-Jun and p38 pathways cooperate in ceramide-induced neuronal apoptosis. Neuroscience 2003;119(2):387-97.

Wu YP, Proia RL. Deletion of macrophage-inflammatory protein 1 alpha retards neurodegeneration in Sandhoff disease mice. Proc. Natl. Acad. Sci. USA 2004;101(22):8425-30.

Zheng Y, Ryazantsev S, Ohmi K, Zhao HZ, Rozengurt N, Kohn DB, Neufeld EF. Retrovirally transduced bone marrow has a therapeutic effect on brain in the mouse model of mucopolysaccharidosis IIIB. Mol. Genet. Metab. 2004;82:286–295.

Zhu X, Raina AK, Rottkamp CA, Aliev G, Perry G, Boux H, Smith MA. Activation and redistribution of c-Jun N-terminal kinase/stress activated protein kinase in degenerating neurons in Alzheimer's disease. J Neurochem. 2001;76(2):435-41.

Acknowledgements

I would like to express my sincere gratitude to my supervisor, Prof. Di Natale. She provided me with many helpful suggestions, important advice and constant encouragement during the course of this work.

Special thanks are due to Dr. Di Domenico for her extremely valuable experience, support and insight especially at the beginning of this study.

I wish also to express my cordial appreciation to Dr. Villani for advices on technical problems.

available at www.sciencedirect.com

ScienceDirect

www.elsevier.com/locate/brainres

BRAIN RESEARCH

Research Report

Mucopolysaccharidosis IIIB: Oxidative damage and cytotoxic cell involvement in the neuronal pathogenesis

Guglielmo R.D. Villani[a,*], *Carmela Di Domenico*[a], *Annapaola Musella*[a], *Francesca Cecere*[a], *Daniele Di Napoli*[b], *Paola Di Natale*[a]

[a]*Department of Biochemistry and Medical Biotechnologies, University of Naples Federico II, Via S. Pansini 5, 80131 Naples, Italy*
[b]*Center for Animal Experimentation, Cardarelli Hospital, 80128 Naples, Italy*

ARTICLE INFO

Article history:
Accepted 13 March 2009
Available online 3 May 2009

Keywords:
Mucopolysaccharidosis IIIB
Pathogenesis
Neurodegeneration
Oxidative stress
Cell-mediated cytotoxicity

ABSTRACT

Sanfilippo B syndrome (Mucopolysaccharidosis IIIB, MPS IIIB) is a lysosomal storage disease due to mutations in the gene encoding alpha-N-acetylglucosaminidase and is characterized by a severe neurological disorder. Although several studies have been reported for the murine model of the disease, the molecular basis and the sequence of events leading to neurodegeneration remain to be clarified. We previously suggested the possible involvement of the reactive oxygen species in the disease pathogenesis. In the present paper we extended the analysis of oxidative stress by evaluating the production of superoxide ions throughout the CNS and by evaluating the effect of the stress on the cellular macromolecules. These approaches applied to one-month-old, three-month-old and six-month-old mice revealed that oxidative stress is present in the affected cerebrum and cerebellum tissues from one month from birth, and that it results primarily in protein oxidation, both in the cerebrum and cerebellum, with lipid peroxidation, and especially DNA oxidation, appearing milder and restricted essentially to the cerebellum. We also identified additional genes possibly associated with the neuropathology of MPS IIIB disease. Real time RT-PCR analysis revealed an altered expression of the Sod1, Ret, Bmp4, Tgfb, Gzmb and Prf1 genes. Since Gzmb and Prf1 are proteins secreted by NK/cytotoxic T-cells, these data suggest the involvement of cytotoxic cells in the neuronal pathogenesis. Extending our previous study, findings reported in the present paper show that oxidative stress and all the analyzed stress-related pathological changes occur very early in the disease course, most likely before one month of age.

1. Introduction

Mucopolysaccharidosis IIIB (MPS IIIB, Sanfilippo syndrome type B) is a lysosomal disease due to mutations in the gene encoding alpha-N-acetylglucosaminidase (NAGLU, EC 3.2.1.50), which is required for the degradation of heparan sulphate (HS) (Neufeld and Muenzer, 2001). The clinical phenotype of the disease is characterized, primarily, by profound neurological deterioration and behavioral disturbances associated to relatively mild somatic manifestations; the genetic basis of MPS IIIB, extensively studied in the past years, demonstrates a broad molecular heterogeneity (Neufeld and Muenzer, 2001). Although a murine model of the disease has been available since 1999 (Li et al., 1999), and although it was recently studied

* *Corresponding author*. Fax: +39 0817463150.
E-mail address: villani@dbbm.unina.it (G.R.D. Villani).

0006-8993/$ – see front matter © 2009 Elsevier B.V. All rights reserved.
doi:10.1016/j.brainres.2009.03.071

on a clinical basis (Heldermon et al., 2007), the pathogenetic basis of the neurological disease is still unclear; i.e. the relationship between abnormal lysosomal storage of partially degraded HS and the neurodysfunction.

For lysosomal diseases, as for others neurodegenerative diseases, much evidence points to the involvement, in the neurological pathology, of an inflammatory response that includes astrocyte and microglia activation followed by the expression and secretion of potentially neurotoxic cytokines and chemokines (Myerowitz et al., 2002; Wu and Proia, 2004). Also for MPS IIIB a drastic induction of reactive astrocytes was reported to be related to the expression of the glial fibrillary acidic protein (GFAP) and GFAP-positive cell density (Li et al., 2002) as well as the involvement of microglia (Ohmi et al., 2003). Our group also confirmed the finding of an upregulation of several genes involved in astrogliosis (Villani et al., 2007). However, a recent study demonstrated that the absence of microglia cell priming by HS oligosaccharides did not change the onset of the expression of several markers, although the onset of brain inflammation was delayed for several months (Ausseil et al., 2008).

Indeed, other evidence on the reduction of the brain function in the mouse model of MPS IIIB pointed to important alterations in the maintenance of neuroplasticity involving fibroblast growth factors (FGF) and their receptors (FGFR) (Li et al. 2002) and to alterations of the neurotrophins Bdnf and Cbln1, as well as to alterations of the microglial NADPH oxidase complex (Villani et al., 2007), suggesting that alterations in the neurotrophin and ROS levels could participate in neuronal dysfunction.

The balance between ROS production and antioxidant defenses determines the degree of oxidative stress: increased ROS levels may result in a damaging of macromolecules and constitute a stress signal that activates specific redox-sensitive signaling pathways that have damaging functions (Dröge and Schipper, 2007). The present study aims to extend the analysis of the oxidative stress previously found to be involved in the MPS IIIB murine model (Villani et al., 2007) by evaluating its effect on the intracellular macromolecules in nervous tissues of the affected mice; moreover, additional genes were analyzed as possibly associated with the neuropathology of MPS IIIB disease. We demonstrate here that oxidative stress has modifying effects on cell macromolecules and that stress and its effects are evident already at one month from birth.

2. Results

2.1. *Analysis of NADPH oxidase activity*

Taking into account our previous results demonstrating an increase in the superoxide ion production in the whole brain and cerebellum of old MPS IIIB mice, in the present study we extended the analysis of the NADPH oxidase activity in young animals, in three different regions of the cerebrum identified

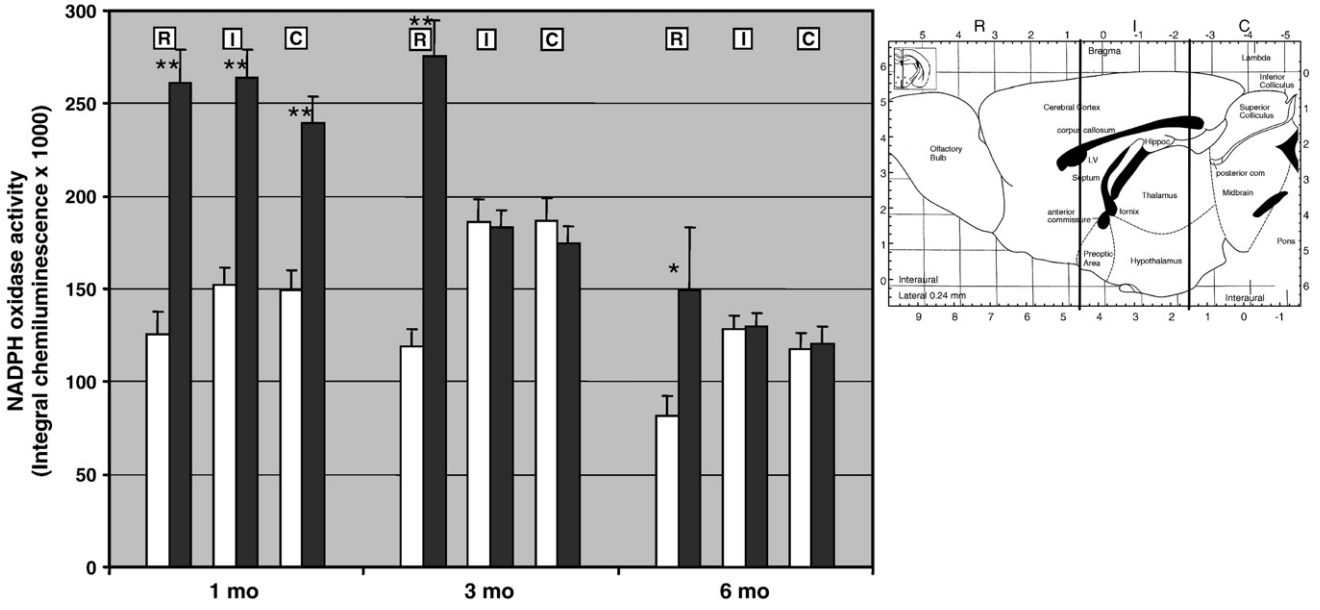

Fig. 1 – Analysis of NADPH oxidase activity. NADPH oxidase activity was determined in the brain homogenates prepared by pooling tissues from three different regions of the cerebrum: rostral (R), intermediate (I) and caudal (C) fragment, obtained from one-, three- and six-month-old normal (white bars) and MPS IIIB (black bars) mice ($n = 4$ for each group). A lucigenin-based assay was performed as described in the Experimental procedures. Reactions were started by adding the proteins, and the production of superoxide ions was measured every 10 s for 15 min by monitoring chemiluminescence. The data, collected as relative luminescence units, were plotted versus time, and the area under the chemiluminescence intensity curve (integral chemiluminescence) was used for analysis. Values are mean ± SD of three experiments performed on different sets of mice (*$P < 0.05$; **$P < 0.01$).

as the rostral (R), intermediate (I) and caudal (C) fragment. The results are shown in Fig. 1. At one month from birth the affected mice showed, in all the cerebrum segments analyzed, an increased production of superoxide ions (as demonstrated by the suppression of chemiluminescence following addition of SOD, data not shown): 208%, 173% and 160% for the rostral, intermediate and caudal segment, respectively. At three months and six months from birth the increase in the superoxide ion production was restricted only to the rostral segment of the cerebrum (232% and 182% compared to normal levels, respectively).

Following these results, we analyzed the oxidation status of the cellular macromolecules in affected tissues at different animal ages by evaluating the protein carbonyl content, lipid peroxidation and DNA oxidation.

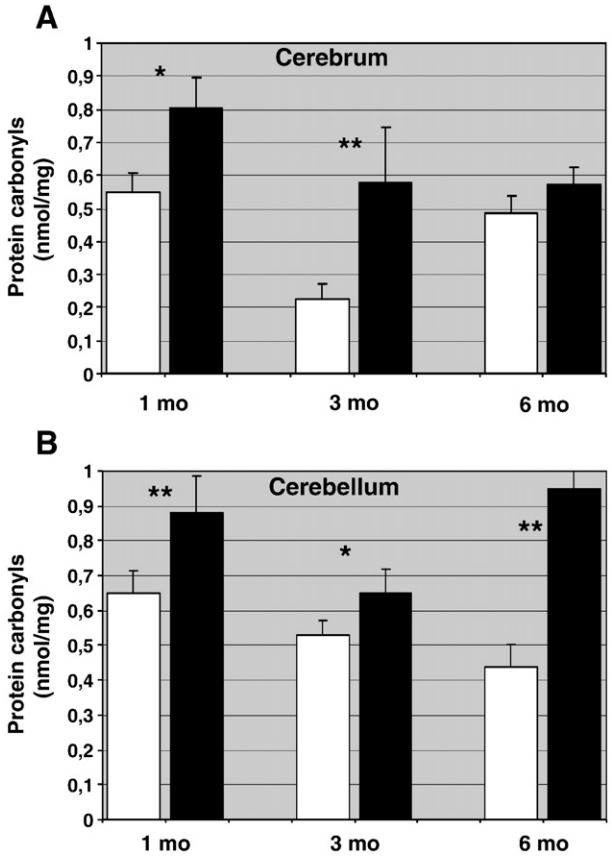

Fig. 2 – Oxidative damage: protein oxidation analysis. The protein oxidation analysis was performed using a protein carbonyl ELISA kit as reported in the Experimental procedures. Tissue samples (cerebrum, panel A, or cerebellum, panel B) from affected (black bars) or age-matched normal (white bars) mice, 1, 3, 6 months old ($n=5$ for each age), were pooled and homogenized in water on ice; immediately after homogenization the protein determination was performed using the Lowry assay and 20 μg of proteins was TCA precipitated to be used in the ELISA assay described in the Experimental procedures. Values, reported as nmol/mg protein carbonyl concentration, are mean ± SD of three experiments performed on different sets of animals (*$P<0.05$; **$P<0.01$).

2.2. *Oxidative damage: protein oxidation analysis*

Protein carbonyls may originate from backbone fragmentation, hydrogen atom abstraction at alpha carbons, or attack on several amino acid side-chains (Lys, Arg, Pro, Thr, etc.), and from the formation of adducts between amino acids and products of lipid peroxidation. Moreover, several reactions of protein radicals can result in the production of other radicals, contributing to cause damage to other biomolecules (Sultana et al., 2006). Protein carbonyls are chemically stable compared with the other products of oxidative stress and so are sensitive indices of oxidative injury. Therefore, we performed the protein oxidation analysis using a protein carbonyl ELISA kit. As shown in Fig. 2, increased levels of protein oxidation were obtained for both the cerebrum and cerebellum, at each time point from birth. For the cerebrum, the main increase was observed at 3 months of age (259%), while a protein carbonyl content corresponding to 146% and 118% compared to normal controls was obtained for the one-month-old and six-month-old mice, respectively (Fig. 2, panel A). Conversely, for the cerebellum the highest carbonyl levels were seen at 6 months from birth (218% compared to normal brains); an increase of 135% and 123% was observed at 1 month and 3 months from birth, respectively (Fig. 2, panel B).

2.3. *Oxidative damage: lipid peroxidation analysis*

Lipid peroxidation is one of the major sources of free radical-mediated injury that directly damages membranes and generates a number of secondary products. In particular, markers of lipid peroxidation have been found to be elevated in brain tissues and body fluids in several neurodegenerative diseases (Sultana et al., 2006).

Lipid peroxidation quantified by the classic measurement of malondialdehyde (MDA) and 4-hydroxy nonenal (4-HNE), the degradation products of polyunsaturated fatty acid hydroperoxides, can often lead to an inaccurate estimation of lipid peroxidation (Mihaljević et al., 1996). We, therefore, evaluated the lipid peroxidation in the affected tissues by using a lipid hydroperoxide assay that measures the hydroperoxides (HDP) directly utilizing the redox reactions with ferrous ions. In the cerebrum a slight increase in lipid peroxidation was observed only in the three-month-old affected mice (135% compared to normal tissue), while at 1 month and 6 months from birth the HDP levels of the affected tissues were similar to the levels found in the normal controls (108% and 107%, respectively) (Fig. 3, panel A). For the cerebellum, a 134% and 145% increase was obtained for the three-month-old and six-month-old mice, respectively; HDP levels similar to that found for the normal tissues were observed at one month from birth (Fig. 3, panel B).

2.4. *Oxidative damage: DNA oxidation analysis*

8-OHdG is produced during DNA repair and its measurement is a useful marker of oxidative damage. The analysis of the oxidative damage on DNA in the MPS IIIB animals showed that in the cerebrum there was no significant difference compared to normal tissues, with only a slight increase in 8-OHdG adducts observed for one-month-old and six-month-old mice

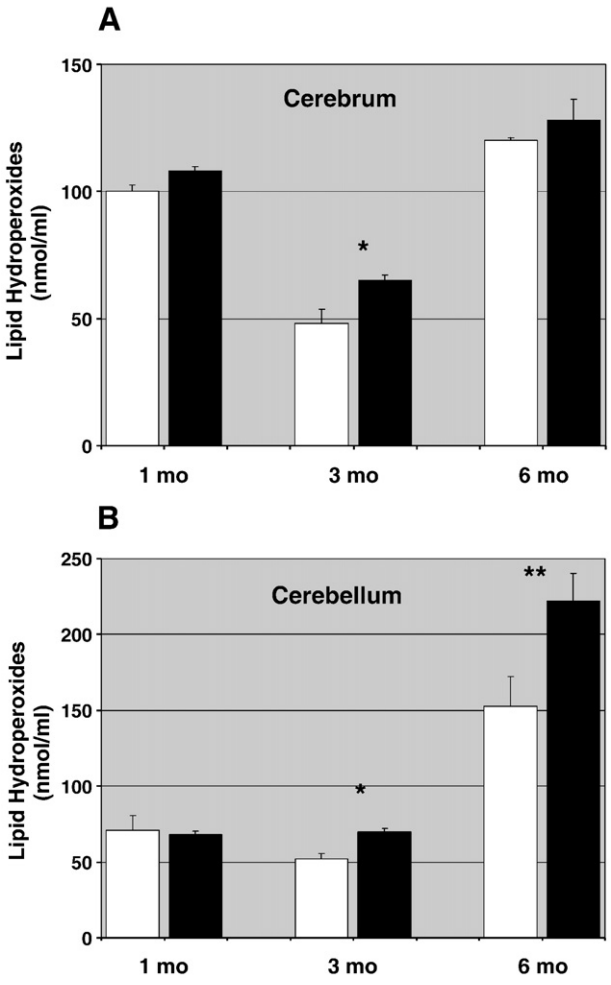

Fig. 3 – Oxidative damage: lipid peroxidation analysis. Tissues (cerebrum, panel A, or cerebellum, panel B) from affected (black bars) or age-matched normal (white bars) mice ($n=4$ for each age) were excised at 1, 3 and 6 months from birth, pooled, homogenized in water and the hydroperoxides were extracted according to the kit instructions; 400 μl of the extracts were used to quantify lipid hydroperoxides according to manufacturer's instructions (see Experimental procedures). Concentration of hydroperoxides is expressed as nmol/ml; values are mean ± SD of three experiments performed on different sets of animals (*$P<0.05$; **$P<0.01$).

(113% and 112% compared to normal animals, respectively) (Fig. 4, panel A). Conversely, affected cerebella had increased levels of 8-OHdG adducts mainly at one and three months from birth (150% and 144% over the normal levels, respectively) while tissues from six-month-old mice showed an increase of 120% over the normal controls (Fig. 4, panel B); however, the differences were not statistically significant except for the intermediate age.

2.5. *Searching for altered genes: real time RT-PCR analysis in old mice*

As a preliminary experiment, this analysis was performed twice on tissues from six-month-old MPS IIIB mice and age-matched normal controls (single sets of $n=7$ animals). Pools of RNAs were used to generate cDNAs to be subjected to the screening. Selected members of different families of genes were analyzed in the rostral, intermediate and caudal fragment of the cerebrum: 1) oxidative stress-related genes; 2) DNA repair-related genes; 3) neuronal plasticity-related genes; 4) neurotrophin genes; 5) inflammation-related genes and 6) apoptosis-related genes. The results are shown in Table 1; fold changes (fc) were considered significant if ≥2 fold or ≤0.5 fold.

Among the oxidative stress-related genes, only Sod1 showed a significant variation (fc 2.7) in the intermediate region of the cerebrum, with a minor increase in the other two

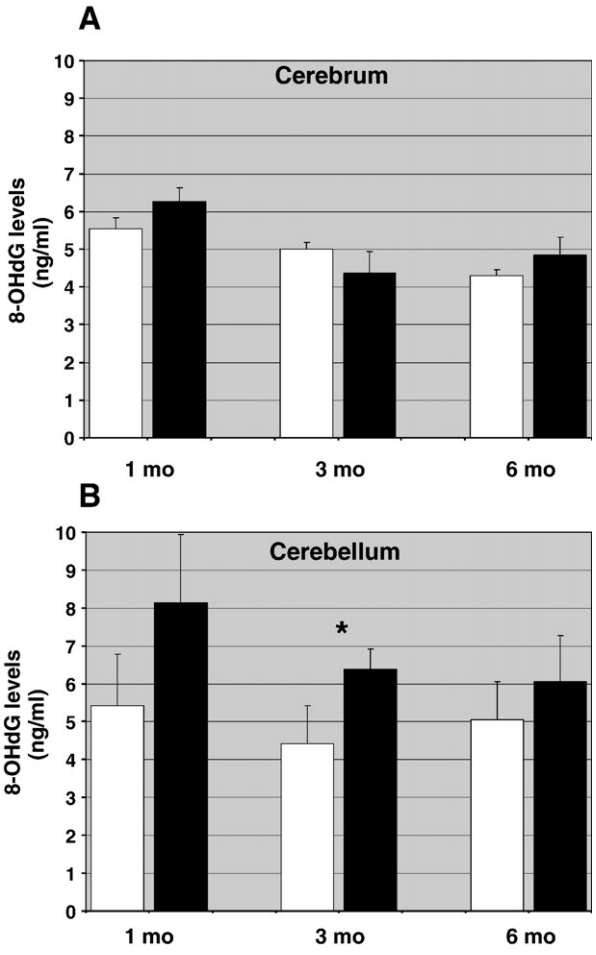

Fig. 4 – Oxidative damage: DNA oxidation analysis. DNA was purified from tissue samples (cerebrum, panel A, or cerebellum, panel B, from affected or age-matched normal mice, $n=4$ for each group) excised at 1, 3 or six months of age. DNA preparations obtained from three mice were pooled and quantified and 200 μg was pretreated with nuclease P1 as described in the Experimental procedures; hydrolysates were filtered and applied to the wells of the ELISA plate and the quantitative measurement of 8-OHdG adducts was obtained (see Experimental procedures). Values, representing ng/ml of 8-OHdG adducts, are mean ± SD of three experiments performed on different sets of animals (*$P<0.05$). White bars: normal mice; black bars: affected mice.

Table 1 – Real time RT-PCR analysis: genes found deregulated in the cerebrum from six-month-old MPS IIIB mice.

GeneBank accession no.	Gene symbol	Gene name	Fold change		
			R	I	C
Oxidative stress-related genes:					
NM_011434	Sod1[a]	Superoxide dismutase 1, soluble	1.18	2.7	1.64
NM_013671	Sod2	Superoxide dismutase 2, mitoc.	0.83	1.78	0.98
NM_011435	Sod3	Superoxide dismutase 3, extrac.	0.90	0.78	0.87
NM_009007	Rac1	RAS-related C3 botulinum substrate 1	0.97	1.95	0.78
NM_010344	Gsr	Glutathione reductase	1.9	0.68	0.9
NM_008160	Gpx1	Glutathione peroxidase 1	1.5	0.68	0.84
NM_009804	Cat	Catalase	1.35	1.29	0.93
NM_011723	Xdh	Xanthine dehydrogenase	0.86	0.84	1.12
NM_009662	Alox5	Arachidonate 5-lipoxygenase	1.29	1.38	1.07
NM_011563	Prdx2	Peroxiredoxin 2	0.85	1.26	1.15
DNA repair-related genes:					
NM_010957	Ogg1	8-oxoguanine DNA-glycosylase 1	0.95	1.22	0.70
NM_176953	Lig4	Ligase IV	0.84	0.92	1.59
NM_008446	Kif4	Kinesin family member 4	0.87	0.72	1.88
NM_020032	Pol1	Polymerase (DNA directed), lambda	1.37	0.68	0.85
Neuronal plasticity-related genes:					
NM_146243	(Actr2) Arp2	Actin-related protein 2 homolog	0.63	1.16	0.65
NM_023735	(Actr3) Arp3	Actin-related protein 3 homolog	0.76	1.08	0.6
NM_024441	Hsp27	Heat shock protein 2	0.71	1.12	0.56
NM_010907	NFkbi	Nuclear factor of kappa light polypeptide gene enhancer in B-cells inhibitor	0.92	1.35	0.55
NM_011952	Erk1	Mitogen-activated protein kinase 3	0.53	1.40	0.90
NM_011951	P38	Mitogen-activated protein kinase 14	0.55	1.30	0.66
NM_001080780	Ret[a]	Ret proto-oncogene	0.57	1.89	0.50
Genes found altered by previous screening on filter arrays:					
Neurotrophins genes:					
NM_010253	Gal	Galanin	0.56	1.05	0.63
NM_007554	Bmp4[a]	Bone morphogenetic protein 4	1.72	2.00	0.83
NM_008742	Ntf3	Neurotrophin 3	0.57	1.64	0.74
Inflammation-related genes:					
NM_011577	Tgfb[a]	Transforming growth factor, beta 1	1.68	2.14	0.84
NM_007700	IKK1	Conserved helix-loop-helix ubiquitous kinase	0.71	1.23	1.51
Apoptosis-related genes:					
NM_007499	Atm	Ataxia telangiectasia mutated homolog	0.72	0.60	0.66
NM_013542	Gzmb[a]	Granzyme B	1.27	6.35	2.9
NM_011073	Prf1[a]	Perforin 1 (pore forming protein)	3.32	8.20	2.50
NM_009810	Casp3	Caspase 3	1.48	1.08	0.67

Analyses were performed on pooled RNA from six-month-old MPS IIIB mice or age-matched controls ($n=7$). R = rostral segment; I = intermediate segment; C = caudal segment.

[a] Genes showing a two fold variation (fold change ≥2 or ≤0.5) in at least one of the three analyzed cerebrum regions were further analyzed in different sets of 1 month old, 3 months old and 6 months old affected mice (see Fig. 5).

regions analyzed. None of the analyzed DNA repair-related genes presented significant alterations, while in the group of genes potentially involved in neuronal plasticity, only Ret showed a significant decrease in the caudal region (fc 0.5) together with increased levels in the intermediate segment (fc 1.89). Among the neurotrophin genes, Bmp4 resulted in an increased expression in the rostral and intermediate regions (fc 1.72 and 2.00, respectively). Similar behavior was observed for the inflammation-related Tgfb gene (fc 1.68 and 2.14 in the rostral and intermediate segment, respectively), while an increased expression in all the cerebrum fragments analyzed (R, I and C) was found for the apoptosis-related genes Gzmb (fc 1.27, 6.35 and 1.90, respectively) and Prf1 (fc 3.32, 8.20 and 2.50, respectively) (Table 1).

2.6. *Searching for altered genes: real time RT-PCR analysis in young mice*

The genes found, from the previous analysis, with a significant variation (fold change ≥2 or ≤0.5) in at least one of the three cerebrum regions were further examined in the three different segments of the cerebrum from one-month-old and three-month-old affected mice; the results, obtained from multiple pools of $n>4$ different animals in each replicate, are

shown in Fig. 5. The most important alterations concerned the apoptosis-related and inflammation-related genes, namely Prf1, Gzmb and Tgfb.

For Prf1 and Gzmb an increased expression was found from one to six months of age in almost all the analyzed cerebrum fragments: Prf1 at one month from birth resulted in a significant increase only in the caudal segment (fc 2.0, $P<0.05$) while at three months of age increments were >2 in all the three cerebrum segments (fc 2.2, $P<0.01$, fc 4.7, $P<0.01$, and fc 4.0, $P<0.05$, for R, I and C, respectively); in the six-month-old mice the highest Prf1 expression (fc 8.2, $P<0.01$) was found in the intermediate segment (Fig. 5). As reported in the previous section, also Gzmb showed the highest expression in the intermediate region of the six-month-old affected cerebrum, but its levels were significantly increased also in other regions and times of age, particularly in the caudal segment of the one-month-old animals (fc 4.2, $P<0.01$).

Tgfb was mostly expressed in the intermediate area of the cerebrum at one month of age (fc 3.2, $P<0.05$) and in the same area similar levels persisted also at the other ages (fc 2.9, $P<0.01$, and fc 2.2, $P<0.05$, at three or six months from birth, respectively); consistent levels were observed in the rostral area (fc approximately 1.7, $P<0.05$) while a lesser expression was found in the caudal region (Fig. 5).

Among the other analyzed genes, Bmp4 and Ret were increased in their expression mainly in the intermediate area at every age. Bmp4 was found in this area with a fc of 2.1, 1.8 and 2 at one, three and six months, respectively ($P<0.05$ for every age); a similar value (fc 1.72, $P<0.05$) was found in the rostral area at six months of age (Fig. 5). Ret in the intermediate area showed fc values of 1.5, 1.7 and 1.9 for one-month-old, three-month-old and six-month-old mice, respectively ($P<0.05$ for every age); a slight increase was also observed in the rostral (fc 1.5, $P<0.05$) and caudal area of three-month-old mice (fc 1.4, not statistically significant), while it was decreased in the rostral and caudal segments at six months of age (fc 0.6, $P<0.01$, and 0.5, $P<0.01$, respectively) (Fig. 5). Sod1 presented in the intermediate segment with fc of 0.55 ($P<0.01$), 1.4 ($P<0.05$) and 2.7 ($P<0.01$) at one, three and six months of age, while its expression was consistent or slightly increased in the caudal region and significantly decreased in the rostral area at one and three months of age (fc 0.51, $P<0.01$, and 0.38, $P<0.01$, respectively).

3. Discussion

Several processes appear to take part to the neuronal pathogenesis in the MPS IIIB disease. An inflammatory process was suggested to be involved in the brain pathology of the murine model, involving astrocytes and microglia activation followed by the secretion of potentially neurotoxic cytokines and chemokines (Li et al., 2002; Ohmi et al., 2003; Villani et al., 2007), as demonstrated for other neurodegenerative diseases (Myerowitz et al., 2002; Wu and Proia, 2004). However, inflammation is only one of the determinants of the

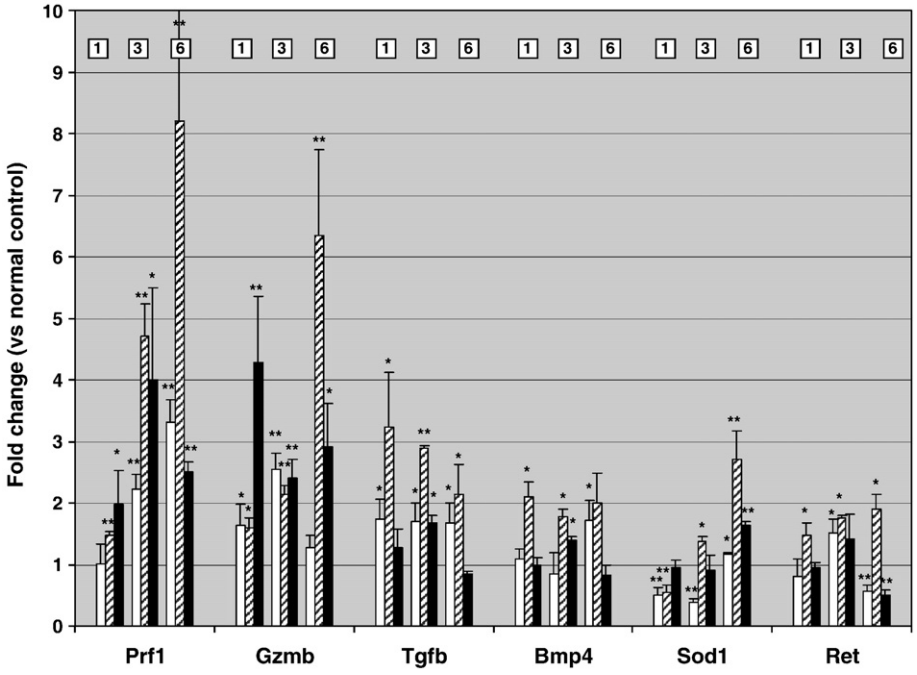

Fig. 5 – Relative levels of Prf1, Gzmb, Tgfb, Bmp4, Sod1 and Ret in the cerebrum of MPS IIIB mice. Results from real time analysis performed on RNAs obtained from cerebrum segments dissected at different times from birth: 1 = one month; 3 = three months; 6 = six months. Equal amounts of RNA from each mouse were pooled before generating the cDNAs. Abl cDNA was used to normalize the level of the gene of interest in both mutant and control preparations. Data (mean ± SD of three experiments performed on three different sets of animals, $n \geq 4$ in each replicate) are expressed as fold change in the MPS IIIB mice compared to the normal controls (*$P<0.05$; **$P<0.01$). White bars: segment R of the cerebrum; striped bars: segment I; black bars: segment C.

neurodegenerative process, since a recent study on doubly mutant mice C57Bl/6$^{NaGlu-/-,TLR4-/-}$ demonstrated that the absence of microglia cell priming by HS oligosaccharides did not change the onset of the disease markers, although the onset of brain inflammation was delayed for several months (Ausseil et al., 2008).

We recently suggested that alterations of ROS levels and, hence, oxidative stress could be involved in the neuronal dysfunction in the murine model of MPS IIIB (Villani et al., 2007). Oxidative stress is one of the most important mediators in the progressive decline of cellular function during aging and in age-related neurodegenerative diseases (Poon et al., 2006). In the brain, free radical-mediated oxidative stress plays a critical role in the decline of cellular function as a result of the oxidation of nucleic acids, lipids, and proteins, which alters the structure and function of these macromolecules. Upregulation of NADPH oxidase was first reported in an experimental model of Parkinson's disease (Wu et al., 2003). We demonstrated the upregulation of this multimeric enzyme also in the brain of MPS IIIB mice, resulting in an increased production of superoxide ions (Villani et al., 2007).

In the present study we extended the analysis of oxidative stress by measuring the superoxide ion production in different areas of the cerebrum and in cerebellum, and by evaluating its effect on the cellular macromolecules. Our data indicate that oxidative stress is already present in young mice (one month old) and that it results primarily in protein oxidation, while lipid peroxidation and DNA oxidation appear milder and restricted essentially to the cerebellum.

A number of studies indicate a strong role for increases in protein oxidation as a primary cause of cellular dysfunction during neurodegeneration (for review: Butterfield et al., 2006; Sultana et al., 2006). However, not all proteins are oxidized: many proteins preserve their activity, suggesting that specific molecules are target of oxidative modification during aging and in neurodegenerative disorders (Poon et al., 2006; Butterfield et al., 2006). In general, carbonylated and nitrated proteins involved in neuronal dysfunction are related to energy metabolism, excitotoxicity, apoptosis and neuronal communication (Sultana et al., 2006; Dröge and Schipper, 2007); for instance, most of the proteins found oxidated in AD and in other neurodegenerative diseases can be linked to energy dysfunction (Butterfield et al., 2006; Martınez et al., 2008). Interestingly, recent evidence demonstrated, in the MPS IIIB mouse model, the accumulation of subunit c of mitochondrial ATP synthase (SCMAS), which could also suggest a mitochondrial dysfunction in this disease (Ryazantsev et al., 2007). Carbonylation was also demonstrated in brain aging and in neurodegenerative diseases for proteins related to recycling of damaged proteins through the proteasome (Sultana et al., 2006; Stefanis and Keller 2006; Dröge and Schipper, 2007). Most of the protein damage is irreparable and damaged molecules should be removed. One way to remove them is their dispatch to the lysosomes, which contain hydrolytic enzymes to degrade proteins taken into the cells by endocytosis as well as cytoplasmic proteins and organelles (autophagy). However, in lysosomal diseases, due to abnormal storage, lysosomes may be impaired in their demolishing function; impairment of the autophagic pathway was recently suggested in MPS IIIA and multiple sulfatase deficiency mouse models (Settembre et al., 2008). On the other hand, also oxidative stress can contribute to autophagic impairment (Dröge and Schipper, 2007): in these conditions the main pathway to remove unwanted proteins could be the proteasome, which recognizes targets marked by attachment of ubiquitin, that is an ATP-dependent process. Indeed, massive accumulation of ubiquitin has been found in affected brains in several mucopolysaccharidoses and also in MPS IIIB (Savas et al., 2004; Ryazantsev et al., 2007).

It is interesting that, at each time point from birth we found the greatest superoxide production in the rostral area of the MPS IIIB murine cerebrum; the analyzed area includes the somatosensory cortex, the striatum and structures related to the olfactory bulb. Interestingly, in a recent study the analysis of human brain tissue in MPS II and MPS IIIB patients revealed that in most of the analyzed patients the frontal cortex was one of the main sites of immunoreactivity for 8-OHdG and neuron-specific enolase (NSE); in the same areas the presence of mild TUNEL-immunoreactive nuclei was reported, while neuronal loss was essentially restricted to the substantia nigra of the affected brains (Hamano et al., 2008). Moreover, Ryazantsev et al. (2007) found that in the murine MPS IIIB model SCMAS accumulated from one month of age primarily in the entirhinal and somatosensory cortex. The frontal lobe and the olfactory system appear to be particularly subject to protein oxidation also in other neurodegenerative diseases such as progressive supranuclear palsy (PSP) (Martınez et al., 2008) and Alzheimer disease (Butterfield et al., 2006; Moreira et al., 2005).

Our findings on the mechanisms involved in brain disease of the MPS IIIB model prompted us to evaluate the expression of additional genes by real time analysis. Among the analyzed oxidative stress-related genes only Sod1 was found to be altered in the affected cerebrum, appearing downregulated mainly in the rostral segment of young affected animals: this seems to correlate with the increased levels of superoxide ion mainly present in the rostral region of the cerebrum. However, further studies are required to establish if ROS is the cause for the decreased Sod1 expression or vice versa. For the DNA repair-related genes and for the neuronal plasticity-related genes, no significant alteration was observed, except for the Ret gene, which appeared to be slightly misregulated. The misregulation evidenced here for Ret, as well as for the other analyzed genes, could be ascribed to anyone of the multiple nuclei placed in the brain; however, recent evidences seem to link Ret signaling to the degeneration of the nigrostriatal system; mice with selective ablations for the gene encoding the receptor for Gdnf (Ret, Gdnfr) show progressive loss of dopaminergic neurons in the substantia nigra, degeneration of nerve terminals in the striatum and pronounced glial activation (Kramer et al., 2007). Gdnf and Bdnf neurotrophic factors can contribute to the fate of neurons: they may determine whether the neurons resist or succumb to neurodegeneration. The demonstrated alteration, in the MPS IIIB murine model, of the Bdnf (Villani et al., 2007) and Ret expression (this paper) support the hypothesis of the involvement of the nigrostriatal system in the brain pathogenesis of the disease. Interestingly, we also observed an upregulation of other neuroprotective members of this family of trophic factors: Tgfb, previously reported as having a protective effect

against motor neuron degeneration (Ho et al., 2000) and Bmp4, widely involved in the development of the central nervous system (Mikawa et al., 2006); this upregulation could represent a countervailing mechanism to attenuate the effect of a misregulation of Bdnf and Gdnfr.

We also analyzed some apoptosis-related genes; among these, the Prf1 and Gzmb genes showed a clear and marked increase in their expression in the affected cerebra, mainly in the intermediate segment. Perforin (Prf1) and granzyme B (Gzmb) are both proteins involved in granule-dependent killing mediated by cytotoxic T lymphocytes (CTL) and natural killer cells (NK). CTL are initially activated by recognizing antigens presented, together with the proteins of class I major histocompatibility complex (MHC), on the surface of an antigen-presenting cell; NK cells do not require pre-activation (Cullen and Martin, 2008). Granzyme B is a major constituent of CTL/NK cell granules and promotes apoptosis through two main pathways: one involving direct activation of caspases and the other mediated through granzyme B-initiated promotion of mitochondrial permeabilization. Destruction of neurons by cytotoxic T-cells has been reported as a pathogenic mechanism in some neurodegenerative disorders (Bien et al., 2002; Metz et al., 2007; Howe et al., 2007) in which cytotoxic T lymphocytes seem to contribute to the damage and apoptotic death of cortical neurons. Our results, as well as the data very recently reported by DiRosario et al. (2009), suggest that T-cell-mediated cytotoxicity could contribute to the dysfunction of neurons in the brain of MPS IIIB mice. It is also interesting to note that, in accordance with this hypothesis, Ohmi et al. (2003) reported, in the cortex of mouse models of MPS IIIB and MPS I, an increased expression of complement C1q, for which more recently van Montfoort et al. (2007) demonstrated a novel role in augmenting the presentation of the antigen captured in immune complexes to CD8+ T lymphocytes.

Our present findings on the increased expression of Prf1 and Gzmb address the apoptotic mechanisms involved in the neuronal pathology of murine MPS IIIB. However, previous data (Li et al., 2002; Villani et al., 2007) showed no clear evidence of apoptosis in this animal model using immunohistochemistry or TUNEL test analysis. On the other hand, Hamano et al. (2008) reported a mild occurrence of TUNEL-immunoreactive nuclei in affected patients, predominantly in swollen neurons in the frontal and temporal cortices and in the globus pallidus. What could account for the markedly increased expression of perforin and granzyme B found in the affected cerebra of the murine model? One possibility is that the cytotoxic T-cell attack, probably taking place in MPS IIIB brains, does not necessarily lead to immediate apoptosis but may in part cause sublethal cell injury, as suggested for other neurodegenerative disorders (Behrens et al., 1997; Bien et al., 2002). It is also possible that the low levels of apoptosis, demonstrated only in the older animals, are due to the cumulative cell loss caused by degeneration, apoptosis and inflammation at younger ages. Finally, another possibility is that MPS IIIB neurons are intrinsically resistant to apoptosis and this resistance could be related to the expression of specific inhibitory factors; as support to this speculation it is an intriguing observation that Bcl-XL, an anti-apoptotic protein, is upregulated during oxidative stress in neuronal cultures (Luetjens et al., 2001). In conclusion, the occurrence of neuronal death due to apoptosis requires further studies in MPS IIIB disease.

In summary, our data suggest, for the brain pathology in the MPS IIIB mouse model, the participation of cytotoxic cells causing neuron injury and confirm the involvement of oxidative stress resulting in a damaging effect on the cell macromolecules, mainly the proteins. More importantly, this study provides time-course data demonstrating for the first time that pathological changes occur very early in the disease course, most likely before one month of age.

4. Experimental procedures

4.1. *Animals and tissues*

The MPS IIIB mouse model used in the present study showed a biochemical phenotype generally similar to that of the human disorder; in this model, no excess heparan sulphate was reported in the soluble GAG fraction of the brain although ganglioside levels were increased (Li et al., 1999). The mice were genotyped by PCR at 1 month from birth, as previously described (Di Natale et al., 2005). Heterozygotes were either intercrossed for experimental use or subjected to 12 back-crossing to C57BL/6 mice to put the mutation on a congenic background. At the time of sacrifice, MPS IIIB mice and age-matched normal animals, aged 1, 3 and 6 months, were killed by cervical dislocation performed after profound anesthesia obtained by intraperitoneal injection of 100 mg/kg ketamine and 1 mg/kg metedomidine. Cerebrum and cerebellum were immediately removed; cerebrum, for some of the experiments, was placed on a brain blocker (David Kopf Instruments, CA) and subdivided into parts on ice-cold tissue culture plate: rostral (R), up to anterior commissure, intermediate (I), including hippocampus, thalamus and hypothalamus, and caudal (C), from the posterior commissure up to 4th ventricle (Fig. 1, adapted from Paxinos and Watson, 2007). Fragments were then transferred to ice-cold microcentrifuge tubes and immediately frozen in liquid nitrogen. The procedures on the mice were approved by the Italian Ministry of Public Health.

4.2. *Analysis of NADPH oxidase activity*

NADPH oxidase activity was measured using a chemiluminescence detection system in homogenates prepared, in 100 mM phosphate buffer, pH 7, by pooling cerebrum fragments (R, I or C) from three different sets of MPS IIIB or normal mice, containing the same number of males and females, sacrificed at 1, 3 and 6 months of age (n=4 for each group). In these assays, 150 μg of proteins was added to a mix containing 50 μM lucigenin, 50 mM phosphate buffer, 1 mM EGTA, 150 mM sucrose, 0.1 mM NADH and 0.1 mM NADPH. In some experiments superoxide dismutase (SOD) 30 U/ml was added to the previous mixture to verify that the main reactive oxygen specie detected in the reaction was the superoxide ion (data not shown). Reactions were started by adding the proteins, and the production of superoxide ions was measured every 10 s for 15 min by monitoring chemiluminescence using a Turner Biosystems 20/20^n luminometer. The data, collected as

relative luminescence units, were plotted versus time, and the area under the curve was used for analysis.

4.3. Protein oxidation analysis

For the protein oxidation analysis, cerebrum or cerebellum from three different sets of affected ($n=5$) or age-matched normal mice ($n=5$), containing approximately the same number of males and females, were excised at 1, 3 or 6 months from birth, pooled and homogenized in water on ice; immediately after homogenization a protein determination was made using the Lowry assay. Twenty μg of proteins was TCA precipitated (by adding 0.8 volumes of ice-cold 28% w/v TCA followed by centrifugation at 10,000 *g* for 3 min) and used in the subsequent assay. Quantification of protein carbonyls was performed by using the Protein Carbonyl ELISA kit (Zentech, Alexis Corporation, Switzerland).

4.4. Lipid peroxidation analysis

For the lipid peroxidation dosage, tissues (cerebrum or cerebellum) were excised from three different sets of affected ($n=4$) or age-matched normal mice ($n=4$), containing the same number of males and females, at 1, 3 or 6 months from birth, pooled, homogenized in water, 50 mg/ml, and the hydroperoxides (HDP) were extracted according to the kit instructions; the extracts were stored at −80 °C if not immediately processed. Quantification of lipid peroxidation was performed using the Lipid Hydroperoxide (LPO) Assay Kit (Cayman Chemical Company, MI, USA).

4.5. DNA oxidation analysis

DNA to be used for the quantification of DNA oxidation was purified by the classic phenol:chloroform extraction method from tissue samples (cerebrum or cerebellum from affected, $n=4$, or age-matched normal mice, $n=4$) obtained from three different sets of one-, three- and six-month-old animals with the same number of males and females. DNAs were pretreated as follows: 200 μg of sample, obtained by pooling the DNA preparation from three mice, was dissolved in 135 μl of water; after addition of 15 μl 200 mM sodium acetate containing 6 units of nuclease P1 (Japan Institute For the Control of Aging, Japan) samples were incubated for 1 h at 37 °C after argon substitution. Fifteen microliters of 1 M Tris–HCl buffer, pH 7.4, and 2 units of alkaline phosphatase (Promega, Madison WI, U.S.A.) were then added and incubation continued for 1 h after argon substitution. Hydrolysates were filtered through Millipore Ultra free C3LGC device at 14,000 rpm for 10 min and 50 μl of filtrate was applied to the wells of the ELISA plate. Quantification of oxidative DNA adduct 8-hydroxy-2′ deoxyguanosine (8OHdG) was performed using the Highly Sensitive 8-OHdG ELISA kit (Japan Institute for the Control of Aging, Japan).

4.6. Statistical analysis

All the statistical analyses given in this paper were performed using Student's *t*-test or, for the real time PCR experiments, ANOVA; 95% confidence limits were selected. The statistical software used for all the analyses was from Glantz (1998).

4.7. Isolation of RNA

Three different sets of affected MPS IIIB mice ($n\geq4$) containing approximately the same number of males and females, 1, 3 and 6 months old at the time of sacrifice, and age-matched normal controls ($n\geq4$) were killed by cervical dislocation after anesthesia and the cerebrum was removed, subdivided into parts (R, I and C as in Fig. 1) and immediately frozen in liquid nitrogen; total RNA was isolated from 50 mg of tissue using the RNeasy Lipid Tissue (Qiagen, MD U.S.A.) following the manufacturer's protocol. The concentration and purity of the RNA preparations were determined by measuring the absorbance at 260, 280 and 230 nm by spectrophotometer. Equal amounts of RNAs from at least four mice (normal or MPS IIIB) were then pooled before generating the cDNAs to be used in the following experiments.

4.8. RT-PCR

The cDNA was synthesized using 3 μg total RNA in the presence of random primers, dNTPs, RNAse Inhibitor and Reverse Transcriptase (all from Promega, Madison WI U.S.A.) following the manufacturer's protocol. The PCR was performed in 25 μl reaction solution containing 12.5 μl RT^2 Real-Time SYBR Green/Fluorescein PCR Master Mix (from SuperArray Inc.), 1.0 μl of template cDNA and 0.2 μM PCR Primer set. The PCR conditions were as follows: 95 °C 15 min, 40 cycles of 95 °C for 30 s, 55 °C for 30 s, and 72 °C for 5 min. Relative expression of mRNA for the target genes was performed by the comparative C_T ($\Delta\Delta C_T$) method using the Abl gene as control. A validation experiment was performed for each gene of interest and its control to determine the conditions for optimal concentration of primers and templates. The normalized C_T (ΔC_T) was obtained by subtraction of the C_T for Abl from the C_T for the gene of interest. The difference between the ΔC_T for mutant and control samples gave rise to the $\Delta\Delta C_T$ value that was used for the calculation of the relative mRNA expression using the formula $2^{-\Delta\Delta CT}$. The relative mRNA levels were expressed as fold change in MPS IIIB mice over control mice. Oligonucleotides were obtained from PrimerBank (Wang and Seed, 2003; http://pga.mgh.harvard.edu/primerbank) or designed using Oligo Explorer (Gene Link, Hawthorne, NY); all primers were from PRIMM srl, Milan, Italy. Sequences of primer pairs used for Abl (reference gene) and for each gene of interest are available on request.

Acknowledgments

This study was supported by the following grants:

1) Associazione Italiana Mucopolisaccaridosi e Malattie Affini (Milan, Italy).

2) Telethon n. GGP07043.

3) Grant from MIUR-Italy, PRIN 2006.

REFERENCES

Ausseil, J., Desmaris, N., Bigou, S., Attali, R., Corbineau, S., Vitry, S., Parent, M., Cheillan, D., Fuller, M., Maire, I., Vanier, M.T., Heard, J.M., 2008. Early neurodegeneration progresses independently of microglial activation by heparan sulfate in the brain of mucopolysaccharidosis IIIB mice. PLoS ONE 3 (5), e2296.

Behrens, L., Bender, A., Johnson, M.A., Hohlfeld, R., 1997. Cytotoxic mechanisms in inflammatory myopathies. Co-expression of Fas and protective Bcl-2 in muscle fibres and inflammatory cells. Brain 120 (Pt 6), 929–938.

Bien, C.G., Bauer, J., Deckwerth, T.L., Wiendl, H., Deckert, M., Wiestler, O.D., Schramm, J., Elger, C.E., Lassmann, H., 2002. Destruction of neurons by cytotoxic T cells: a new pathogenic mechanism in Rasmussen's encephalitis. Ann. Neurol. 51 (3), 311–318.

Butterfield, D.A., Abdul, H.M., Newman, S., Reed, T., 2006. Redox proteomics in some age-related neurodegenerative disorders or models thereof. NeuroRx 3 (3), 344–357.

Cullen, S.P., Martin, S.J., 2008. Mechanisms of granule-dependent killing. Cell Death Differ. 15 (2), 251–262 Electronic publication 2007 Nov 2.

Di Natale, P., Di Domenico, C., Gargiulo, N., Castaldo, S., Gonzalez Y Reyero, E., Mithbaokar, P., De Felice, M., Follenzi, A., Naldini, L., Villani, G.R.D., 2005. Treatment of the mouse model of mucopolysaccharidosis type IIIB with lentiviral-NAGLU vector. Biochem. J. 388, 639–646.

DiRosario, J., Divers, E., Wang, C., Etter, J., Charrier, A., Jukkola, P., Auer, H., Best, V., Newsom, D.L., McCarty, D.M., Fu, H., 2009. Innate and adaptive immune activation in the brain of MPS IIIB mouse model. J. Neurosci. Res. 87 (4), 978–990.

Dröge, W., Schipper, H.M., 2007. Oxidative stress and aberrant signaling in aging and cognitive decline. Aging Cell 6, 361–370.

Glantz, S.A., 1998. Statistics in Biomedical Disciplines, 2nd Ed. McGraw-Hill Medical.

Hamano, K., Hayashi, M., Shioda, K., Fukatsu, R., Mizutani, S., 2008. Mechanisms of neurodegeneration in mucopolysaccharidoses II and IIIB: analysis of human brain tissue. Acta Neuropathol. 115, 547–559.

Heldermon, C.D., Hennig, A.K., Ohlemiller, K.K., Ogilvie, J.M., Herzog, E.D., Breidenbach, A., Vogler, C., Wozniak, D.F., Sands, M.S., 2007. Development of sensory, motor and behavioral deficits in the murine model of Sanfilippo syndrome type B. PLoS ONE 2 (1), e772.

Ho, T.W., Bristol, L.A., Coccia, C., Li, Y., Milbrandt, J., Johnson, E., Jin, L., Bar-Peled, O., Griffin, J.W., Rothstein, J.D., 2000. TGFbeta trophic factors differentially modulate motor axon outgrowth and protection from excitotoxicity. Exp. Neurol. 161 (2), 664–675.

Howe, C.L., Adelson, J.D., Rodriguez, M., 2007. Absence of perforin expression confers axonal protection despite demyelination. Neurobiol. Dis. 25 (2), 354–359 Electronic publication 2006 Nov 16.

Kramer, E.R., Aron, L., Ramakers, G.M., Seitz, S., Zhuang, X., Beyer, K., Smidt, M.P., Klein, R., 2007. Absence of Ret signaling in mice causes progressive and late degeneration of the nigrostriatal system. PLoS Biol. 5 (3), e39.

Li, H.H., Yu, W.H., Rozengurt, N., Zhao, H.Z., Lyons, K.M., Anagnostaras, S., Fanselow, M.S., Suzuki, K., Vanier, M.T., Neufeld, E.F., 1999. Mouse model of Sanfilippo syndrome type B produced by targeted disruption of the gene encoding alpha-N-acetylglucosaminidase. Proc. Natl. Acad. Sci. U. S. A. 96, 14505–14510.

Li, H.H., Zhao, H.Z., Neufeld, E.F., Cai, Y., Gomez-Pinilla, F., 2002. Attenuated plasticity in neurons and astrocytes in the mouse model of Sanfilippo syndrome type B. J. Neurosci. Res. 69 (1), 30–38.

Luetjens, C.M., Lankiewicz, S., Bui, N.T., Krohn, A.J., Poppe, M., Prehn, J.H., 2001. Up-regulation of Bcl-xL in response to subtoxic beta-amyloid: role in neuronal resistance against apoptotic and oxidative injury. Neuroscience 102 (1), 139–150.

Martınez, A., Dalfo, E., Muntane, G., Ferrer, I., 2008. Glycolitic enzymes are targets of oxidation in aged human frontal cortex and oxidative damage of these proteins is increased in progressive supranuclear palsy. J. Neural. Transm. 115, 59–66.

Metz, I., Lucchinetti, C.F., Openshaw, H., Garcia-Merino, A., Lassmann, H., Freedman, M.S., Atkins, H.L., Azzarelli, B., Kolar, O.J., Brück, W., 2007. Autologous haematopoietic stem cell transplantation fails to stop demyelination and neurodegeneration in multiple sclerosis. Brain 130 (Pt 5), 1254–1262 Electronic publication 2007 Feb 9.

Mihaljević, B., Katusin-Razem, B., Razem, D., 1996. The reevaluation of the ferric thiocyanate assay for lipid hydroperoxides with special considerations of the mechanistic aspects of the response. Free Radic. Biol. Med. 21 (1), 53–63.

Mikawa, S., Wang, C., Sato, K., 2006. Bone morphogenetic protein-4 expression in the adult rat brain. J. Comp. Neurol. 499 (4), 613–625.

Moreira, P.I., Smith, M.A., Zhu, X., Nunomura, A., Castellani, R.J., Perry, G., 2005. Oxidative stress and neurodegeneration. Ann. N. Y. Acad. Sci. 1043, 545–552.

Myerowitz, R., Lawson, D., Mizukami, H., Mi, Y., Tifft, C., Proia, R.L., 2002. Molecular pathophysiology in Tay-Sachs and Sandhoff diseases as revealed by gene expression profiling. Hum. Mol. Genet. 11 (11), 1343–1350.

Neufeld, E.F., Muenzer, J., 2001. The mucopolysaccharidoses, In: Scriver, CR, Beaudet, AL, Sly, WS, Valle, D (Eds.), The Metabolic and Molecular Bases of Inherited Disease, 8th Ed. McGraw-Hill, New York, pp. 3421–3452.

Ohmi, K., Greenberg, D.S., Rajavel, K.S., Ryazantsev, S., Li, H.H., Neufeld, E.F., 2003. Activated microglia in cortex of mouse models of mucopolysaccharidosis I and IIIB. Proc. Nat. Acad. Sci. USA 100, 1902–1907.

Paxinos, D.G., Watson, C., 2007. The Rat Brain in Stereotaxic Coordinates, 6th Ed. Academic Press.

Poon, H.F., Vaishnav, R.A., Getchell, T.V., Getchell, M.L., Butterfield, D.A., 2006. Quantitative proteomics analysis of differential protein expression and oxidative modification of specific proteins in the brains of old mice. Neurobiol. Aging 27, 1010–1019.

Ryazantsev, S., Yua, W.H., Zhao, H.Z., Neufeld, E.F., Ohmia, K., 2007. Lysosomal accumulation of SCMAS (subunit c of mitochondrial ATP synthase) in neurons of the mouse model of mucopolysaccharidosis III B. Mol. Genet. Metab. 90 (4), 393–401.

Savas, P.S., Hemsley, K.M., Hopwood, J.J., 2004. Intracerebral injection of sulfamidase delays neuropathology in murine MPS-IIIA. Mol. Genet. Metab. 82, 273–285.

Settembre, C., Fraldi, A., Jahreiss, L., Spampanato, C., Venturi, C., Medina, D., de Pablo, R., Tacchetti, C., Rubinsztein, D.C., Ballabio, A., 2008. A block of autophagy in lysosomal storage disorders. Hum. Mol. Genet. 17 (1), 119–129 Electronic publication 2007 Oct 3.

Stefanis, L., Keller, J.N., 2006. The Proteasome in Neurodegeneration. Springer, New York.

Sultana, R., Pierluigi, M., Butterfield, D.A., 2006. Protein oxidation and lipid peroxidation in brain of subjects with Alzheimer's disease: insights into mechanism of neurodegeneration from redox proteomics. Antioxid. Redox Signal 8 (11–12), 2021–2037.

van Montfoort, N., de Jong, J.M., Schuurhuis, D.H., van der Voort, E.I., Camps, M.G., Huizinga, T.W., van Kooten, C., Daha, M.R., Verbeek, J.S., Ossendorp, F., Toes, R.E., 2007. A novel role of complement factor C1q in augmenting the presentation of antigen captured in immune complexes to CD8+ T lymphocytes. J. Immunol. 178 (12), 7581–7586.

Villani, G.R.D., Gargiulo, N., Faraonio, R., Castaldo, S., Gonzalez y Reyero, E., Di Natale, P., 2007. Cytokines, neurotrophins, and oxidative stress in brain disease from mucopolysaccharidosis IIIB. J. Neurosci. Res. 85, 612–622.

Wang, X., Seed, B., 2003. A PCR primer bank for quantitative gene expression analysis. Nucleic Acids Res. 31 (24), 1–8 e154.

Wu, Y.P., Proia, R.L., 2004. Deletion of macrophage-inflammatory protein 1a retards neurodegeneration in Sandoff disease mice. Proc. Nat. Acad. Sci. 101 (22), 8425–8430.

Wu, D.C., Teismann, P., Tieu, K., Vila, M., Jackson-Lewis, V., Ischiropoulos, H., Przedborski, S., 2003. NADPH oxidase mediates oxidative stress in the 1-methyl-4-phenyl-1,2,3,6-tetrahydropyridine model of Parkinson's disease. Proc. Natl. Acad. Sci. U. S. A. 100 (10), 6145–6150 Electronic publication 2003 Apr 29.

blood

Prepublished online Sep 16, 2010;
doi:10.1182/blood-2010-04-278234

Gene therapy augments the efficacy of hematopoietic cell transplantation and fully corrects Mucopolysaccharidosis type I phenotype in the mouse model

Ilaria Visigalli, Stefania Delai, Letterio S. Politi, Carmela Di Domenico, Federica Cerri, Emanuela Mrak, Raffaele D'Isa, Daniela Ungaro, Merel Stok, Francesca Sanvito, Elisabetta Mariani, Lidia Staszewsky, Claudia Godi, Ilaria Russo, Francesca Cecere, Ubaldo del Carro, Alessandro Rubinacci, Riccardo Brambilla, Angelo Quattrini, Paola Di Natale, Katherine Ponder, Luigi Naldini and Alessandra Biffi

Blood (print ISSN 0006-4971, online ISSN 1528-0020), is published semimonthly by the American Society of Hematology, 1900 M St, NW, Suite 200, Washington DC 20036.

Running title: HSC gene therapy corrects MPS I disease

Gene therapy augments the efficacy of hematopoietic cell transplantation and fully corrects Mucopolysaccharidosis type I phenotype in the mouse model

Ilaria Visigalli[1,2,#], Stefania Delai[1,3,#], Letterio S. Politi[4], Carmela Di Domenico[5], Federica Cerri[6], Emanuela Mrak[7], Raffaele D'Isa[8], Daniela Ungaro[9], Merel Stok[10], Francesca Sanvito[11], Elisabetta Mariani[12], Lidia Staszewsky[13], Claudia Godi[4], Ilaria Russo[13], Francesca Cecere[5], Ubaldo del Carro[9], Alessandro Rubinacci[7], Riccardo Brambilla[8], Angelo Quattrini[6], Paola Di Natale[5], Katherine Ponder[14], Luigi Naldini[1,2], Alessandra Biffi[1,*]

[1]San Raffaele Telethon Institute for Gene Therapy, Regenerative Medicine, Gene and Cell Therapy, [2]Vita Salute San Raffaele University, [4]Neuroradiology Group, Imaging Core, [6]Experimental Neuropathology Unit, Neuroscience Dept., [7]Bone Metabolism Unit, [8]Molecular Genetics of Behavior Unit, Neuroscience Dept., [9]Movement Disorders Unit, Neuroscience Dept., [11]Mouse HistoPathology Unit, [12]Bone Physiopathology Program (BoNetwork), San Raffaele Scientific Institute, Milan, Italy; [3]University of Perugia, Italy; [5]Department of Biochemistry and Medical Biotechnology, University of Naples Federico II, Naples, Italy; [10]Erasmus MC, Rotterdam, NL; [13]Department of Cardiovascular Research, Mario Negri Institute, Milan, Italy; [14]Division of Hematology, Department of Internal Medicine, Washington University School of Medicine, St. Louis, MO, USA.

*Please address correspondence to: Alessandra Biffi, MD; HSR-TIGET, San Raffaele Scientific Institute, Via Olgettina 58, Milan – Italy; Phone (39) 02.2643.4681; Fax (39) 02.2643.4668; e-mail: biffi.alessandra@hsr.it.

[#]These authors equally contributed to the work.

ABSTRACT

Type I Mucopolysaccharidosis (MPS I) is a lysosomal storage disorder caused by the deficiency of α-L-iduronidase, which results in glycosaminoglycan accumulation in tissues. Clinical manifestations include skeletal dysplasia, joint stiffness, visual and auditory defects, cardiac insufficiency, hepatosplenomegaly and mental retardation, the latter being present exclusively in the severe Hurler variant. The available treatments - enzyme replacement therapy and hematopoietic stem cell transplantation (HCT) - can ameliorate most disease manifestations, but their outcome on the skeletal and brain disease could be further improved. We here demonstrate that hematopoietic stem cell (HSC) gene therapy based on lentiviral vectors (LV) completely corrects the disease manifestations in the mouse model. Of note, the therapeutic benefit provided by gene therapy on critical MPS I manifestations, such as the neurological and skeletal disease, greatly exceeds the one exerted by HCT, the standard of care treatment for Hurler patients. Interestingly, therapeutic efficacy of HSC gene therapy is strictly dependent from the achievement of supra-normal enzyme activity in the hematopoietic system of transplanted mice, which allows enzyme delivery to the brain and skeleton for disease correction. Overall, our data provides evidence of an efficacious treatment for MPS I Hurler patients warranting future development towards clinical testing.

INTRODUCTION

Type I Mucopolysaccharidosis (MPS I) is one of the most frequent lysosomal storage disorders (LSD) and is due to the inherited deficiency of α-L-iduronidase (IDUA) activity, which results in the accumulation of its unprocessed substrates (glycosaminoglycans – GAGs) in many organs[1]. The disorder is systemic and clinically heterogeneous. Clinical manifestations include skeletal dysplasia, joint stiffness, visual and auditory defects, cardiac insufficiency, hepatosplenomegaly and mental retardation. The clinical spectrum ranges from the severe Hurler syndrome (MPS I-H) to the attenuated Scheie syndrome. Mental retardation is distinctive only of MPS I-H, which is fatal in childhood if untreated, thus representing the variant with the most urgent need for new therapies. Enzyme replacement therapy (ERT)(parenteral administration of exogenous enzyme that can be internalized by tissue cells *via* the mannosium-6-phosphate receptor) is recommended only for MPS I patients without primary neurological disease, due to the inability of the enzyme to efficiently cross the blood-brain barrier; moreover, neutralizing antibodies can attenuate its efficacy[2]. When performed at early ages, hematopoietic stem cell transplantation (HCT) from healthy donors alleviates most of the disease manifestations in MPS I-H patients, likely by migration of the transplant-derived leukocytes into organs, where they can clear the storage and secrete the functional enzyme for correction of the metabolic defect in resident cells[3]. However, despite recent improvements in the outcome of HCT, the morbidity and mortality associated with the procedure are still not negligible, mostly due to rejection and graft-versus-host

disease. Moreover, the amount of enzyme that transplantation can provide to the organism can be limiting, especially since donors are often heterozygous siblings. Indeed, a relationship between circulating enzyme levels after transplant and the urinary GAGs has been shown[4]: the low enzyme levels achieved with heterozygote donor transplant lead to less adequate reduction in GAG levels. Likely due to partial metabolic correction at disease sites, the impact of HCT on central nervous system (CNS) and skeletal disease, despite being substantial in ameliorating patients' phenotype, could still benefit from further improvement[5].

The benefits of different gene therapy approaches were established in MPS I animal models. Intravenous delivery of viral vectors, which can establish a tissue source for systemic enzyme distribution, was effective in controlling disease manifestations in MPS I animal models upon neonatal treatment[6-9]. However, residual disease still affected the nervous and skeletal tissues and the aorta of mice treated with this approach in adulthood[10,11]. This limited efficacy could be due to insufficient enzyme delivery *via* the bloodstream to tissues, such as the brain, protected by physiological barriers or poorly vascularized, like the skeleton, and/or to immune-mediated clearance of the liver-secreted enzyme.

Hematopoietic stem cell (HSC) gene therapy has also been developed. When oncoretroviral vectors were used for gene transfer, HSC gene therapy proved to be effective in restoring the enzyme activity and providing therapeutic effects on visceral organs of MPS I mice. However, the CNS disease was not adequately corrected[12]. Others and we demonstrated that lentiviral vectors (LV) constitute a valuable alternative to oncoretroviral vectors, enabling more

efficient marking of murine and human hematopoietic stem and progenitor cells (HSPC) and robust, long-term transgene expression in their progeny[13-19]. LV were employed to transduce HSPC and direct IDUA expression in an erythroid-specific manner by the use of a lineage-specific promoter in the MPS I mouse model[20]. This approach generated an intravascular enzyme source, namely gene modified erythrocytes, which could efficiently release the enzyme in the plasma for distribution to the affected tissues. Interestingly, the treatment reproduced the efficacy of in vivo gene therapy approaches and of HCT, but did not provide an increased benefit in correcting neurological disease manifestations. Conversely, we previously showed that transplantation of HSPC transduced with ubiquitously expressing LV prevents and corrects neurological disease manifestations in mice affected by another LSD (metachromatic leukodystrophy-MLD)[18,21], for which HSC gene therapy has now entered clinical testing. The efficacy of the approach was shown to be dependent on the CNS infiltration of myeloid cells producing supra-normal enzyme quantities and conveying the protein through the blood brain barrier[18]. According to these results, we hypothesized that LV-driven, supra-normal IDUA reconstitution above wild type (WT) levels in HSPC and their differentiated progeny could improve the outcome of the previously tested approaches in correcting the neurological (and skeletal) disease in MPS I. We thus addressed here this hypothesis and challenged MPS I disease in mice with the transplantation of WT and LV-transduced *Idua*$^{-/-}$ HSPC, in which enzymatic activity was restored to supra-normal levels.

MATERIALS and METHODS

Mice studies

Idua$^{-/-}$ mice (C57BL/6 background)[22] were imported in our animal facility as a kind gift of Prof. J.M. Heard and intercrossed to obtain an inbred strain. Rag2$^{-/-}$ γchain$^{-/-}$ mice[23] were obtained from the Central Institute for Experimental Animals (Nogawa, Japan). All procedures were approved by the Animal Care and Use Committee of the Fondazione San Raffaele del Monte Tabor (IACUC 325) and communicated to the Ministry of Health and local authorities according to Italian law.

Transduction and transplantation of hematopoietic progenitors

Eight-week-old WT or MPS I mice were sacrificed with CO_2 and the bone marrow (BM) was harvested by flushing femurs and tibiae. HSPC were purified for lineage$^-$ selection using the Enrichment of Murine Hematopoietic Progenitors kit (Stem Cell Technologies Inc., Vancouver, British Columbia, Canada), and transduced at Multiplicity of Infection (MOI) 100 with IDUA- or GFP-encoding LV (IDUA-LV, GFP-LV)[21]. Transduced cells (10^6 cells/mouse) were injected in the tail vein of 8-week-old WT or MPS I mice after lethal irradiation (12Gy). Transduced cells were also cultured for 14 days for IDUA activity measurement (liquid culture[21]) and for PCR quantitative analysis for the LV sequences (clonogenic assays)[18].

Behavioral studies

Spontaneous locomotor activity was recorded in 41x41x33 (height) cm Perspex activity cages (Ugo Basile, Comerio, Varese, Italy), equipped with infrared light photocell beams. The lower arrays of aligned infrared emitters and detectors measured the number of transitions (horizontal activity), while vertical arrays measured rearing. Mice were placed individually in the activity cages and their activity was recorded in a low luminosity environment in a daily session of 10 minutes for three consecutive days. The percentage change between the first and third trial was employed as outcome measure.

Auditory brainstem response (ABR) measurement

Needle scalp electrodes were used to record sound-evoked bioelectrical potentials for evaluation of the central and peripheral auditory function and to identify hearing deficits related to the auditory pathway from the cochlea to the auditory midbrain[24]. Five positive peaks in the ABR waves are expected. In the mouse, peak I refers to cochlear processing, peak II to processing in the cochlear nucleus complex, peak III in the complex of the superior olive, peak IV in the lateral lemniscus and peak V in the colliculus inferior.

ABR to pure tones were recorded in anesthetized animals. We recorded latency of peaks I, III, IV, V and the latency between peaks I-III, III-V and I-V. We calculated the average and SD of the latency of each peak in WT mice. In each mouse and for each peak a score based on the difference between the latency recorded and the respective average in WT animals ± SD was then calculated. Abnormalities in the latencies were graded in a 3-degrees ordinal scale (0=normal finding, i.e. individual peak latency not exceeding control mean peak latency ± 1

SD; 1= slight increase, with latency ranging between 1 and 2 SDs; 2= increase, with latency between 2 and 3 SDs; 3= great increase with latency greater than 3 SDs, or ABR absence). This allowed not to drop out mice without ABR responses and to properly evaluate ABR absence as the highest degree of functional impairment due to pathology.

Computerized Tomography

CT scans were performed on a human-grade 64-channel multi-slice apparatus (Light Speed VCT, GE Healthcare USA). The imaging protocol included a bi-planar scout and a helical volumetric CT acquisition with coverage of the whole body, with a tube speed rotation of 0.5 seconds (s), 0.625mm slice thickness and 0.3mm/s table motion, 120KV, 680mA, reconstruction field of view of 17 cm and matrix of 512x512. CT images were filtered with both the standard parenchyma and the high-resolution bone algorithms.

Skull width was measured on axial reformatted images considering the largest diameter; femur length was determined by measuring its long axis in between the two epiphysis; humerus width was measured in the middle of the diaphysis. The analysis was performed using OsiriX v.3.5.1 software.

On a dedicated workstation (Advantage 4.4, GE Healthcare USA) both the zygomatic regions were manually isolated; an automatic segmentation with bone threshold >160U.H. was applied to the regions of interest and corresponding volumes were measured through a manufacturer's software.

Animal sacrifice modalities

At sacrifice mice were trans-cardially perfused with saline for 15 minutes, upon administration of 0.02ml/g body weight tribromoethanole (Avertine; Sigma). Thereafter, organs were collected as described in Supplemental Methods.

IDUA activity assay

Enzyme activity was measured fluorometrically as described[12]. See Supplemental Methods for details.

Analysis of glycosaminoglycans in tissues and urine

GAGs were quantified as described[25-27]. See Supplemental Methods for details.

Histopathology

Semithin sections were conducted as described[18]. Sections (0.5–1μm thick) were stained with toluidine blue and examined by light microscopy. For quantification of vacuoles aggregates, digitalized images of sections from all tissues, at the same level, were obtained with a digital camera (Leica DFC300F) at x100 magnification. At least three images from four different animals *per* group were acquired with the Leica QWin software (Leica Mycrosystem). An arbitrary score (from 0 to 4) was given by the investigators (two blinded and experienced pathologists, A.Q. and F.C.) on the basis of the percentage of vacuoles observed in each x100 field.

Quantitative PCR analysis

Vector copies *per* genome were quantified by TaqMan analysis as described[17,18].

Peripheral quantitative CT

Peripheral Quantitative CT (pQCT) measurements were performed *ex vivo* on fixed tibiae and femurs. The SSI was calculated by the manufacturer's software as follows: SSI = ∑i = 1,n r2 • aCD/ ND • rmax, where "r" is the distance of a voxel from the center of gravity, "rmax" is the maximum distance of a voxel from centre of gravity, "a" is the area of a voxel, "CD" is the cortical density and "ND" is the density of normal cortical bone tissue equal to 1200mg/cm^3, as measured by pQCT when no spaces are included. To account for changes in the mineralization of bone and therefore for changes in material properties, the section modulus was normalized for this value in the pQCT software. See Supplemental Methods for details.

Statistics

Statistical analyses were made by either Student's *t* test or one-way Anova for repeated measurements using Bonferroni's test for *post-hoc* analysis after significant main effect of the treatment (confidence interval 95%).

RESULTS

Gene therapy and not HCT allows efficient delivery of the functional enzyme to all MPS I affected tissues

We transduced lineage$^-$ HSPC isolated from the BM of *Idua*$^{-/-}$ and *Idua*$^{+/+}$ mice with IDUA-LV or GFP-LV, as described[18]. *Idua*$^{-/-}$ IDUA-LV transduced cells showed an average vector copy number per genome (VCN) of 11±3 (tested on clonogenic progenitors) and over-expressed the enzyme (whose expression was driven by the human PGK promoter) at up to 200 fold the levels detected in mock-transduced *Idua*$^{+/+}$ HSPC, after 14 days of in vitro liquid culture (data not shown). The transduced cells were transplanted into 2 month-old lethally irradiated MPS I and WT littermates according to the procedure shown in Figure 1A. Interestingly, while transplantation of WT GFP-LV transduced cells reconstituted a normal IDUA activity in the peripheral blood mononuclear cells (PBMCs), supra-normal enzyme expression (up to 150 fold the low WT levels) was measured in the PBMCs of gene therapy treated (GT) mice short- and long-term after the transplant (Figure 1B). Supra-normal enzymatic activity was also measured 6 months after the transplant in the serum (Figure 1C) and in all the tested tissues of GT mice, including the brain, where activity levels up to 4.5 fold the WT were detected (Figure 1D). Of note, transplantation of GFP-transduced WT HSPC (HCT), despite being capable of reconstituting a normal enzymatic activity in the spleen of the MPS I mice, reconstituted only below-normal enzyme activity in the liver, kidney and heart, and failed to deliver detectable amounts of the functional enzyme to the brain (Figure 1D).

The efficiency of enzyme delivery to the brain of GT mice significantly correlated with the level of enzymatic activity in PBMCs and with the VCN measured in the BM (Figure S1A-C). In particular, IDUA activity values in PBMCs above 1500 nmol/mg/h (average value of GT mice) and VCN higher than 5 in the BM (average VCN measured on the BM of the GT mice cohort) consistently allowed efficient delivery of IDUA to the brain (up to ≥ 2 fold the levels of WT controls) (Figure 1D-E).

Supra-normal enzymatic activity allows metabolic correction in the affected tissues

To evaluate the extent of metabolic correction at diseased sites upon transplantation of either gene corrected or WT HSPC, we performed a semi-quantitative assessment of the storage on tissue sections from treated and control animals. Cytoplasmic vacuoles were scored, being distended lysosomes from which GAGs were leached by fixation. Storage was abundant in the kidney, liver (within hepatocytes and Kuppfer cells), spleen (predominant in the red pulp), heart (abundant in the endothelium and myocytes) and in the brain (where storage occurs within endothelial cells and neurons) of MPS I mock-transplanted animals (Figure 2A-B). Variable reduction of storage was observed in HCT mice, with reduction being more evident in hematopoietic lineage cells rather than in resident non-hematopoietic cell populations (see storage in hepatocytes in Figure 2A). Almost complete clearance of the storage was observed only in the spleen, where the highest enzyme activity was measured and where the hematopoietic lineage is the most affected (Figure 2B and Figure 1D).

Conversely, a significantly greater benefit was observed in GT mice, in which the storage material was almost undetectable in all examined tissues (Figure 2A and 2B). Storage was cleared from both hematopoietic and non-hematopoietic lineage cells, suggesting the occurrence of cross-correction of the resident populations.

GAGs were also quantified in the urine and in the diseased tissues of mock-transplanted and treated mice (Figure 2C-D). Normalization of urinary (Figure 2C) and tissue GAGs (Figure 2D) was observed in GT mice, demonstrating complete correction of the metabolic defect, both systemically and at relevant diseased sites; transplantation of WT HSPC resulted in complete storage removal from the spleen, but only in partial clearance of GAGs from the other tissues (liver and kidney are shown as representative)(Figure 2D).

The elevation of heparin cofactor II-thrombin (HCII-T) complex is a biomarker for MPS I that appears to correlate with disease severity and is responsive to treatment[28,29]. HCII-T presence was tested on the serum of treated and control animals by western blot analysis. Reduction of HCII-T complex down to WT levels was observed in the serum of GT mice (Figure 2E), further confirming that metabolic correction was attained.

Differential neurological outcome of gene therapy and HCT

Six months after the treatment, treated and control mice underwent behavioral studies. To study adaptive behavior and identify memory deficits, a repeated open field test was performed exposing the mice to the same open field for 3 repeated trials conducted in 3 sequential days. Horizontal and rearing activities were scored and the percentage of change between performance at

first and at third trials was used as outcome measure. While the defective adaptive behavior of MPS I mice at horizontal activity testing was not ameliorated in HCT mice, which had barely detectable IDUA activity in the brain, it was normalized in GT mice, which showed up to 4.5 fold the WT enzyme activity in the CNS (Figure 3A and 1D). Interestingly, the extent of correction of the behavioral phenotype well correlated with the VCN measured in the BM and with the IDUA activity measured in the brain of the treated mice (Figure S1D-E). A threshold value for IDUA activity in the brain allowing for efficacious correction of the neurological phenotype in GT mice could be established at 20nmol/mg/h, which corresponds to the mean brain activity value of the entire cohort (Figure 3B). Similar results were observed when measuring rearing activity (data not shown).

To further assess the efficacy of gene therapy in correcting MPS I-associated damage in the nervous system, we examined the Purkinje cell layer of the cerebellum of treated and control animals: we quantified the integrity of the layer (number of Purkinje cells within all the circumvolutions of each section) and evaluated the degeneration of the cells present in the layer (Figure 3C-D). Interestingly, the reduced density of Purkinje cells observed in mock-transplanted MPS I mice was normalized to WT density by gene therapy (Figure 3C). Moreover, the degeneration of the Purkinje cells was greatly reduced in GT animals as compared to mock-transplanted affected controls (Figure 3C-D). HCT exerted only a partial benefit on the Purkinje cells (Figure 3 C-D).

Differential skeletal outcome of gene therapy and HCT

Treated and control mice underwent total body Computed Tomography (CT) scans to characterize their skeleton. The width of the skull and of the humerus and femur, as well as the length of the femur were measured on CT scans. Moreover, the volume of the zygomatic bones was measured on three-dimensional reconstructions. Interestingly, direct inspection (Figure 4A), CT imaging (Figure 4B) and bone measurements on CT scans (Figure 4C-F) demonstrated an almost complete normalization of all analyzed parameters in GT mice as compared to mock-transplanted affected siblings, whereas HCT provided a partial benefit on skeletal abnormalities. The extent of correction of the skeletal phenotype was greater in the presence of higher IDUA expression in PBMCs of GT mice, as shown for the femur length, which is representative of the other tested parameters (Figure 4G). Similar results were obtained by the assessment of the densitometric and geometrical parameters of the appendicular long bones (femur and tibia) at pQCT. The bone phenotype of the affected mice was characterized by increased size and density at comparison with WT animals (data not shown). The polar Strength Strain Index (SSI) of the femur and tibia was analyzed as a representative parameter accounting for the resistance of the long bones towards torsion (obtained from pQCT cross sectional scanning), based on bone density and size. The SSI of GT mice was significantly lower than that of mock-transplanted affected littermates and not distinguishable from the SSI of WT animals (Figure 4H). Moreover, the SSI of GT mice was also significantly lower than that of HCT mice, confirming the poor efficacy of the latter procedure in correcting the MPS I-associated skeletal disease (Figure 4H).

Histopathologic evaluation of the epiphysis of the long bones from control and treated animals confirmed the CT and pQCT findings. Disorganization of the growth plate, with irregular morphology and cell distribution, was demonstrated in both mock-transplanted MPS I mice and animals treated by HCT; on the contrary, the growth plate of GT animals appeared undistinguishable from that of WT mice for morphology and cellular organization (Figure 5A). In order to quantitatively describe the morphology of the growth plate in the different groups of animals, we performed a morphometric analysis (as detailed in Figure S2). Briefly, we measured i) the ratio between the perimeter and the length of the growth plate as a quantitative measure of its altered morphology (the higher is the ratio, the most irregular and undulate is the growth plate) and ii) the number of chondrocytes aligned in columns perpendicular to the major axis of the growth plate (chondrocytes aligned in perpendicular columns are instrumental for correct bone growth in length and thus are pre-requisites for a normal function of the growth plate). These measurements confirmed that the growth plate in mock-treated MPS I mice has a highly irregular morphology and is disorganized, having a very high perimeter/length ratio and a very low number of aligned chondrocytes as compared to WT mice (Figure 5B and C). Interestingly, gene therapy was associated to a normalization of the morphology of the growth plate, with normalized perimeter/length ratio and increased number of aligned chondrocytes; minor correction of both parameters was observed upon transplantation of WT HSPC (Figure 5B and C).

Restoration of auditory function and retinal thickness in GT mice

GT and control animals underwent neurophysiological studies for measurement of their Auditory Brainstem Responses (ABR) (Figure 6A-B). Interestingly, while up to 60% of mock-transplanted MPS I mice were deaf at ABR testing, only 20% of the GT animals showed a substantial hearing impairment. Moreover, scoring of latencies of peaks I, III, IV and V demonstrated a significantly reduced latency of all tested waves in GT as compared to mock-transplanted MPS I mice (the latency of peaks I, referring to cochlear processing, and IV, referring to processing in the lateral lemniscus, are shown as representative) (Figure 6B), confirming amelioration of the auditory function in affected mice upon treatment.

Measuring the thickness of the retina of treated and control mice allowed us assessing the impact of gene therapy on the visual system. In particular, the reduction of retinal thickness observed in mock-treated MPS I mice was corrected to values in the range of WT controls by gene therapy (Figure 6C-D).

Other phenotype outcome measures

Treated and control mice underwent echo-cardiographic evaluation to study the disease-associated cardiac abnormalities. However, the study failed to provide relevant information, likely due to a confounding influence of the lethal irradiation. Indeed, echo-cardiography revealed valve disease (thickening of mitral and aortic valves, isolated or combined mitral and aortic regurgitation) in 60% and 70% of the mock-transplanted WT and MPS I animals, respectively. Furthermore, mock-transplanted MPS I mice did not present a

significant left ventricular dilatation or increased wall thickness, but rather showed a thickened pericardium (see also Figure S3). Splenomegaly was not observed in treated and mock-transplanted animals as compared to untreated MPS I controls due to the irradiation procedure (Figure S3).

Tolerability of gene transfer and enzyme supra-normal expression in murine and human HSPC

To evaluate the tolerability of the treatment, mice underwent bleeding for hemocytometric evaluation and cytofluorimetry (peripheral blood immunophenotype for T and B lymphocytes and myeloid cells) before sacrifice. Moreover, gross necroscopy was performed on each animal and liver, spleen, thymus plus any suspect lesion were processed for pathology. No hematological abnormalities or altered proportion of blood lineages were detected in the peripheral blood of tested animals after recovery from transplant (Figure S4). Southern-blot analysis detecting the LV sequence (by a PRE-specific probe[21]) on the spleen DNA from a small subset of treated and control mice demonstrated a smear suggestive of absence of predominant clones (data not shown). Pathology identified two liver- and spleen-infiltrating B cell lymphomas, one in a mock-transplanted MPS I mouse and one in the gene therapy cohort; the lesions were vector-negative (data not shown). These findings are consistent with the reported high incidence of B cell lymphomas in the C57Bl6 strain[30,31]. The repopulation and differentiation ability of the transduced cells in the lethally irradiated recipients (Figure S4) indicates that IDUA supra-normal expression does not affect the function of murine HSPC (engraftment failure frequency <10%).

In the perspective of a future clinical translation of this approach, we assessed the feasibility and tolerability of IDUA supra-normal expression at the levels shown to be therapeutic in mice on human CD34+ HSPC isolated from normal cord blood. Transduction performed according to established protocols[17] allowed obtaining enzyme supra-normal expression up to 150 folds above un-transduced controls (measured after 14 days of in vitro liquid culture) (Figure S5 A) in the presence of a number of LV integrations (1.05 ± 0.35, measured after 14 days of in vitro semisolid culture of progenitors – colonies from CFC assay) lower than that required to obtain similar expression levels in murine HSPC. Importantly, when transplanted into sub-lethally irradiated $Rag2^{-/-}$ $\gamma chain^{-/-}$ mice[23], IDUA over-expressing cells long-term repopulated the hematopoietic organs of chimeric mice with efficiency comparable to un-transduced cells (Figure S5B) and underwent multilineage differentiation (Figure S5C-E). Importantly, the cells retained IDUA supra-normal expression long-term in vivo (Figure S5F). Of note, IDUA activity measured in the murine tissues was proportional to the human cell engraftment in each organ (Figure S5G).

DISCUSSION

The data here described, which result from a comparison of the transplantation of engineered *versus* WT HSPC, indicate that gene therapy represents an effective and applicable therapeutic opportunity for MPS I patients warranting future development towards clinical testing. Indeed, we here demonstrate that gene-corrected cells are capable of robust and effective delivery of the functional IDUA enzyme to diseased tissues, including the CNS, where supra-normal enzymatic activity was measured. This finding is particularly relevant in light of the inability of WT HSPC transplantation as well as of other tested gene therapy approaches to deliver comparable amounts of enzyme to the brain. The efficient delivery of IDUA to diseased sites was associated with metabolic correction of the affected tissues, as shown by the clearance of accumulated GAGs within hematopoietic and non-hematopoietic cells. This finding suggests the occurrence of active secretion of the functional enzyme by the gene corrected progeny of the transplanted cells and its re-uptake by the resident populations. Importantly, the efficient clearance of the storage material achieved by gene therapy allowed obtaining complete correction of the MPS I-associated phenotype. To our knowledge, we here provide first evidence of correction to normal of the MPS I neurological and skeletal defects. In particular, behavioral defects as well as neurodegeneration in the CNS were corrected, with dependence from enzymatic activity levels. Similarly, IDUA over-expression in the hematopoietic system allowed correcting the disease-associated morphological, morphometric and densitometric abnormalities of the skeleton and a dose-

effect relationship was shown. Despite functional data on the correction of the heart disease could not be obtained due to limitations of the procedure, the differential clearance of the storage in the heart confirmed the higher proficiency of gene therapy as compared to HCT also at this disease site. Further studies employing either sub-lethal irradiation or pharmacological myeloablation will better investigate this finding. Furthermore, when other outcome measures were considered, GT mice showed a significantly improved phenotype up to almost complete normalization of each of the tested parameters. Overall, these results indicate that LV-mediated gene therapy has a superior proficiency as respect to both HCT and other previously tested HSC gene therapy approaches, which were shown to reduce the manifestations of MPS I in mice in a similar way to HCT in humans[12,20]. Notably, disease correction was obtained upon treatment of adult animals. Furthermore, these data demonstrate that LV-mediated gene transfer into HSPC and their progeny is critical for attaining IDUA supra-normal delivery to those tissues requiring high enzyme levels for metabolic and functional correction.

Increasing evidences of partial amelioration of histopathological abnormalities related to lysosomal storage after systemic vector or enzyme administration in LSD animal models treated in adulthood are accumulating[32-36]. These results, which in some cases are not associated to an overt benefit in terms of neurological symptoms alleviation, are far from being understood. Anyhow, the efficacy of HSC gene therapy could also be related to some IDUA protein being secreted by the transduced hematopoietic cells into the bloodstream.

From the circulation the enzyme could have crossed the blood-brain-barrier and reached the brain independently from the infiltration of gene-corrected myeloid cells. However, the results recently obtained by Wang and colleagues using an erythroid specific expression cassette in the context of a HSPC transplant protocol, demonstrate that enzyme delivery to the brain by serum enzyme crossing the blood-brain-barrier can provide only partial benefit to the MPS I neurological disease[20]. We can thus hypothesize that the amount of enzyme delivered to the CNS by this approach is lower than what we obtained, indicating that myeloid cells over-expressing the enzyme could significantly increase IDUA delivery to the CNS (and possibly to the skeleton). Of note, these results were obtained in the context of a procedure well known to induce tolerance to the foreign protein without the need for long-term immuno-suppression of the host[10].

Therapeutic efficacy shown by gene therapy is here strictly dependent from supra-normal levels of IDUA activity within the hematopoietic system of treated mice: high levels of enzyme are indeed required to correct the metabolic and functional defect in the MPS I brain and skeleton. Such a requirement for lysosomal enzyme robust delivery to disease sites could be met only upon the efficient transduction of HPSC by advance generation LV. An experimental threshold of 1500nmol/mg/h measured on circulating hematopoietic cells (~100 fold the activity detected in the PBMC of WT animals) could be identified as critical for achieving the largest benefit in treated mice. Importantly, in terms of potential for clinical translation, we demonstrated that similar expression levels could be obtained in human

HSPC with a limited amount of LV integrations (1 LV copy *per* cell on average) due to the higher proficiency of the human phosphoglycerate kinase promoter in human cells. Moreover, we tested the tolerability of LV-mediated IDUA expression at these supra-normal values in both murine and human HSPC. The unaffected long-term repopulation and differentiation potential of the transduced IDUA over-expressing HSPC demonstrated that supra-normal IDUA activity does not detectably affect HSPC functional properties, as tested in vivo. Further follow up studies will allow demonstrating the long-term safety of this approach. However, the safety and the overall therapeutic potential of HSC gene therapy are already supported by a large amount of preclinical studies[37,38] and, most importantly, by the recently reported promising follow up of the adrenoleukodystrophy patients treated by means of LV-based HSC gene therapy[19].

In conclusion, we here demonstrate that LV-mediated HSC gene therapy allows efficacious enzyme delivery to all MPS I affected tissues, resulting in complete correction of disease manifestations, including neurological and skeletal abnormalities that are refractory to correction by other therapeutic approaches. Therefore, LV-based HSC gene therapy represents an efficacious strategy for the treatment of storage diseases with systemic and CNS involvement, and, upon further development, might become an attractive option for MPS I-H patients, potentially capable of addressing the disease manifestations refractory to correction by ERT and HCT.

ACKNOWLEDGMENTS

We are indebted to J.M. Heard for providing MPS I mice, R. Latini for echo-cardiography studies, M. Ponzoni for pathology, A. Rovelli, S. Cenci and G. Wagemaker for critical discussion of the data. This research was supported by grants from the National MPS Society to AB and the Italian Telethon to AB and LN.

AUTHORSHIP CONTRIBUTION

I.V., S.D., L.S.P. performed research and analyzed the data, C.D.D., F.C., E.M., R.D'I., D.U. M.S. F.S., E.M. C.G., I.L. F.C. performed research, L.S., U.D.C., A.R., R.B., A.Q., P.D.N. analyzed the data, L.N. and K.P. interpreted the data and edited the manuscript, A.B. designed experiments, interpreted the data and wrote the manuscript.

CONFLICT OF INTEREST

None of the authors declares any conflict of interest.

REFERENCES

1. Hopwood JJ, Morris CP. The mucopolysaccharidoses. Diagnosis, molecular genetics and treatment. *Mol Biol Med*. . 1990;7(5):381-404.
2. Pastores GM. Laronidase (Aldurazyme): enzyme replacement therapy for mucopolysaccharidosis type I. *Expert Opin Biol Ther*. 2008;8(7):1003-1009.
3. Staba SL, Escolar ML, Poe M, et al. Cord-Blood Transplants from Unrelated Donors in Patients with Hurler's Syndrome. *N Engl J Med*. 2004;350(19):1960-1969.
4. Wynn RF, Wraith JE, Mercer J, et al. Improved metabolic correction in patients with lysosomal storage disease treated with hematopoietic stem cell transplant compared with enzyme replacement therapy. *J. Pediatr*. 2009;154(4):609-611.
5. Muenzer J, Fisher A. Advances in the treatment of mucopolysaccharidosis type I. *N Engl J Med*. 2004;350(19):1932-1934.
6. Traas AM, Wang P, Ma X, et al. Correction of clinical manifestations of canine mucopolysaccharidosis I with neonatal retroviral vector gene therapy. *Mol Ther*. 2007;15(8):1423-1431.
7. Metcalf JA, Ma X, Linders B, et al. A Self-inactivating gamma-Retroviral Vector Reduces Manifestations of Mucopolysaccharidosis I in Mice. *Mol Ther*. 2009;[Epub ahead of print] PMID: 19844196.
8. Chung S, Ma X, Liu Y, Lee D, Tittiger M, Ponder KP. Effect of neonatal administration of a retroviral vector expressing alpha-l-iduronidase upon lysosomal storage in brain and other organs in mucopolysaccharidosis I mice. *Mol Genet Metab*. 2007;90(2):181-192.
9. Liu Y, Xu L, Henning AK, et al. Liver-directed neonatal gene therapy prevents cardiac, bone, ear, and eye disease in mucopolysaccharidosis I mice. *Mol Ther*. 2005;11:35-47.
10. Ma X, Liu Y, Tittiger M, et al. Improvements in Mucopolysaccharidosis I Mice After Adult Retroviral Vector-mediated Gene Therapy with Immunomodulation. *Mol Ther*. 2007;15(5):889-902.
11. Herati RS, Ma X, Tittiger M, Ohlemiller KK, Kovacs A, Ponder KP. Improved retroviral vector design results in sustained expression after adult gene therapy in mucopolysaccharidosis I mice. *J Gene Med*. 2008;10(9):972-982.
12. Zheng Y, Rozengurt N, Ryazantsev S, Kohn DB, Satyake N, Neufeld EF. Treatment of the mouse model of mucopolysaccharidosis I with retrovirally tyransduced bone marrow. *Molecular Genetics and Metabolism*. 2003;79:233-244.
13. Miyoshi H, Smith KA, Mosier DE, Verma IM, Torbett BE. Transduction of human CD34+ cells that mediate long-term engraftment of NOD/SCID mice by HIV vectors. *Science*. 1999;283:682-686.
14. Guenechea G, Gan OI, Inamitsu T, et al. Transduction of human CD34+ CD38- bone marrow and cord blood-derived SCID-repopulating cells with third-generation lentiviral vectors. *Mol Ther*. 2000;1:566-573.
15. Guenechea G, Gan OI, Dorrell C, Dick JE. Distinct classes of human stem cells that differ in proliferative and self-renewal potential. *Nat. Immunol*. 2001;2:75-82.
16. Ailles L, Schmidt M, Santoni de Sio FR, et al. Molecular evidence of lentiviral vector-mediated gene transfer into human self-renewing, multi-potent, long-

term NOD/SCID repopulating hematopoietic cells. *Mol Ther*. 2002;6(5):615-626.

17. Capotondo A, Cesani M, Pepe S, et al. Safety of Arylsulfatase A Overexpression for Gene Therapy of Metachromatic Leukodystrophy. *Hum Gene Ther*. 2007;18:821-836.

18. Biffi A, Capotondo A, Fasano S, et al. Gene therapy of metachromatic leukodystrophy reverses neurological damage and deficits in mice. *J. Clin. Invest*. 2006;116(1):3070-3082.

19. Cartier N, Hacein-Bey-Abina S, Bartholomae CC, et al. Hematopoietic stem cell gene therapy with a lentiviral vector in X-linked adrenoleukodystrophy. *Science*. 2009;326(5954):818-823.

20. Wang D, Zhang W, Kalfa TA, et al. Reprogramming erythroid cells for lysosomal enzyme production leads to visceral and CNS cross-correction in mice with Hurler syndrome. *Proc Natl Acad Sci U S A*. 2009;106(47):19958-19963.

21. Biffi A, De Palma M, Quattrini A, et al. Correction of Metachromatic Leukodystrophy in the Mouse Model by Transplantation of Genetically Modified Hematopoietic Stem Cells. *J. Clin. Invest*. 2004;113(8):1118-1129.

22. Ohmi K, Greenberg DS, Rajavel KS, Ryazantsev S, Li HH, Neufeld EF. Activated microglia in cortex of mouse models of mucopolysaccharidoses I and IIIB. *Proc. Natl. Acad. Sci. USA*. 2003;100:1902-1907.

23. Traggiai E, Chicha L, Mazzucchelli L, et al. Development of a human adaptive immune system in cord blood cell-transplanted mice. *Science*. 2004;304(5667):104-107.

24. Kurt S, Groszer M, Fisher SE, Ehret G. Modified sound-evoked brainstem potentials in Foxp2 mutant mice. *Brain Res*. 2009;1289:30-36.

25. Björnsson S. Simultaneous preparation and quantitation of proteoglycans by precipitation with alcian blue. . *Anal. Biochem*. . 1993;210:282-291.

26. Ausseil J, Desmaris N, Bigou S, et al. Early neurodegeneration progresses independently of microglial activation by heparan sulfate in the brain of mucopolysaccharidosis IIIB mice. . *PLoS ONE* 2008;3(5):e2296.

27. Whitley CB, Ridnour MD, Draper KA, Dutton CM, Neglia JP. Diagnostic test for Mucopolysaccharidosis I. Direct method for quantifying excessive urinary glycosaminoglycan excretion. *Clin Chem*. 1989;35(3):374-379.

28. Randall DR, Colobong KE, Hemmelgarn H, et al. Heparin cofactor II-thrombin complex: a biomarker of MPS disease. *Mol Genet Metab*. 2008;94(4):456-461.

29. Langford-Smith K, Arasaradnam M, Wraith JE, Wynn R, Bigger BW. Evaluation of heparin cofactor II-thrombin complex as a biomarker on blood spots from mucopolysaccharidosis I, IIIA and IIIB mice. *Mol Genet Metab*. 2009; [Epub ahead of print] PMID: 19926322.

30. Blackwell BN, Bucci TJ, Hart RW, Turturro A. Longevity, body weight, and neoplasia in ad libitum-fed and diet-restricted C57BL6 mice fed NIH-31 open formula diet. *Toxicol Pathol*. 1995;23(5):570-582.

31. Tittiger M, Ma X, Xu L, Ponder KP. Neonatal intravenous injection of a gamma retroviral vector has a low incidence of tumor induction in mice. *Hum Gene Ther*. 2008;11:1217-1223.

32. Hartung SD, Frandsen JL, Pan D, et al. Correction of metabolic, craniofacial, and neurologic abnormalities in MPSI mice treated at birth with adeno-

associated virus vector transducing the human alpha-L-iduronidase gene. *Mol Ther*. 2004;9(6):866-875.

33. Sferra TJ, Backstrom K, Chuansong W, Rennard R, Miller M, Hu Y. Widespread correction of lysosomal storage following intrahepatic injection of a recombinant adeno-associated virus in the adult MPS VII mouse. *Mol Ther*. 2004;10(3):478-491.

34. Matzner U, H. Enzyme replacement improves nervous system pathology and function in a mouse model for metachromatic leukodystrophy. *Human Molecular Genetics*. 2005;14(9):1139-1152.

35. Kobayashi H, Carbonaro D, Pepper K, et al. Neonatal gene therapy of MPS I mice by intravenous injection of a lentiviral vector. *Mol Ther*. 2005;11(5):776-789.

36. Lee WC, Courtenay A, Troendle FJ, et al. Enzyme replacement therapy results in substantial improvements in early clinical phenotype in a mouse model of globoid cell leukodystrophy. *FASEB J*. 2005;19(11):1549-1551.

37. Montini E, Cesana D, Schmidt M, et al. Hematopoietic stem cell gene transfer in a tumor-prone mouse model uncovers low genotoxicity of lentiviral vector integration. *Nat Biotechnol*. 2006;24(6):687-696.

38. Montini E, Cesana D, Schmidt M, et al. The genotoxic potential of retroviral vectors is strongly modulated by vector design and integration site selection in a mouse model of HSC gene therapy. *J Clin Invest*. 2009;119(4):964-975.

FIGURE LEGENDS

Figure 1. Reconstitution of IDUA activity in MPS I mice upon transplantation of wild type or gene corrected HSPC.

(**A**) Experimental scheme. *Idua*$^{-/-}$ and *Idua*$^{+/+}$ cells were transduced with IDUA-LV or GFP-encoding LV (in which transgene expression was driven by the human phosphoglycerate kinase [PGK] promoter) and then transplanted (1x10^6 cells/mouse) into lethally irradiated mice, as indicated. **GT**: gene therapy treated *Idua*$^{-/-}$ mice; **HCT**: *Idua*$^{-/-}$ mice transplanted with WT HSPC transduced with GFP-LV; **MPS I**: *Idua*$^{-/-}$ mice transplanted with GFP-LV transduced *Idua*$^{-/-}$ HSPC (mock-transplanted affected controls); **WT**: *Idua*$^{+/+}$ mice transplanted with GFP-LV transduced *Idua*$^{+/+}$ HSPC (mock-transplanted WT controls). (**B**-**D**) IDUA activity was measured in the PBMCs (B), in the serum (C) and in the tissues indicated below the "x" axis (D) of mice transplanted with either mock-transduced or gene corrected HSPC at 4 weeks (B) or 6 months after the transplant (at sacrifice) (B, C and D). Each dot represents one mouse, average values are shown (black line). (**E**) Gene therapy treated mice were divided into two groups according to the IDUA activity measured in total PBMCs (at 6 months from the transplantation)(left chart) and to the vector copy number *per* genome (VCN) measured on total BM cells (right chart). IDUA activity measured in the brain is shown for animals having IDUA activity in PBMCs below (<) or above (>) 1500nmol/mg/h and carrying less (<) or more (>) than 5 LV copies *per* genome in the BM (being 1500 and 5 the average values measured in the

entire pool of gene therapy treated mice). Mean ± min/max are shown. **= p<0.01; ***=p<0.001 at Student's *t* test.

Figure 2. Supra-normal enzymatic activity allows storage removal in the MPS I affected tissues.

(**A**) Morphological analysis of 1-μm sections, toluidine blue stained, from different organs of treated and control animals, as indicated. Representative images show the lysosomal distention in the indicated tissues in MPS I mice (no distention is present in WT animals). Kidney: arrows and arrowheads identify lysosomal storage, which is evident in the tubules (arrows), in the glomeruli (arrowheads)(* marks the glomeruli) and in interstitial fibroblasts; liver: arrows highlight storage within hepatocytes, and storage is also present within Kuppfer cells; spleen: pathological storages (arrows) are predominant in the red pulp; heart: pathological storage is abundant in the endothelium and in myocytes (arrows); frontal cortex: pathological storage is present within neurons (arrows) and in endothelial cells (v=vessels); subjective score in MPS I: 3-4 in the different examined tissues. Magnification 100X and 200X. Residual storage is present in all tissues of mice treated with HCT. Two representative animals [HCT(a) and HCT (b), both having donor cell engraftment >70%, as assessed by quantification of donor GFP+ cells in peripheral blood by cytofluorimetric analysis] are shown demonstrating a different grade of storage [subjective score HCT(a): 1-2 and HCT (b): 2-3 in the different examined tissues]. Magnification 100X and 200X. A strong reduction of the storage is evident in all the examined tissues from a representative GT mouse having a VCN of 5 in the BM (subjective score: 0-1

in the different examined tissues). Magnification 100X. (**B**) Lysosomal distention/cell engulfment was scored (see methods for details) in liver, spleen, heart, kidney and cortex of treated and control mice. Mean ± SEM are shown; n=4 representative mice analyzed *per* group (≥3 representative images *per* mouse). *=p<0.05; **= p<0.01; ***=p<0.001 at One Way Anova. (**C**-**D**) GAGs were quantified in the urine (C) and in the tissues (D, as indicated below x axis; liver, spleen and kidney were chosen as representative tissues) of treated and control mice. Mean ± SEM are shown; n≥4 representative mice analyzed *per* group. *=p<0.05; **= p<0.01; ***=p<0.001 at One Way Anova. (**E**) Western Blot for heparin co-factor II-thrombin (HCII-T) complex was performed on the serum of MPS I, GT and WT mice. GAPDH (lower image) was used as internal control.

Figure 3. Differential neurological outcome of gene therapy and HCT.

(**A**) Repeated open field test was performed on treated and control mice 6 months after the transplantation. Horizontal activity of MPS I (n=20), HCT (n=18), **GT (n=17)** and WT (n=14) mice is reported as percentage (%) of change between the 1st and the 3rd day. (**B**) GT mice were divided into two groups according to the IDUA activity measured on their brain. The % change in horizontal activity between 1st and 3rd trial is shown for animals having brain IDUA activity lower (<, n=8) or higher (>, n=9) than 20nmol/mg/h (being 20nmol/mg/h the average activity value measured on the brain of the entire population of GT mice). Mean ± SD are shown; *=p<0.05; **=p<0.01; ***=p<0.001 at one-way Anova in (A) and Student's *t* test in (B). (**C**) Purkinje cell frequency (expressed as % of the cells counted in WT mice)(dense area)

and % of degenerated Purkinje cells among the total cells (scattered area) in cerebellum slices from affected, WT, HCT and GT treated mice are shown (see methods for details). Mean ± SD values are shown; n≥4 representative mice analyzed *per* group (≥3 representative sections *per* mouse). (**D**) Representative semithin section images from the Purkinje cell layer of treated and control mice, as indicated. The pictures show degenerating Purkinje cells, which besides accumulating GAGs display shrunken cell bodies and darkly stained nuclei (arrows, "gl" marks granular layer), in mock-transplanted MPS I mice; in HCT mice residual storage and Purkinje cell degeneration were seen, while in the GT treated mice we observed a complete rescue of the pathological phenotype. Magnification 100X in the images from the upper row, 200X in the bottom row.

Figure 4. Differential skeletal outcome of gene therapy and HCT.

(**A-B**) Pictures (A) and 3D reconstructions of CT scans (B) from MPS I, WT, HCT and GT mice 6 months after the treatment, showing the different gross appearance of the treated and control mice (the GT mouse shown in [A] and [B] had a VCN of 5.4 on bone marrow; the HCT mouse had a donor cell engraftment of 74% on PBMCs). (**C-F**) Measurements of skull width (C), zygomus volume (D), femur length (E) and humerus width (F) were performed on CT scan images as shown on the right side of each chart (see methods for details) from MPS I (n=19), HCT (n=14), GT (n=15) and WT (n=14). For avoiding sex biases, the femur length of only the male mice is reported (MPS I n=10, HCT n=10, GT n=8, WT n=8); similar results were obtained in females. (**G**) Gene therapy treated mice were divided into two groups according to the

IDUA activity measured on their PBMCs. The femur length is shown for animals (males and females) having PBMC IDUA activity lower (<) or higher (>) than 1500nmol/mg/h (being 1500nmol/mg/h the average activity value measured in the entire population of gene therapy treated mice). (**H**) Strength Strain Index (SSI) (calculated as described in the methods section) was evaluated by pQCT on the diaphysis of the femur (left chart) and tibia (right chart) from MPS I (n=19), HCT (n=14), GT (n=15) and WT (n=14). Mean and min/max values are shown; *= $p<0.05$; **=$p<0.01$; ***=$p<0.001$ at one-way Anova in (C-F) and (H); *=$p<0.05$ at Student's *t* test in G.

Figure 5. Differential effect on the growth plate of gene therapy and HCT. (**A**) Representative pictures of the proximal epiphysis of the tibiae from mock-transplanted and treated mice (hematoxylin and eosin staining), as indicated. The growth plate is disorganized and has an irregular morphology in both mock-transplanted MPS I and HCT mice (the GT mouse shown in [A] and [B] had a VCN of 6 on bone marrow; the HCT mouse had a donor cell engraftment of 80% on PBMCs). Magnification 5X and 20X. (**B**-**C**) The ratio between the perimeter and the length of the growth plate (B) was calculated and the number of chondrocytes aligned in columns perpendicular to the major axis of the growth plate (C) was counted (see Figure S2 for detailed explanation) for 5 representative MPS I, HCT, GT and WT mice (≥3 representative sections *per* mouse). Mean and min/max values are shown; *= $p<0.05$; **=$p<0.01$; ***=$p<0.001$ at one-way Anova.

Figure 6. Effect of gene therapy on auditory brainstem responses and retina integrity.

(**A**-**B**) ABR were measured on gene therapy treated (n=9) and control mice (n=9 for WT and 5 for MPS I) 6 months after treatment. (A) Representative response after auditory stimulation in WT, MPS I and GT mice: for each mouse 3 series of waves (obtained by average of 500 electrical signals each) were recorded (shown in the upper panel). In the lower panel the resultant wave obtained by the average of the three traces is shown. The latency of wave I and IV was measured as shown by the pink and green lines, respectively. (B) ABR scores of wave I (left chart) and wave IV (right chart) latencies are shown. (**C**-**D**) Retinal thickness (D) of MPS1, GT, and WT mice (n=3) measured on 20x magnification pictures upon DAPI staining, as shown in the representative images in (C). n=3 mice analyzed *per* group (≥6 representative images *per* mouse). PE = photoreceptor layer; ONL = outer nuclear layer; INL = inner nuclear layer; GCL = ganglion cell layer. The white bar in picture on the left shows the measured thickness. Mean and SD are shown (*= $p<0.05$; **=$p<0.01$; ***=$p<0.001$ at One-way Anova).

Figure 1

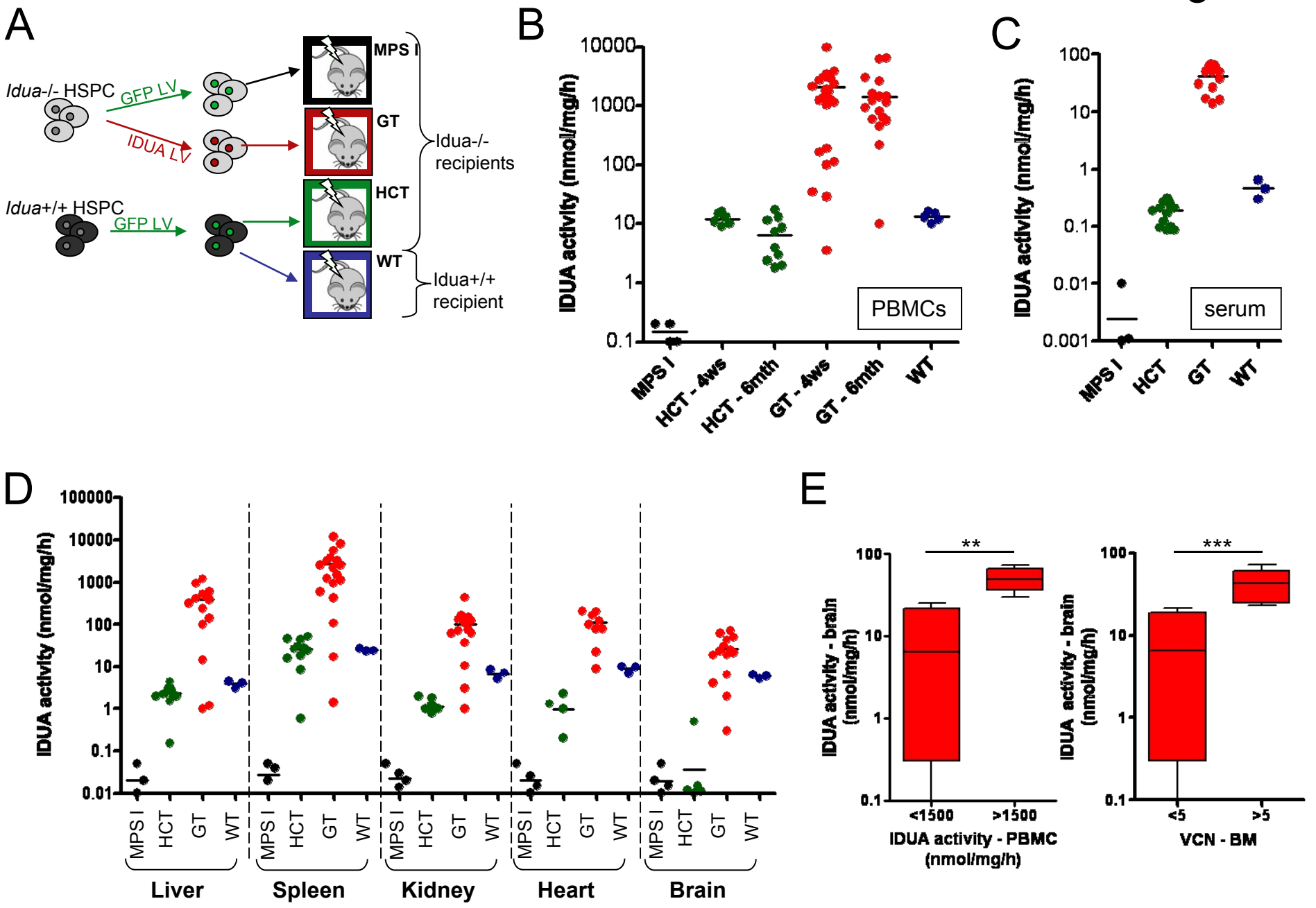
A
Idua-/- HSPC
GFP LV
IDUA LV
Idua+/+ HSPC
GFP LV
MPS I
GT
HCT
WT
Idua-/- recipients
Idua+/+ recipient
B
IDUA activity (nmol/mg/h)
PBMCs
MPS I
HCT - 4ws
HCT - 6mth
GT - 4ws
GT - 6mth
WT
C
IDUA activity (nmol/mg/h)
serum
MPS I
HCT
GT
WT
D
IDUA activity (nmol/mg/h)
MPS I
HCT
GT
WT
Liver
Spleen
Kidney
Heart
Brain
E
IDUA activity - brain (nmol/mg/h)
**
<1500
>1500
IDUA activity - PBMC (nmol/mg/h)
IDUA activity - brain (nmol/mg/h)
***
<5
>5
VCN - BM

Figure 2

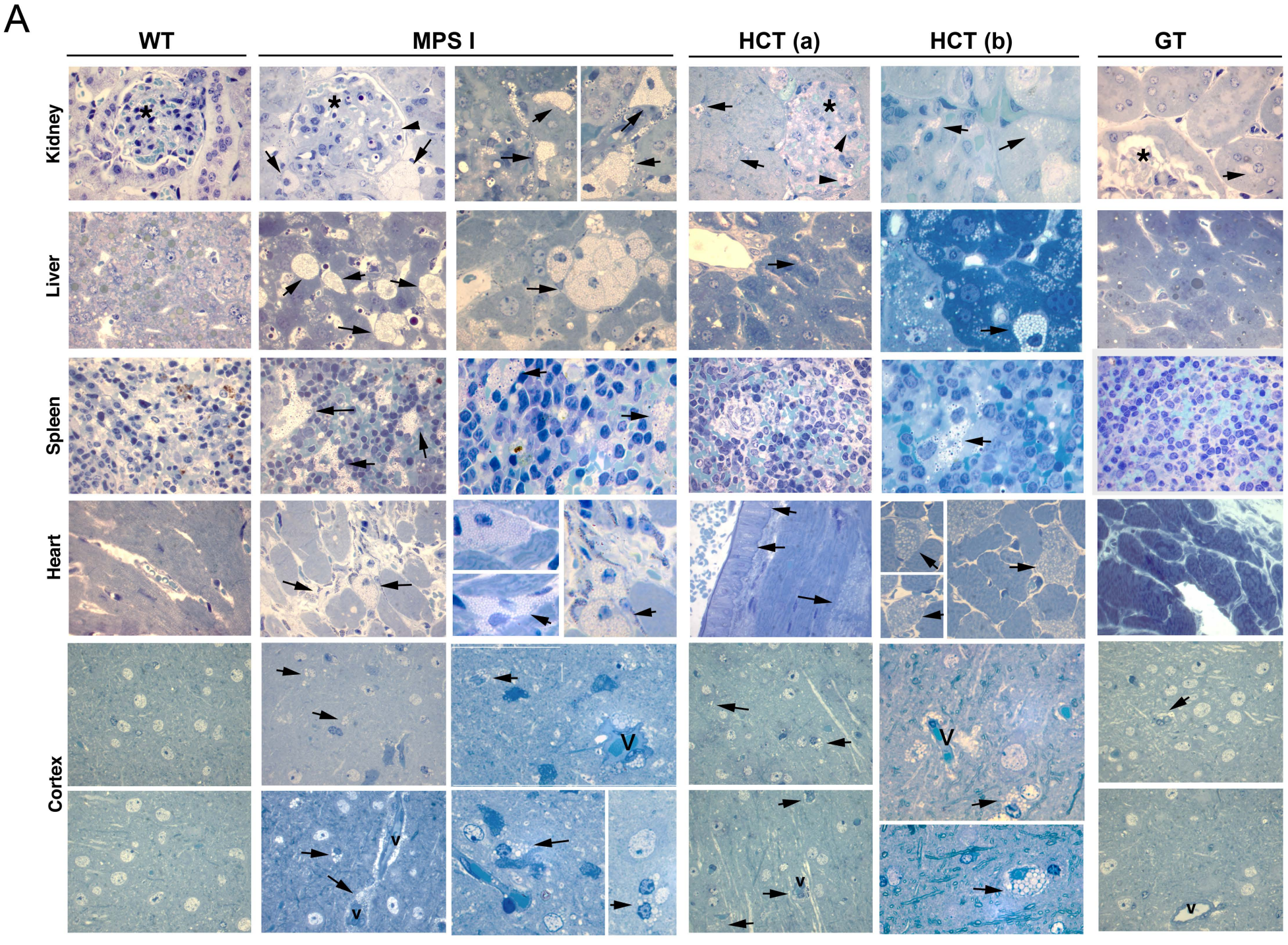

Figure 2

B

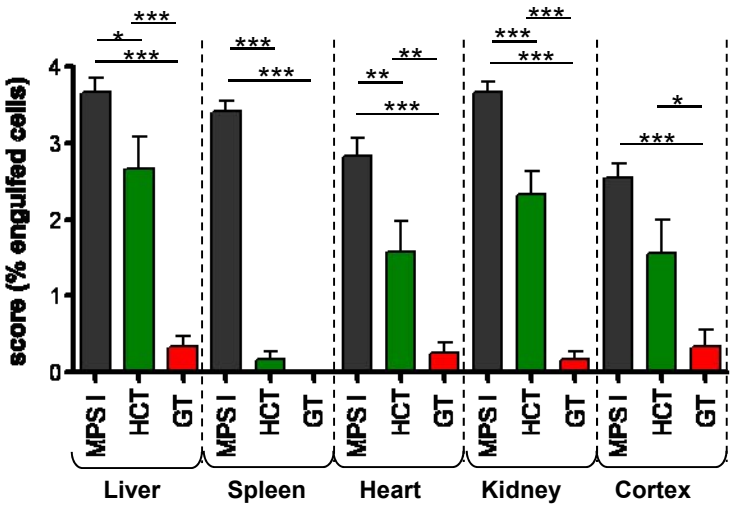

C

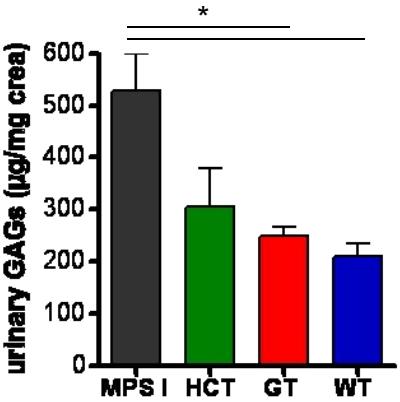

D

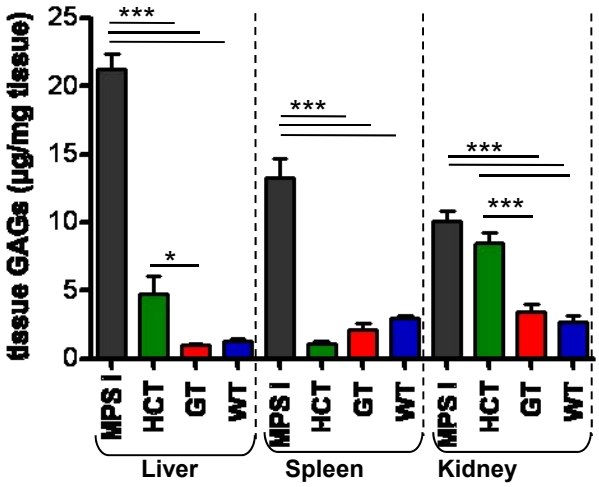

E

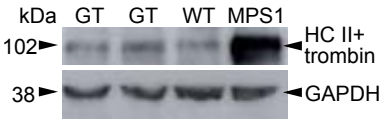

Figure 3

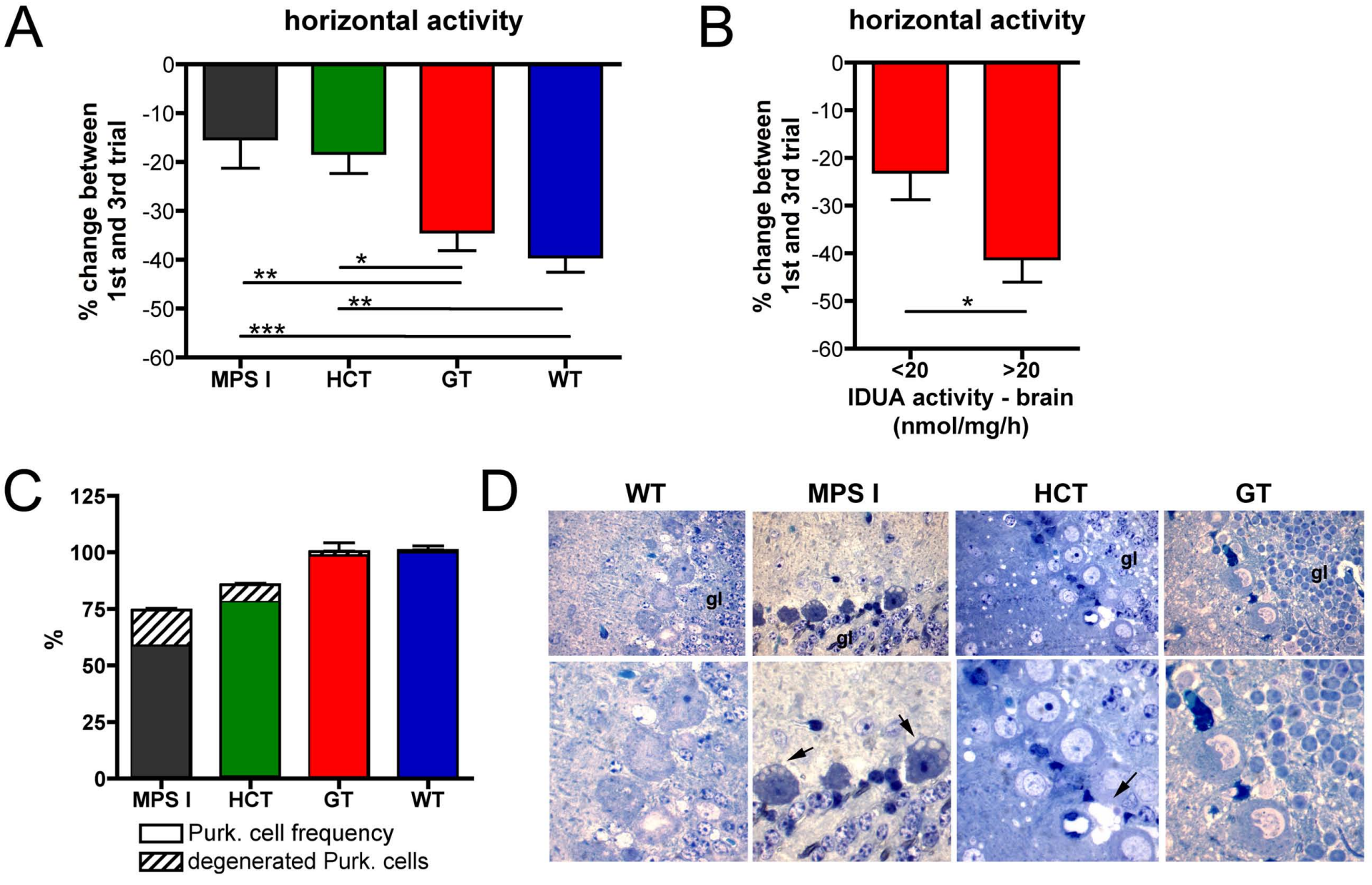
A
horizontal activity
% change between 1st and 3rd trial
0
-10
-20
-30
-40
-50
-60
**
*
**
***
MPS I
HCT
GT
WT
B
horizontal activity
% change between 1st and 3rd trial
0
-10
-20
-30
-40
-50
-60
*
<20
>20
IDUA activity - brain (nmol/mg/h)
C
125
100
75
50
25
0
%
MPS I
HCT
GT
WT
Purk. cell frequency
degenerated Purk. cells
D
WT
MPS I
HCT
GT
gl

Figure 4

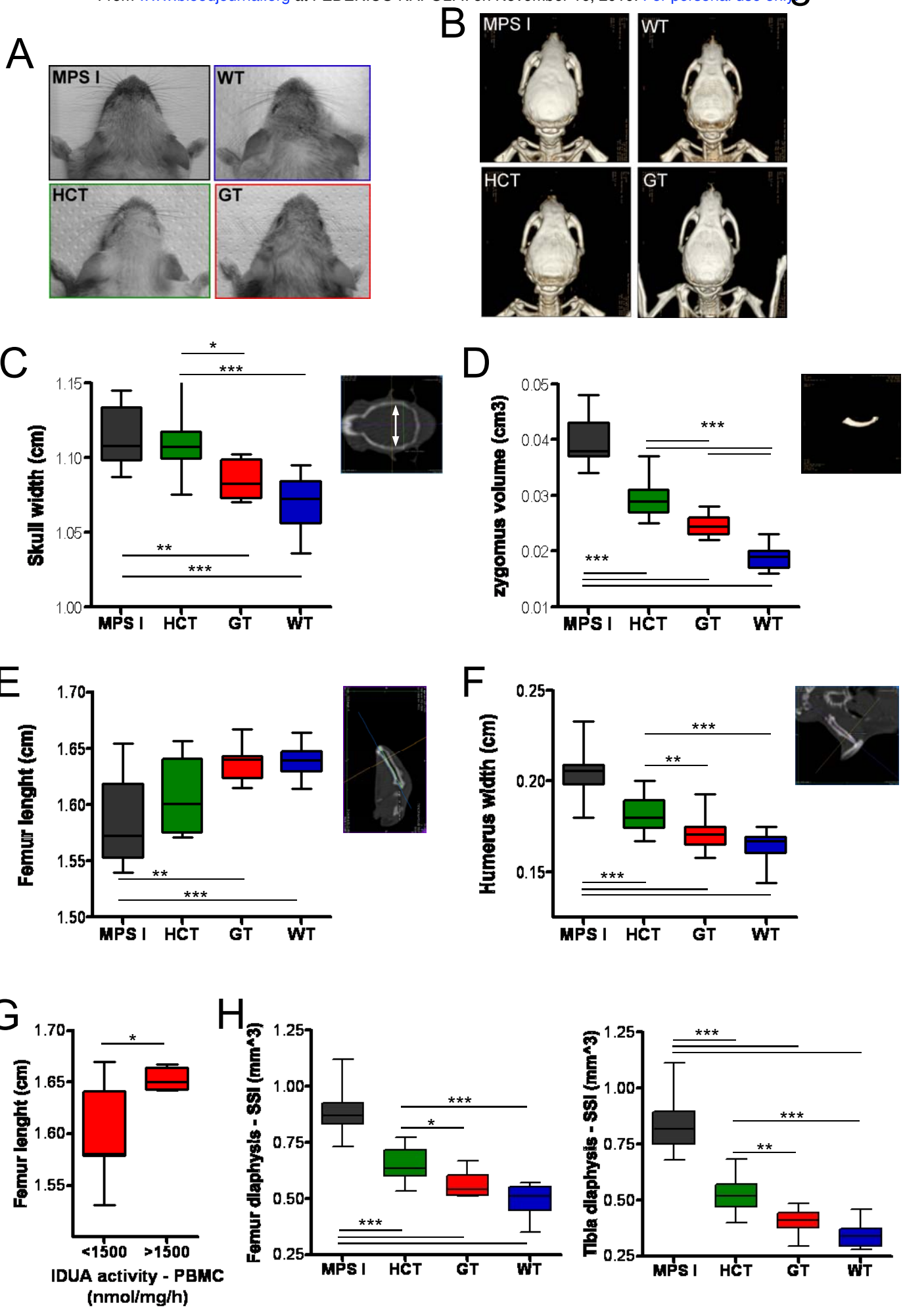

Figure 5

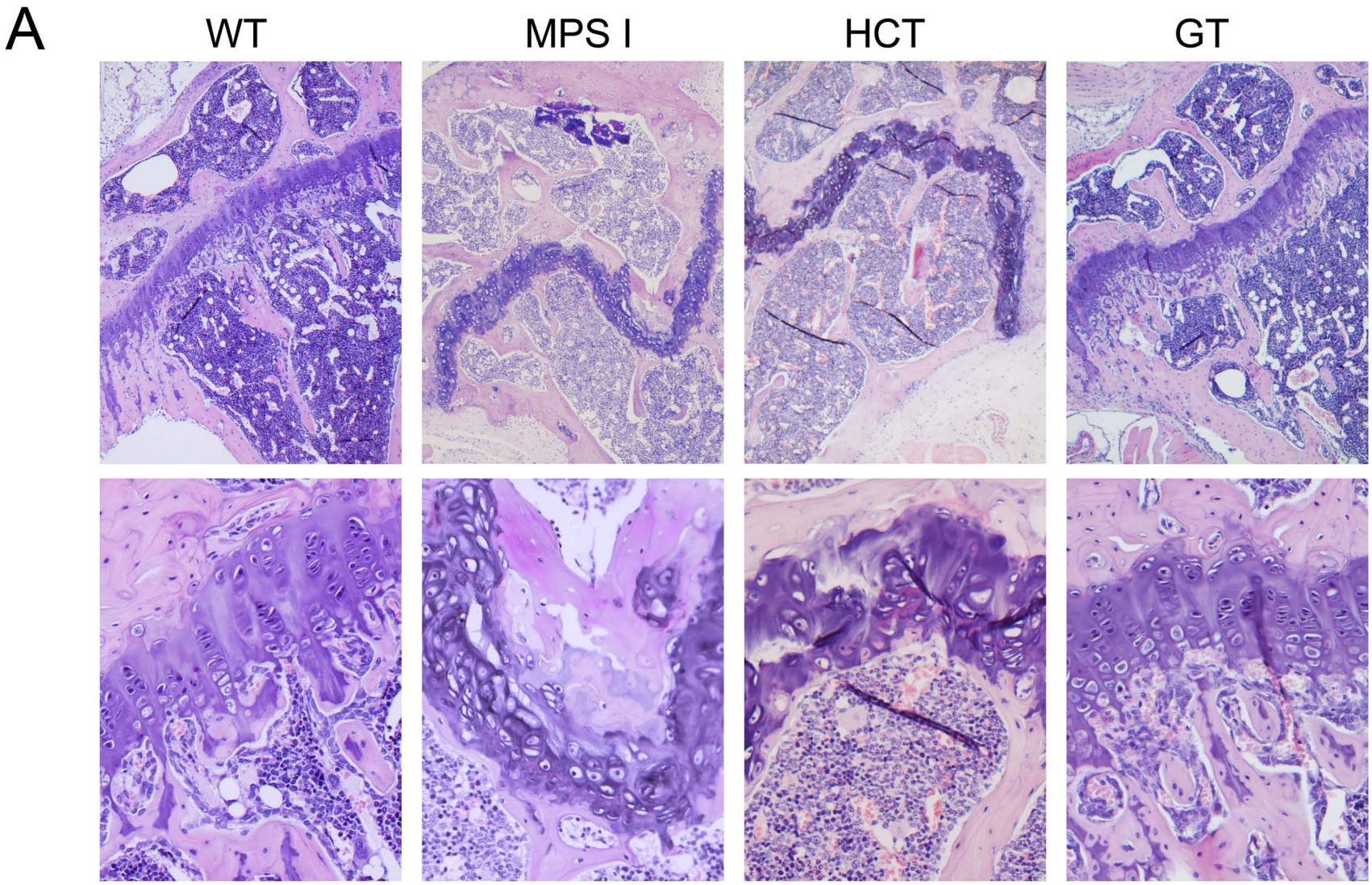
A
WT
MPS I
HCT
GT

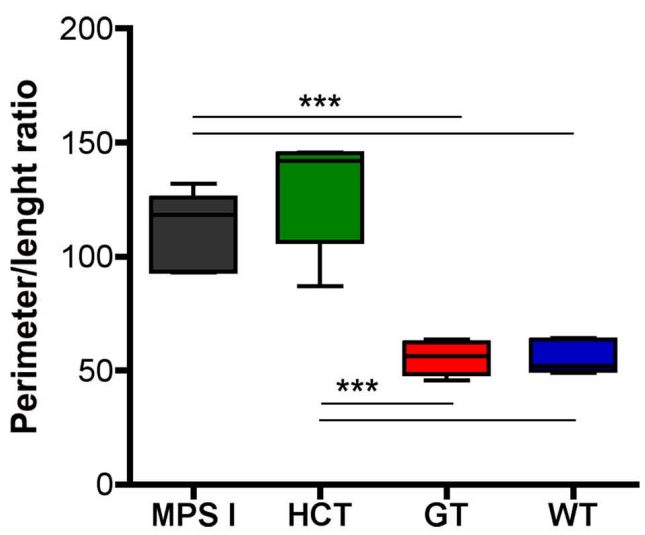
B
Perimeter/lenght ratio
200
150
100
50
0
***
***
MPS I
HCT
GT
WT

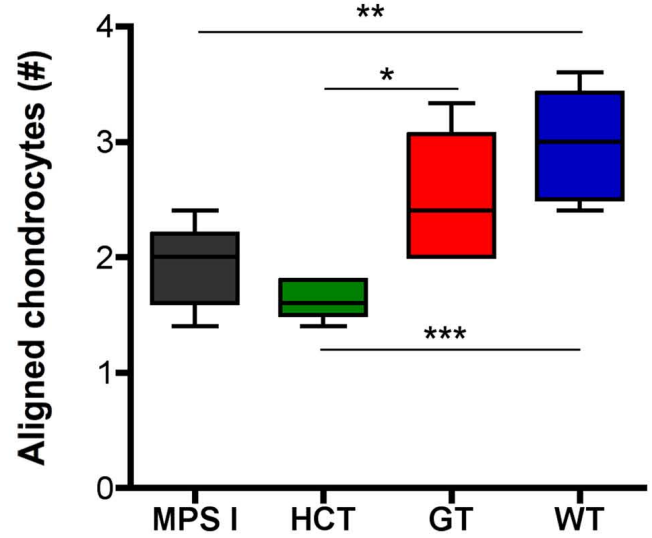
C
Aligned chondrocytes (#)
4
3
2
1
0
**
*
***
MPS I
HCT
GT
WT

Figure 6

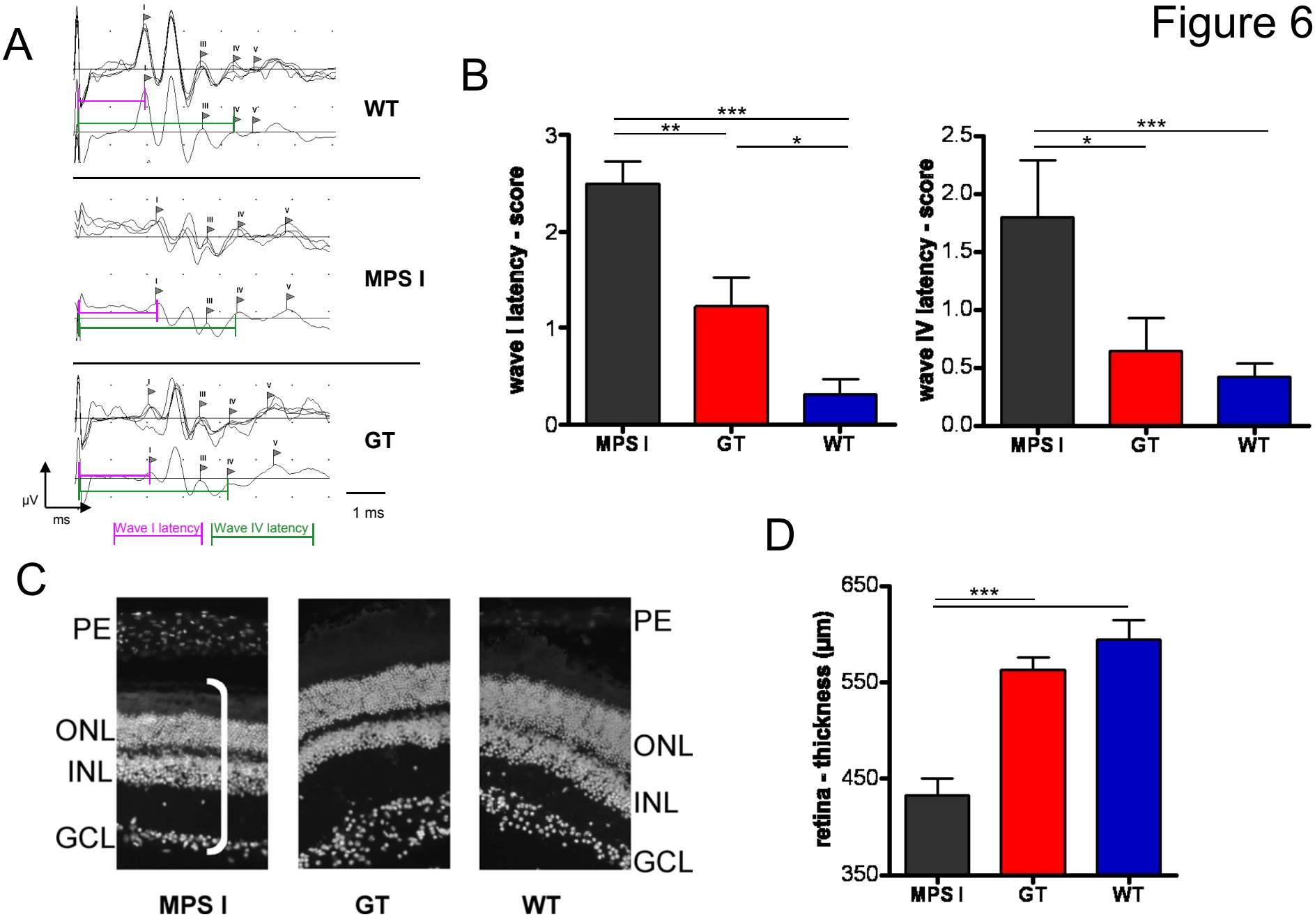
A
WT
MPS I
GT
μV
ms
1 ms
Wave I latency
Wave IV latency
B
wave I latency - score
MPS I
GT
WT
wave IV latency - score
C
PE
ONL
INL
GCL
MPS I
GT
WT
D
retina - thickness (μm)
650
550
450
350
***